TU Delft

Delft University of Technology

Document Version
Final published version

Citation (APA)
Bozali, B. (2026). *Development and Applications of Textile-Based Sensors and Actuators*. [Dissertation (TU Delft), Delft University of Technology]. https://doi.org/10.4233/uuid:9c0897c9-9289-4065-a9d2-54ee366c0404

Important note
To cite this publication, please use the final published version (if applicable).
Please check the document version above.

Copyright
In case the licence states “Dutch Copyright Act (Article 25fa)”, this publication was made available Green Open Access via the TU Delft Institutional Repository pursuant to Dutch Copyright Act (Article 25fa, the Taverne amendment). This provision does not affect copyright ownership.
Unless copyright is transferred by contract or statute, it remains with the copyright holder.

Sharing and reuse
Other than for strictly personal use, it is not permitted to download, forward or distribute the text or part of it, without the consent of the author(s) and/or copyright holder(s), unless the work is under an open content license such as Creative Commons.

Takedown policy
Please contact us and provide details if you believe this document breaches copyrights.
We will remove access to the work immediately and investigate your claim.

This work is downloaded from Delft University of Technology.

Development and Applications of Textile-Based Sensors and Actuators

Dissertation

for the purpose of obtaining the degree of doctor

at Delft University of Technology

by the authority of the Rector Magnificus,

Prof.dr.ir. H. Bijl,

chair of the Board for Doctorates

to be defended publicly on

Monday, 21 September 2026, 12:30

by

BEYZA BOZALI

This dissertation has been approved by the (co)promotors.

Composition of the doctoral committee:

Rector Magnificus	Chairperson
Prof.dr.ir. K.M.B. Jansen,	Delft University of Technology, Netherlands, promotor
Dr. S. Ghodrat,	Delft University of Technology, Netherlands, co-promotor

Independent Members:

Prof.dr. A.R. Balkenende,	Delft University of Technology, Netherlands
Prof.dr.ir. L. Van Langenhove,	Ghent University, Belgium
Prof.dr. V. Koncar,	University of Lille, France
Prof.dr.ir. V. Nierstrasz,	University of Borås, Sweden

Reserve Member:

Prof.dr.ir. E. Karana,	Delft University of Technology, Netherlands

This research is supported by the Turkish Ministry of National Education.

Copyright © Beyza Bozali 2026

All rights reserved.

An electronic version of this dissertation is available at:

http://repository.tudelft.nl

Summary

The integration of sensing and actuation functionalities directly into textiles offers opportunities for developing soft, flexible, and unobtrusive wearable systems. Knitted textiles are particularly promising for this purpose because their inherent stretchability and flexibility allow functional elements to be integrated directly into the textile structure. However, the complex relationship between yarn properties, knit architecture, and functional performance makes the systematic design of knitted sensors and actuators challenging. This thesis investigates how knitted textile structures can be engineered to achieve controlled sensing and heating performance, with a particular focus on understanding the relationships between material and structural parameters and device behaviour.

The research investigates three types of knitted functional textiles: strain sensors, pressure sensors, and heaters. Conductive yarns were integrated into knitted structures using a flatbed knitting process, allowing the functional elements to remain fully textile-based. The work combines experimental characterisation, structural optimisation, wearable demonstrators, and physics-based modelling to investigate how knitting parameters and material selection influence functional performance.

First, knitted strain sensors were developed using conductive and elastic yarns in 1×1 rib structures. The effects of knitting density, conductive yarn position, and the number of conductive courses on sensing behaviour were systematically investigated. Positioning the conductive yarn inside the knitted structure reduced hysteresis and improved the linearity and reproducibility of the sensor response. Sensors with working ranges of up to 40% strain, hysteresis as low as 0.03, and gauge factors up to 1.19 were achieved. These results demonstrate that the mechanical and electrical behaviour of knitted strain sensors can be controlled through structural design and yarn configuration.

The strain-sensing structures were further investigated in wearable applications. Finger-worn sensors demonstrated their potential for monitoring finger movements and supporting rehabilitation-related applications. Textile-based strain sensing was also explored for monitoring respiration and biomechanical movement, demonstrating the potential of knitted sensors for continuous physiological and motion monitoring.

Knitted pressure sensors were subsequently developed to investigate tactile sensing. Different knitted geometries and structural configurations were evaluated to understand their influence on sensitivity and detection range. The results showed that the structural design of the knitted sensor determines its pressure response. Flat structures provided high sensitivity at relatively low pressures, while dome-like structures enabled a wider detection range. These findings demonstrate that knitted pressure sensors can be tailored to different sensing requirements through the design of their textile architecture.

The research also investigated knitted heaters as textile-based actuators. A physics-based model was developed to relate electrical resistance, current distribution, power dissipation, and temperature distribution to the structural design of the heater. Knitted heaters with different conductive-line configurations were experimentally evaluated. The results demonstrated that the number and arrangement of conductive lines strongly influence heating performance and temperature uniformity. The developed modelling approach showed good agreement with experimental measurements and provides a basis for predicting and designing the thermal behaviour of knitted heaters.

Overall, this thesis demonstrates that knitting can be used not only as a manufacturing technique but also as a means of engineering the functional behaviour of textile-based sensors and actuators. Across the investigated systems, yarn properties, knit architecture, conductive layout, and structural parameters were shown to influence electrical, mechanical, and thermal performance. The research therefore contributes to a better understanding of the structure–property–performance relationships of knitted functional textiles and demonstrates how these relationships can be exploited to develop application-specific wearable systems.

Overall, this thesis demonstrates that knitting can be used not only as a manufacturing technique but also as a means of engineering the functional behaviour of textile-based sensors and actuators. Across the investigated systems, yarn properties, knit architecture, conductive layout, and structural parameters were shown to influence electrical, mechanical, and thermal performance. The research therefore contributes to a better understanding of the structure–property–performance relationships of knitted functional textiles and demonstrates how these relationships can be exploited to develop application-specific wearable systems.

The developed technologies show potential for applications in motion monitoring, rehabilitation, physiological monitoring, tactile sensing, and wearable thermal regulation. Further work is required to address long-term durability, washability, multi-axial deformation, scalability, sustainable materials, and the integration of textile components with electronic systems.

Samenvatting

De integratie van sensor- en actuatorfunctionaliteiten rechtstreeks in textiel biedt mogelijkheden voor de ontwikkeling van zachte, flexibele en onopvallende draagbare systemen. Gebreide textielen zijn hiervoor bijzonder veelbelovend, omdat hun intrinsieke rekbaarheid en flexibiliteit het mogelijk maken om functionele elementen rechtstreeks in de textielstructuur te integreren. De complexe relatie tussen gareneigenschappen, breistructuur en functionele prestaties maakt het echter uitdagend om gebreide sensoren en actuatoren systematisch te ontwerpen. Dit proefschrift onderzoekt hoe gebreide textielstructuren kunnen worden ontworpen om gecontroleerde sensor- en verwarmingsprestaties te bereiken, met bijzondere aandacht voor de relaties tussen materiaal- en structurele parameters en het functioneren van de ontwikkelde systemen.

In dit onderzoek worden drie typen functionele gebreide textielen onderzocht: reksensoren, druksensoren en verwarmers. Geleidende garens werden geïntegreerd in gebreide structuren met behulp van een vlakbreimachine, waardoor de functionele elementen volledig uit textiel konden worden vervaardigd. Het onderzoek combineert experimentele karakterisering, structurele optimalisatie, draagbare demonstrators en fysische modellering om te onderzoeken hoe breiparameters en materiaalkeuze de functionele prestaties beïnvloeden.

Ten eerste werden gebreide reksensoren ontwikkeld met geleidende en elastische garens in 1×1-ribstructuren. De effecten van breidichtheid, de positie van het geleidende garen en het aantal geleidende banen op het sensorrespons werden systematisch onderzocht. Het positioneren van het geleidende garen aan de binnenzijde van de gebreide structuur verminderde de hysterese en verbeterde de lineariteit en reproduceerbaarheid van de sensorrespons. Sensoren met een meetbereik tot 40% rek, een hysterese van slechts 0,03 en een gauge factor tot 1,19 werden gerealiseerd. Deze resultaten laten zien dat het mechanische en elektrische gedrag van gebreide reksensoren kan worden gestuurd door de structurele opbouw en de configuratie van de garens.

De reksensorstructuren werden vervolgens onderzocht in draagbare toepassingen. Sensoren die rond de vingers werden gedragen, toonden hun potentieel voor het monitoren van vingerbewegingen en toepassingen gericht op revalidatie. Gebaseerd op hetzelfde principe werd textielgebaseerde reksensoring ook onderzocht voor het monitoren van ademhaling en biomechanische bewegingen. Deze toepassingen tonen het potentieel van gebreide sensoren voor continue monitoring van fysiologische signalen en bewegingen.

Vervolgens werden gebreide druksensoren ontwikkeld voor tactiele detectie. Verschillende gebreide geometrieën en structurele configuraties werden geëvalueerd om hun invloed op gevoeligheid en meetbereik te begrijpen. De resultaten lieten zien dat het structurele ontwerp van de gebreide sensor de drukrespons sterk beïnvloedt. Vlakke structuren boden een hoge gevoeligheid bij relatief lage drukken, terwijl koepelvormige structuren een groter meetbereik mogelijk maakten. Deze bevindingen laten zien dat gebreide druksensoren kunnen worden afgestemd op verschillende sensorbehoeften door de architectuur van de textielstructuur aan te passen.

Daarnaast werden gebreide verwarmers onderzocht als textielgebaseerde actuatoren. Er werd een fysisch model ontwikkeld dat elektrische weerstand, stroomverdeling, vermogensdissipatie en temperatuurverdeling relateert aan het structurele ontwerp van de verwarmer. Gebreide verwarmers met verschillende configuraties van geleidende banen werden experimenteel geëvalueerd. De resultaten toonden aan dat het aantal en de configuratie van de geleidende banen een sterke invloed hebben op de verwarmingsprestaties en de uniformiteit van de temperatuurverdeling. Het ontwikkelde model vertoonde een goede overeenkomst met de experimentele metingen en biedt een basis voor het voorspellen en ontwerpen van het thermische gedrag van gebreide verwarmers.

Over het geheel genomen laat dit proefschrift zien dat breien niet alleen als productietechniek kan worden gebruikt, maar ook als middel om het functionele gedrag van textielgebaseerde sensoren en actuatoren te ontwerpen en te sturen. Voor de onderzochte systemen bleken gareneigenschappen, breiarchitectuur, de configuratie van geleidende elementen en structurele parameters van invloed te zijn op de elektrische, mechanische en thermische prestaties. Het onderzoek draagt daarmee bij aan een beter begrip van de relaties tussen structuur, materiaaleigenschappen en prestaties van functionele gebreide textielen, en laat zien hoe deze relaties kunnen worden benut voor de ontwikkeling van draagbare systemen die zijn afgestemd op specifieke toepassingen.

De ontwikkelde technologieën bieden mogelijkheden voor toepassingen in bewegingsmonitoring, revalidatie, fysiologische monitoring, tactiele detectie en draagbare thermische regulatie. Verdere ontwikkeling is nodig om uitdagingen op het gebied van langdurige duurzaamheid, wasbaarheid, multi-axiale vervorming, opschaling, duurzame materialen en de integratie van textielcomponenten met elektronische systemen aan te pakken.

Contents

1 Introduction 17

1.1 General information about smart textiles and their application areas 18

1.2 Integration methods of smart functions into garments 19

1.2.1 Conductive yarns and knitting for smart textiles 21

1.3 Textile-based sensors and actuators 24

1.3.1 Challenges and research gaps in the development of knitted sensors 25

1.4 Research questions 26

1.5 Thesis Outline 26

References 27

2 Development of knitted strain sensors and their performance evaluation 29

2.1 Materials and Methods 32

2.2 Resistance-Strain Testing Procedure 33

2.3 Electromechanical Properties 34

2.4 Results 34

2.4.1 Electromechanical Performance Analysis of a Knitted Strain Sensor 34

2.4.2 The Effect of Knit Density (NP Number) on the Sensor Performance 35

2.4.3 The Effect of an Elastic Yarn Type on Sensor Performance 37

2.4.4 The Effect of Conductive Yarn Configuration on the Sensor Performance 38

2.4.5 The Effect of Conductive Yarn Type and Conductive Course Number on Sensor Performance 39

2.5 Discussion 42

2.6 Conclusions 44

References 46

Supporting Information 48

3 Application of knitted strain sensors 53

3.1 Materials and Methods 55

3.2 Results 57

3.2.1 Electromechanical performance of the knitted strain sensor 57

3.2.2 Application of knitted strain sensor for rehabilitation purposes 58

3.3 Discussion 61

3.4 Conclusion 61

References 62

4 Development of knitted pressure sensors 65

4.1 Materials and Methods 67

4.2 Results and Discussion 68

4.2.1 Analysis of flat knitted pressure sensors 68

4.2.2 Analysis of dome-like knitted pressure sensors 69

4.3 Conclusion 70

References 71

5 Development of knitted heaters 73

5.1 Theory 75

5.2 Materials and Methods 78

5.3 Results 79

5.3.1 Heater Line Knit Structures 79

5.3.2 Equivalent Resistances of Knitted Heaters 80

5.3.3 Resistance Characterization of the Heater Lines 81

5.3.4 Validation of Measured and Predicted Temperature Profiles 82

5.4 Discussion 85

5.5 Conclusions 88

References 89

Supporting Information 91

6 Conclusions, Limitations and Future Perspectives 93

6.1 Answering the research questions 94

6.2 Contribution to the field of smart textiles 98

6.3 Limitations 98

6.4 Future work on smart textiles 99

References 101

List of publications 102

Abbreviations

The following abbreviations and coding are used in this thesis:

EMG	Electromyography
ECG	Electrocardiography
SMAs	Shape-memory alloys
GF	Gauge factor
WR	Working range
H or H_{ε}	Hysteresis
R_0	Initial resistance
ΔR	Resistance change
$\Delta \varepsilon$	Change in strain
Tex, Dtex	Yarn linear density units
YL	Yarn length in knit design
LD	Linear density (Tex)
WS	Wale spacing
CS	Course spacing
S_h, S_v	Horizontal and vertical size
P	Applied pressure
ΔR	Resistance change
R_0	Initial resistance
S	Sensitivity = $(\Delta R/R_0)/P$
NP	Needle Pitch
D	Dome diameter (used in area calculation)
kPa	Kilopascal (unit of pressure)
Intrinsic conductive polymers	ICPs
Carbon nanotubes	CNTs
R_{eq}	Equivalent resistance
R_h	Heater resistance
ε	Resistance ratio
n	Number of heater lines
T_0	Initial temperature
p_h	Heating power
C_R	Resistivity constant
C_H	Heat transfer parameter

C_p	Heat capacity
L/W	Length to width ratio
ΔT	Temperature change

Statement on the Use of Generative Artificial Intelligence

I acknowledge the use of Large Language Models (LLM) such as ChatGPT, NotebookLLM, Perplexity.ai and Gemini to help brainstorm topics, ideas, and research directions. Furthermore, they helped digest and summarize research papers to identify relevant topics.

These topics were always consulted in the paper itself, and, like the written text in this report, they were never directly copied from LLM outputs. Outputs were only used as a starting point before narrowing down the topics for assessment.

I acknowledge the use of Large Language Models (LLMs) such as ChatGPT, NotebookLLM, Perplexity.ai, and Gemini during the later stages of manuscript preparation. These tools were used selectively to support language refinement, clarity and minor editorial improvements. The core ideas, literature review, analysis, and written content were developed independently by the author. No text was directly copied from LLM outputs. Any suggestions generated by these tools were carefully reviewed and, where relevant, reformulated before inclusion in the manuscript.

Chapter 1

1. Introduction

1.1 General information about smart textiles and their application areas

Smart textiles have gained significant attention owing to their potential applications in textile-based antennas [1], energy harvesting [2], electromagnetic shielding [3] and health monitoring [4]. The integration of various smart functionalities into garments allows us to harness the inherent qualities of textiles, such as comfort, breathability, stretchability and washability. Textile-based smart structures enable real-time monitoring of physiological and environmental parameters, providing continuous feedback for applications such as body temperature regulation, posture tracking and health monitoring. They also serve as an effective platform in the development of tools for measuring external and internal garment temperatures, as well as body temperature [5]. Since they adapt to the human body and facilitate the direct integration of conductive threads, a wide range of textile-based sensors and actuators can be developed for a variety of applications, including healthcare, sports, rehabilitation and occupational use such as for soldiers or industrial workers. In healthcare, textile-based smart structures are promising approaches that stimulate muscles and nerves to facilitate movement in neurological disorders. All these potentials enable smart textiles to monitor, respond and support human physiological and environmental needs, resulting in diverse applications in healthcare, sports and rehabilitation applications.

By embedding electronic functionalities directly into fabrics, smart textiles extend the capabilities of traditional materials, enabling garments to sense, respond and adapt to physiological conditions while maintaining comfort, flexibility and durability. That enables garments to interact with the environment, adapting to factors such as temperature, motion, and biological signals. Beyond passive comfort, textiles actively enhance user experience through integrated functionalities. A crucial development in this field is the emergence of textile-based sensors which utilize the fabric's natural adaptability to detect and transmit physiological and environmental data. These sensors enable applications such as real-time health monitoring, motion tracking and human-machine interaction, further expanding the possibilities of wearable technology. Related applications include sensor gloves and VR suits as well as elbow and knee revalidation aids and sensory compression garments. Figure 1.1 provides a summary of the applications of smart textiles discussed above.

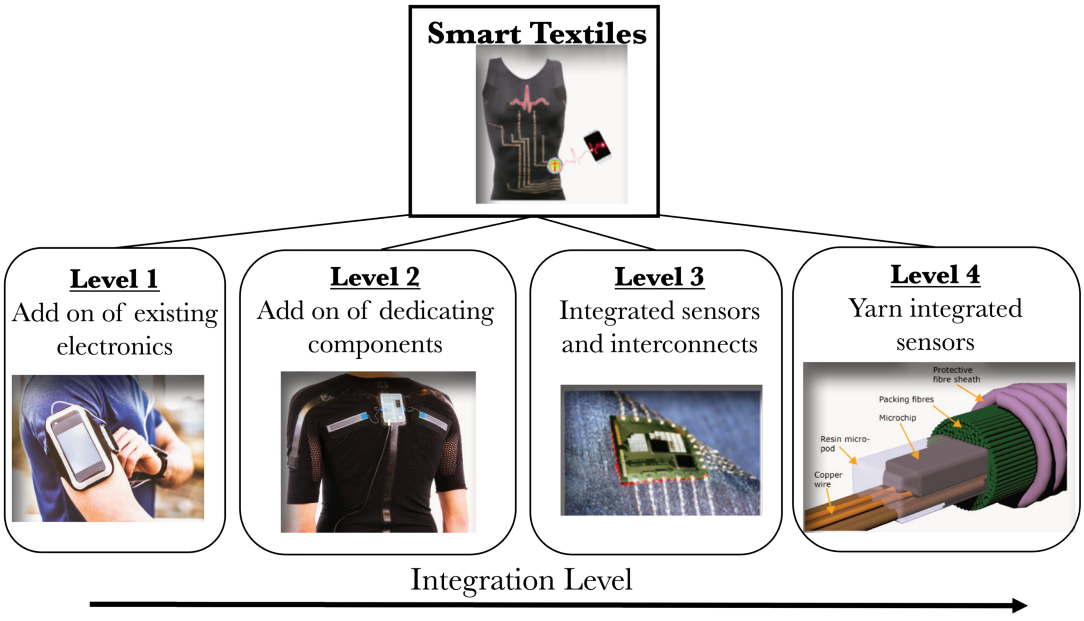


Figure 1.1 Smart textile applications.

1.2 Integration methods of smart functions into garments

The rapid advancement of electronic devices and textile manufacturing technologies has enabled smart garments to change from bulky, rigid systems into lightweight and portable clothing [6]. This transformation is achieved through the integration of electronics into textiles at four distinct levels, as shown in Figure 1.2 . At Level 1, smart textiles involve the addition of external electronic devices that do not require direct contact with the body. This includes snap-on sensors (such as heart rate or motion sensors) that attach via buttons or magnetic patches and can be easily removed for washing or maintenance [7]. Additionally, modular electronics, such as fitness trackers or health monitors, can be inserted into specialized pockets or sewn-in pouches within the fabric.

Level 2 represents a more integrated approach, where dedicated electronic components are embedded into textiles using conductive materials. These components are often incorporated using advanced textile manufacturing techniques such as knitting or weaving, allowing for improved durability and functionality. Although Levels 1 and 2 offer key advantages, including ease of use, versatility and cost-effectiveness, they can be bulky and uncomfortable during movement.

At Level 3, smart textiles advance further by integrating sensors and interconnects directly into the fabric structure. This allows for seamless electronic connectivity, improving flexibility, comfort, and durability without the need for external modules [8]. At this level, if one sensor fails, it cannot be easily separated or replaced without affecting the entire textile structure. Flexible substrates or laminations can also be part of Level 3; however, recyclability remains a major challenge because integrating electronic components into textiles creates hybrid materials that are difficult to separate into their original, recyclable parts [9].

Level 4 represents the most advanced integration and involves yarn-integrated sensors. In this approach, electronic properties are embedded directly at the fiber level. This results in a true integration of textiles and electronics, making garments inherently functional without sacrificing wearability [10]. Although promising for future applications, this approach currently remains at the laboratory scale. Scaling up remains a significant challenge, as flexible substrates can compromise breathability and potentially lead to skin irritation.

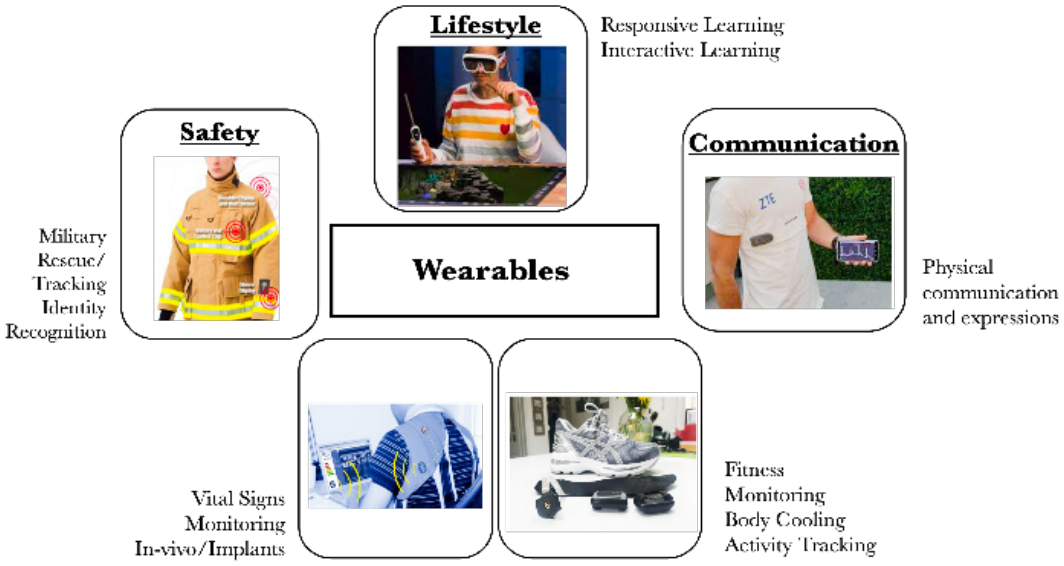


Figure 1.2 Attachment methods of smart functions into garment – Historical development of smart functions integration into textiles (Level 1: Acorn Health, Level 2 [11], Level 3 [12], Level 4 [13]).

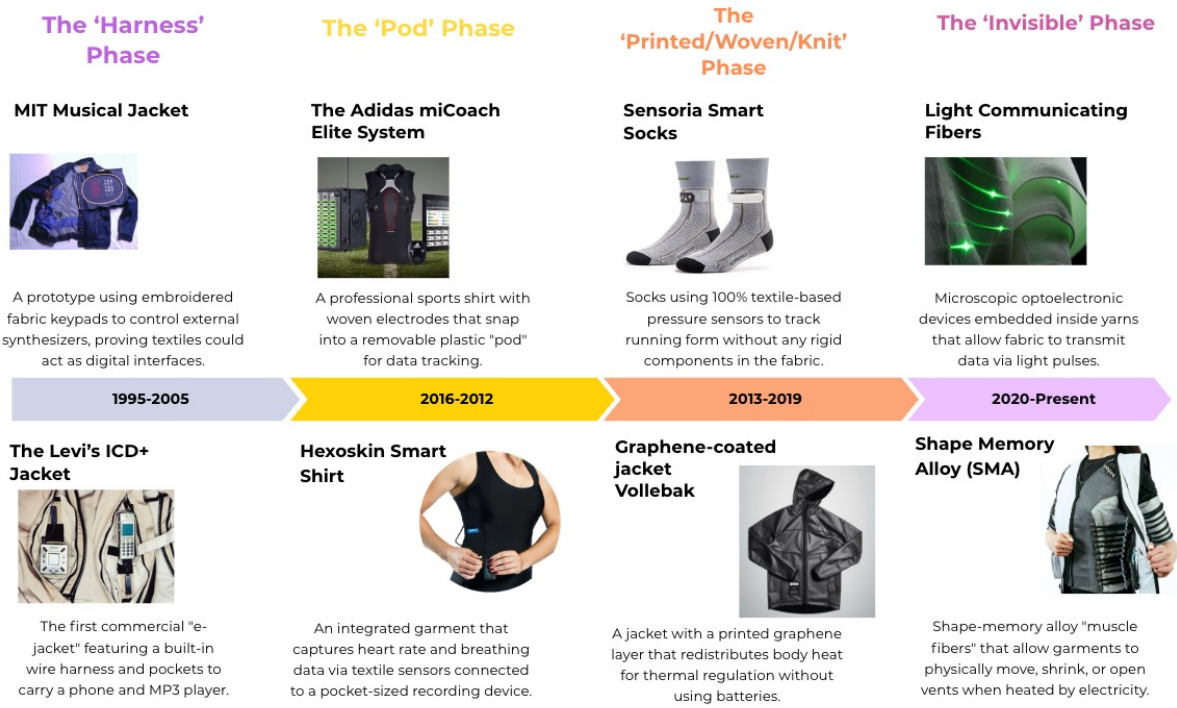


Figure 1.3 Historical progression of smart textile phases.

As shown in Figure 1.3, the evolution of smart textiles is categorized into four distinct technological phases that illustrate the progressive integration of electronics into fabric structures. The initial "Harness" Phase (1995–2005) utilized textiles as passive carriers for bulky hardware, often incorporating internal wire harnesses and dedicated pockets to accommodate external devices. This evolved into the "Pod" Phase (2006–2012), where sensors were integrated into the weave or knit but remained dependent on removable, rigid electronic modules for data processing. The subsequent "Printed/Woven/Knit" Phase (2013–2019) marked a shift toward seamless integration, employing functional materials like graphene coatings and conductive yarns to create 100% textile-based sensors. Currently, the "Invisible" Phase (2020–Present) represents the state-of-the-art, where optoelectronic devices and shape-memory alloys are embedded at the fiber level, allowing the textile to function autonomously as a communication or kinetic medium without visible electronic components.

Despite the significant advancements among these integration levels, several critical challenges remain that must be addressed to enable a high-level implementation of textile-based smart structures. One major challenge is ensuring reliability and robustness, as embedded electronics must withstand mechanical stresses such as bending, stretching and repeated use [14]. A second critical issue is the requirement for washability, which remains difficult to meet without compromising the functionality of integrated components [15]. Mass production and scalable integration of electronics into textiles also present significant issues, particularly in maintaining performance consistency across large volumes [16]. The lack of standardized testing methods and integration protocols hinders effective collaboration between the textile, electronics and information industries limiting progress toward fully commercialized smart garments.

One approach to addressing some of the challenges in smart textiles is the use of conductive yarns to form both sensors and interconnections between electronic components. Textile-based smart elements such as sensors, actuators and interconnections are typically composed of a combination of conductive and non-conductive yarns, which allows them to be seamlessly embedded into fabrics. The advantage of using textile-based sensors is that they can often be produced in a single manufacturing process, while still giving the feel of regular cloth-

ing with desirable properties like stretchability, washability and breathability. However, not all types of sensors have these qualities, for instance, optical sensors are harder to integrate into soft and washable fabrics, which makes their use more limited compared to resistive or capacitive textile-based alternatives. This emphasizes the importance of investigating textile-based structures capable of integrating functionality within the fabric itself to achieve both practicality and performance.

Textile-based smart structures present an approach which involves integrating sensors directly into the textile structure rather than attaching them as separate components. By utilizing commercially available materials, such as conductive yarns and employing standard textile manufacturing techniques, fabrics can be produced with embedded sensing or actuating capabilities. The functionality of these sensors and actuators relies on the integration of conductive and non-conductive yarns within the fabric. This method not only ensures seamless integration but also enhances durability and flexibility making textile-based sensors a promising solution for advancing smart textile applications. Conductive yarns stand out as a particular solution, which is why this thesis focuses on them in detail. The following section therefore discusses conductive yarns and the knitting techniques that enable their integration into smart textiles.

1.2.1 Conductive yarns and knitting for smart textiles

Conductive yarns are key functional elements for developing textile-based smart structures which allow sensors and actuators to be seamlessly integrated into textiles while preserving comfort and flexibility. Several types of conductive yarns are commonly used for textile-based smart structures each offering distinct advantages and limitations:

- Silver-coated nylon yarns: Flexible, washable and stable and widely used in wearable sensors.
- Stainless steel-based yarns: Strong and highly conductive, but prone to filament breakage, resulting in unstable signals.
- Hybrid yarns (polyester or cotton blended with metallic filaments): Provide a balance between conductivity, durability and comfort making them suitable for everyday wear.

Several methods are used to produce conductive yarns, including coating or plating fibers with metals or conductive polymers, blending conductive fibers with conventional ones, core-spun or twisted yarns with a conductive core, and printing conductive inks for patterned circuits. Key properties such as electrical conductivity, flexibility, mechanical strength and washability are critical for a good integration into textiles, ensuring the yarns withstand bending, tension, abrasion, and washing while remaining comfortable.

The performance of conductive yarns depends on several physical and electrical properties:

- Linear density (tex, dtex): A measure of yarn thickness that influences fabric elasticity, where tex represents the weight in grams per 1 kilometer of yarn and dtex (decitex) represents the weight in grams per 10 kilometers of yarn [17].
- Resistivity (Ω/m): The resistance affects the sensitivity in sensors and power consumption in actuators.

These roles demonstrate that conductive yarns are not just passive materials but active design elements that define the performance of smart knitted textiles. Their adaptability makes them important to developing textile-based smart structures. To fully leverage the properties of conductive yarns, an appropriate textile manufacturing technique is required and knitting provides the flexibility and structural control needed to develop effective wearable sensors.

Knitting is a textile manufacturing technique that forms fabrics by interloping yarns. Its inherent flexibility, stretchability and adaptability make it particularly suitable for making textile-based smart structures. The choice of knitting pattern and machine type plays a critical role in defining the mechanical and electrical properties of the fabric.

- The selection of the knitting pattern is important as it determines the mechanical and electrical properties of the fabric. In this study, rib and interlock patterns were employed due to their superior elasticity and dimensional stability. Rib and interlock structures provide excellent elasticity and dimensional stability, making them ideal for integrating sensor elements into wearable textiles.

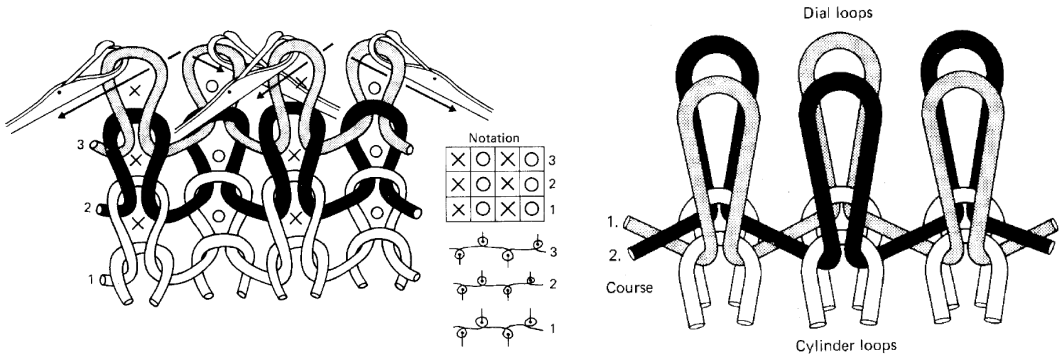


Figure 1.4 Interlock (left) and Rib (right) Structure [18].

- Knitted fabrics are characterized by their course and wale configuration as shown in Figure 1.5. A course is a row of loops running horizontally across the fabric. A wale is a column of loops running vertically along the length of the fabric.

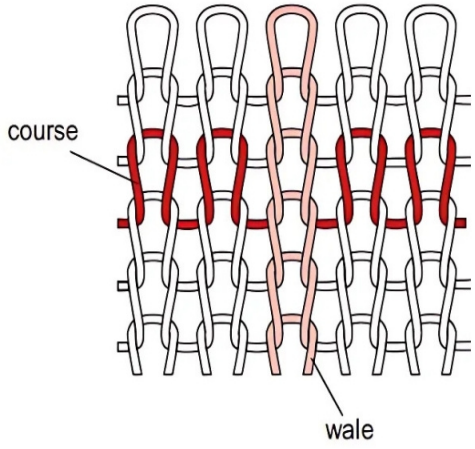


Figure 1.5 Course and wale direction in knit structure [19].

In textile engineering, selecting the appropriate knit architecture is a critical design parameter that dictates the mechanical and electrical performance of wearable sensors. Single jersey provides a thin, smooth substrate, whereas double jersey and Milano rib offer the dimensional stability required to maintain structural integrity.

Furthermore, the high elasticity and recovery of rib structures make them the ideal architecture for responsive strain gauges used in kinematic monitoring. Finally, specialized patterns like Garter, Seed and Tuck knit designs as shown in Figure 1.6 further expand functionality by providing structural cushioning or housing bulky components without increasing overall garment stiffness. A detailed representation of loop formation can also be seen at Figure 1.7.

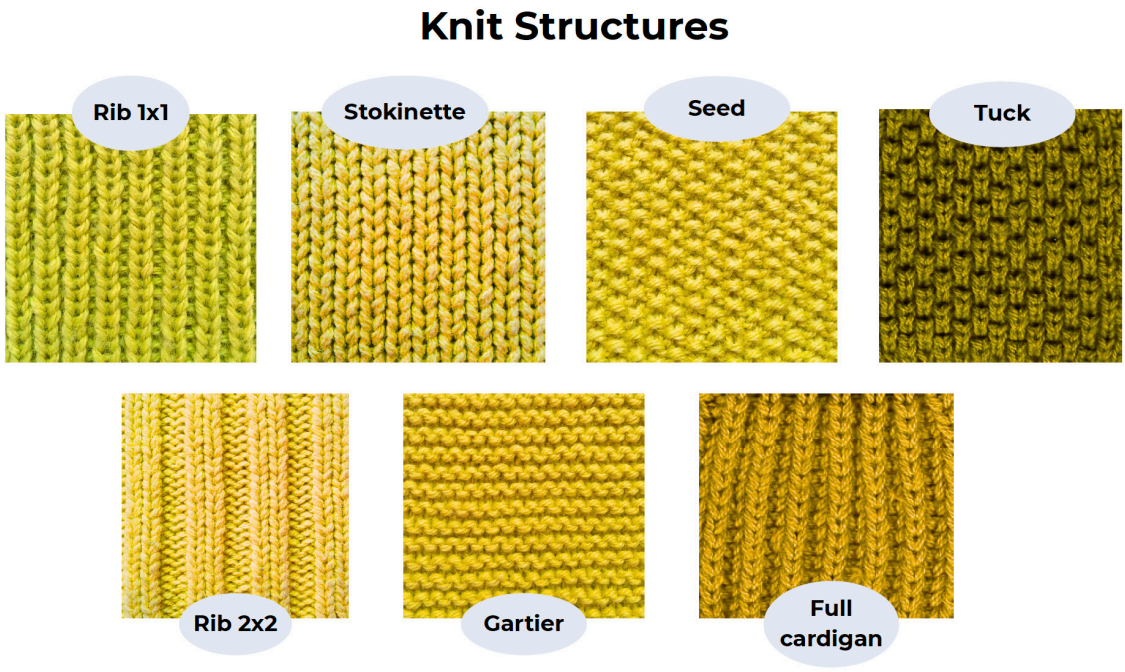


Figure 1.6 Understanding knit fabric textures: From basic rib to complex cardigans.

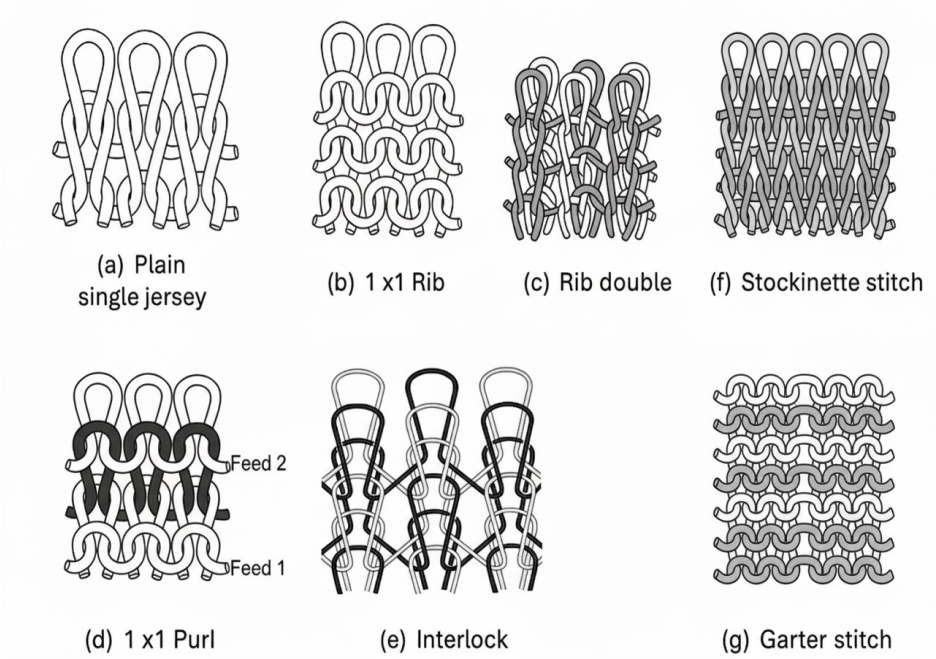


Figure 1.7 An overview of fundamental knit types.

Knitting can be performed using different knitting machines, each offering unique advantages. Flat knitting machines can produce flat fabrics with precise control over the pattern. Circular knitting machines produce tubular fabrics continuously and are ideal for high-speed production. In this thesis, a STOLL flatbed knitting machine as shown in Figure 1.8 was used to produce the smart structures.

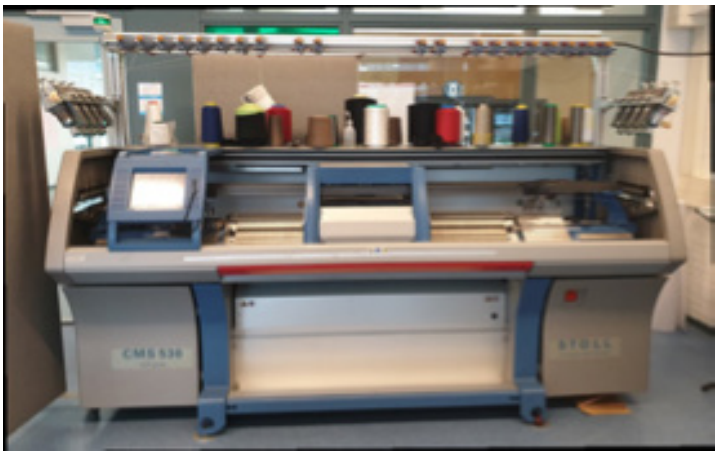


Figure 1.8 Flatbed Stoll CMS 530 knitting machine.

1.3 Textile-based sensors and actuators

With conductive yarns integrated through knitting, the fabrics can be equipped with a variety of sensing and actuating functions to make fully functional smart garments. Textile-based sensors play a promising role in the development of smart fabrics, enabling real-time monitoring and responsive functionalities in various applications. Textile-based sensors can be classified into several types based on their sensing mechanisms, including strain sensors [20], pressure sensors [21], textile electrodes [22] and chemical sensors [23]. Strain sensors often made using conductive polymers, graphene, or carbon nanotubes, detect mechanical deformations such as stretching and bending, making them ideal for applications in posture monitoring, motion tracking and rehabilitation.

Textile-based strain sensors work by converting mechanical deformation of fabrics into electrical signals, typically through piezoresistive, capacitive or optical mechanisms. Knitted structures are particularly suitable for strain sensing, as their inherent elasticity allows resistance to change under mechanical stretch. The performance of these sensors has been systematically evaluated in both knitted and stitched structures, demonstrating the influence of textile architecture on sensitivity, working range, and durability [24]. Furthermore, the integration or coating of conductive materials such as carbon nanotubes, graphene, and PEDOT:PSS can further enhance their sensitivity and durability [25]. Stoppa and Chiolerio also emphasize that textile strain sensors offer excellent flexibility and wearability, making them suitable for smart textiles supporting motion tracking, gait analysis, rehabilitation monitoring, and respiratory measurements [26].

Textile-based pressure sensors rely on piezoresistive or capacitive mechanisms, where applied force alters the electrical properties of conductive textile layers; Atalay et al. demonstrated that 3D-knitted structures are highly effective for mapping distributed pressure in wearable systems [20]. They offer high sensitivity and conformability to complex surfaces. This makes them suitable for integration into garments for real-time pressure monitoring in healthcare, sports, and human–machine interface applications. Bioelectrical sensors made from conductive fabrics or embroidered electrodes allow long-term measurement of ECG, EMG, and EEG without gels; Ankhili et al. showed that textile electrodes significantly improve comfort and suitability for daily use [27]. Chemical textile sensors incorporate electrochemical materials to detect a wide range of physiological and environmental indicators. These sensors can be engineered to monitor parameters such as sweat composition, gases, humidity, and pH, enabling applications in healthcare and sports performance [28].

By taking the textile structure itself as the starting point, functional actuating elements can be created by

adapting how conductive yarns are incorporated into the fabric. Through integration and variation of knitting patterns, these conductive pathways enable the textile to perform actuation functions such as localized heating. Since these conductive elements form an intrinsic part of the knitted structure, they share the same advantages as knitted sensors—flexibility, stretchability, and breathability while providing actuation capabilities without compromising comfort, softness or overall wearability. Knitted heaters exemplify this approach, delivering uniform and controllable thermal output while remaining fully textile-like and seamlessly wearable.

1.3.1 Challenges and research gaps in the development of knitted sensors

While textile sensors and actuators demonstrate the advantages of integrating conductive yarns into textile structures, the implementation of knitted sensors presents additional challenges due to their complex mechanical and electrical behavior. Knitted sensors show nonlinear, anisotropic and hysteretic mechanical behavior due to loop deformation mechanics, which makes their strain–resistance relationship difficult to model [26]. Large hysteresis during repeated stretching and releasing is common, and a drift often happens after wear or washing cycles [20]. These characteristics reduce stability and limit long-term sensing accuracy. Electrical output varies substantially with yarn composition, knit pattern and environmental conditions. Conductive yarn blends, stitch density, and knit geometry strongly influence resistance pathways [29]. Humidity and temperature further affect conductivity, making stable electrical performance under high strain difficult to maintain. This variability complicates sensor reliability. Wearability demands that knitted sensors remain soft, flexible, skin-safe, and washable, but many conductive materials compromise durability. Metal-coated fibers may break, and conductive polymer coatings can degrade due to abrasion or sweat. This degradation reduces both electrical stability and long-term comfort, causing a major obstacle for real-world implementations [30]. Knitted sensors respond to multiple deformation modes, causing unwanted signals, drift and cross-sensitivity between stretch, pressure and bending inputs [24]. Interpreting these signals requires advanced filtering and modelling.

To ensure that the sensors remain fully textile-based, additional electronic units such as microprocessors and power modules can be positioned away from the sensing areas. For example, these units can be located on the back, within a pocket, or in other areas that minimize discomfort while maintaining garment functionality. This approach allows the integration of necessary control and power components without compromising the flexibility, wearability, or washability of the smart textile.

This thesis focuses on developing textile-based smart elements using conductive yarns, with knitting as the primary manufacturing technique. The aim is to construct soft, textile-based sensors and actuators by integrating conductive yarns into the textile structure. This approach builds on the fabric architecture to produce functional, stretchable, breathable, and washable smart elements suitable for practical applications.

While these challenges are well recognized, there remains a lack of systematic understanding of how textile parameters such as knit geometry, yarn selection, and structural density influence electromechanical behavior. In particular, the underlying mechanisms governing hysteresis, nonlinearity, and signal instability are not yet fully linked to design parameters. This limits the ability to derive generalizable design rules for textile-based sensors.

1.4 Research questions

This study is structured around key research questions aimed at understanding, developing and evaluating textile-based smart systems.

RQ1: How can knitted textile structures be engineered to make functional sensors and actuators?

RQ2: What are the fundamental relationships between knit structure, yarn properties (elasticity, conductivity) and the electromechanical performance of knitted devices?

RQ3: What applications are possible with knitted sensors?

By addressing these questions, this study aims to find design rules and material choices that help make knitted sensors and actuators work well. The results will help us understand how textile structures and yarn properties affect performance. They will also provide practical ideas for creating useful applications, such as health-monitoring clothes, wearable interfaces, soft robots or interactive garments

1.5 Thesis Outline

The thesis is organized into six chapters as shown in Figure 1.9, starting with the research objectives and outline in Chapter 1. Chapter 2 presents the design and optimization of knitted strain sensors, focusing on material selection, knitting structures, and sensor configuration. Chapter 3 extends this work by integrating the developed strain sensors into finger-worn wearable devices and evaluating their performance for rehabilitation and movement monitoring. Chapter 4 investigates knitted pressure sensors, examining how geometry, knit structure, and conductive fillers influence pressure sensitivity and usability. Chapter 5 introduces a physics-based modelling for knitted textile heaters and analyses how design parameters affect heating performance and uniformity. Finally, Chapter 6 summarizes the key findings, addresses the research questions and provides a discussion of challenges and future perspectives in smart textile technologies.

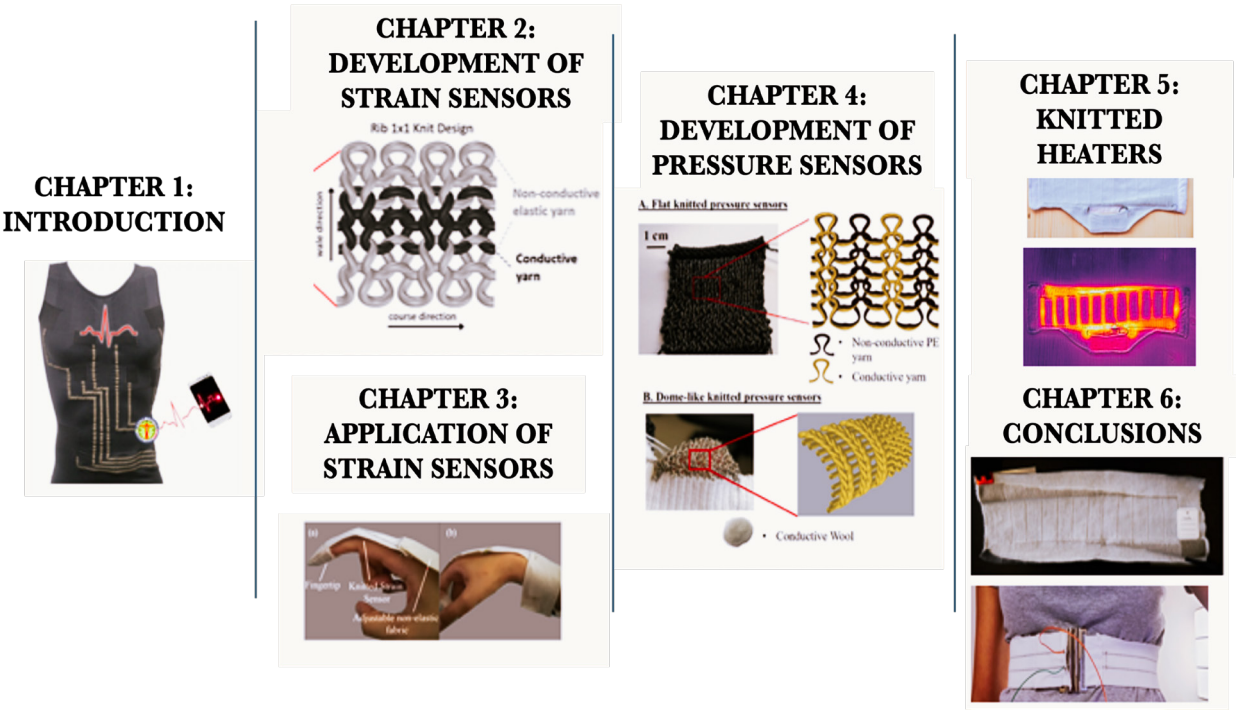


Figure 1.9 Thesis outline.

References

1. Asha Banu, S.M. and K. Meena Alias Jeyanthi, Textile based antenna design for breast cancer detection. Materials Today: Proceedings, 2022. 62: p. 4814-4820.
2. White, P., et al., The Energy Harvesting Performance of a Flexible Triboelectric-Based Electrospun PTFE/PVDF Fibre. Engineering Proceedings, 2023. 30(1): p. 8.
3. Verma, S., et al., Recent Advances for Fabricating Smart Electromagnetic Interference Shielding Textile: A Comprehensive Review. Electronic Materials Letters, 2022. 18(4): p. 331-344.
4. Hatamie, A., et al., Review—Textile Based Chemical and Physical Sensors for Healthcare Monitoring. Journal of The Electrochemical Society, 2020. 167(3).
5. Saidi, A., et al., Advanced Functional Materials for Intelligent Thermoregulation in Personal Protective Equipment. Polymers (Basel), 2021. 13(21).
6. Stoppa, M. and A. Chiolerio, Wearable electronics and smart textiles: a critical review. Sensors (Basel), 2014. 14(7): p. 11957-92.
7. Chen, S.J., et al., A Modular Textile Antenna Design Using Snap-on Buttons for Wearable Applications. IEEE Transactions on Antennas and Propagation, 2016. 64(3): p. 894-903.
8. Tseghai, G.B., et al., Integration of Conductive Materials with Textile Structures, an Overview. Sensors (Basel), 2020. 20(23).
9. Skrzetuska, E. and P. Rzezniczak, Circularity of Smart Products and Textiles Containing Flexible Electronics: Challenges, Opportunities, and Future Directions. Sensors (Basel), 2025. 25(6).
10. Aziz, S., et al., Fast and High-Strain Electrochemically Driven Yarn Actuators in Twisted and Coiled Configurations. Advanced Functional Materials, 2020. 31(10).
11. SmartShirt: Optimising athletic performance through human motion data; Available from: https://elitacwearables.com/projects/smarshirt/.
12. Linz, T., et al., Embroidering electrical interconnects with conductive yarn for the integration of flexible electronic modules into fabric, in Ninth IEEE International Symposium on Wearable Computers (ISWC'05). 2005. p. 86-89.
13. Satharasinghe, A.S., Development of solar energy harvesting textiles. 2019, Nottingham Trent University.
14. Shak Sadi, M. and E. Kumpikaite, Advances in the Robustness of Wearable Electronic Textiles: Strategies, Stability, Washability and Perspective. Nanomaterials (Basel), 2022. 12(12).
15. Rotzler, S., M.v. Krshiwoblozki, and M. Schneider-Ramelow, Washability of e-textiles: current testing practices and the need for standardization. Textile Research Journal, 2021. 91(19-20): p. 2401-2417.
16. Zhu, J. and H.-L. Kao, Scaling E-Textile Production: Understanding the Challenges of Soft Wearable Production for Individual Creators, in Proceedings of the 2022 ACM International Symposium on Wearable Computers. 2022. p. 94-99.
17. ISO, ISO 1144:2016, Textiles — Universal system for designating linear density (Tex System). 2016.
18. Spencer, D.J., Knitting Technology. Third ed. 2001.
19. Available from: https://mypacklove.com/blog/patches/what-are-wales-in-knit-fabric-simple-guide/?srsltid=AfmBOor-Nv8BOCG5Czt4JGdddEBoTr_MnZ2YJ-X_13JlT_bh6P_BnKFw.
20. Atalay, O., Kennon, W. R., & Husain, M. D., Textile-Based Weft Knitted Strain Sensors: Effect of Fabric

Parameters on Sensor Properties. Sensors, 2017.

21. Kamara, V., Kargwal, S. K., Constant, N., Gordon, R., Humphreys, G., & Mankodiya, K., A comparative characterization of smart textile pressure sensors. IEEE Engineering in Medicine and Biology Society (EMBC), 2019: p. 1745-1748.

22. Blachowicz, T., Ehrmann, G., & Ehrmann, A., Textile-based sensors for biosignal detection and monitoring. Sensors, 2021. 21(8): p. 6042.

23. Gualandi, I., Tessarolo, M., Mariani, F., Possanzini, L., Scavetta, E., & Fraboni, B., Textile chemical sensors based on conductive polymers for the analysis of sweat. Polymers, 2021. 13(6): p. 894.

24. Jansen, K.M., Performance evaluation of knitted and stitched textile strain sensors. Sensors, 2020. 20(24): p. 7236.

25. Jia, Y., Shen, L., Liu, J., Zhou, W., Du, Y., Xu, J., & Jiang, F., An efficient PEDOT-coated textile for wearable thermoelectric generators and strain sensors. Journal of Materials Chemistry C, 2019. 7(12): p. 3496-3502.

26. Stoppa, M., & Chiolerio, A, Wearable Electronics and Smart Textiles: A Critical Review. Sensors, 2014. 14: p. 11957–11992.

27. Ankhili, A., Tao, X., Cochrane, C., Koncar, V., Coulon, D., & Tarlet, J. M., Comparative study on conductive knitted fabric electrodes for long-term electrocardiography monitoring: silver-plated and PEDOT: PSS coated fabrics. Sensors, 2018. 18(11): p. 3890.

28. Li, S., Li, H., Lu, Y., Zhou, M., Jiang, S., Du, X., & Guo, C, Advanced textile-based wearable biosensors for healthcare monitoring. Biosensors, 2023. 13(10): p. 909.

29. Kim, Y.-H., Jun, J., Oh, Y.-K., Choi, H.-J., Lee, M.-J., Assessing the role of yarn placement in plated knit strain sensors: A detailed study of their electromechanical properties. Sensors, 2024.

30. M. Krshiwoblozki, S.R., Investigation of the functional ageing of conductive coated fabrics under simulated washing conditions. Materials, 2023.

Chapter 2

2. Development of knitted strain sensors and their performance evaluation

While the previous chapter outlined the motivation and background for smart textiles, this chapter focuses on the development and experimental evaluation of knitted strain sensors. It examines how material choice, knitting structures and sensor configurations influence performance metrics such as sensitivity, working range and hysteresis in wearable applications.[1]

In recent years, knitted strain sensors have been developed that aim to achieve reliable sensing and high wearability, but they are associated with difficulties due to high hysteresis and low gauge factor (GF) values. This study investigated the electromechanical performance of the weft-knitted strain sensors with a systematic approach to achieve reliable knitted sensors. For two elastic yarn types, six conductive yarns with different resistivities, the knitting density as well as the number of conductive courses were considered as variables in the study. We focused on the 1x1 rib structure and in the sensing areas co-knit the conductive and elastic yarns and observed that positioning the conductive yarns at the inside was crucial for obtaining sensors with low hysteresis values. We show that using this technique and varying the knitting density, linear sensors with a working range up to 40% with low hysteresis can be obtained. In addition, using this technique and varying the knitting density, linear sensors with a working range up to 40% strain, hysteresis values as low as 0.03, and GFs varying between 0 and 1.19 can be achieved.

1 *This chapter is based on the following publication: Bozali, Beyza; Ghodrat, Sepideh; Plaude, Linda; van Dam, Joris J. F.; and Jansen, Kaspar M. B. "Development of low hysteresis, linear weft-knitted strain sensors for smart textile applications." Sensors 22, no. 19 (2022): 7688.*

With the recent interest in wearable technology, it has become increasingly important to have textile-based sensors that can be a potential platform for future applications and products. Textile-based sensors are essential components of wearable technology due to their flexibility, breathability and ease of application, and therefore can be used in many different applications, such as monitoring heart rate, pulse and other health signals [1], generating human-machine interface systems [2] and producing textile-based systems for electromagnetic interference shielding (EMI) purposes [3]. Textiles with embedded strain sensors can measure local movements of body parts and can be used to monitor posture and limb locomotion but also e.g., respiration. Related applications include sensor gloves and VR suits as well as elbow and knee revalidation aids and sensory compression garments.

A strain sensor is an electronic device that produces an electrical signal in response to mechanical deformation [4]. Typical strain sensors used for engineering purposes consist of thin metal layers on a polyimide substrate and have a working range which is limited to about 1%. Those types of sensors are therefore inadequate to detect movements of the skin or the clothing layer attached to it which may range up to 40% [5]. Textile-based strain sensors offer a new generation of devices that combine strain sensing functionality with wearability, lightness and high stretchability. They can be comfortably worn and sense a wide range of body strains for a vast number of applications.

Textile-based strain sensors can be produced with standard textile manufacturing methods such as knitting [6], embroidering [7], or stitching [8]. For stitched and embroidered sensors, the response of sensors is determined by the stitch structure and as well as the base fabric characteristics, and therefore the elastic response of the substrate is critical to achieving reliable sensors. Knitted structures are good candidates for designing flexible strain sensors thanks to their high stretch recovery and good stretchability characteristics [9]. The main advantage of knitted sensors is that they can be manufactured at low costs in mass production with existing textile equipment and readily available yarns. In addition, the sensors will be washable, breathable, and stretchable while having a fully textile appearance.

The basic working principle of knitted strain sensors can be explained by loops of conductive yarn embedded in overlapping and adjacent rows. During stretching, the points of contact alter, causing the overall resistance to change. This resistance change is reproducible, and if large enough, it can be used as a sensor signal [10]. The human skin typically deforms up to 40% [11] which thus defines the desired upper limit of body strain sensors [12]. For breathing rate measurements, the strains are in the order of 5%. A useful knitted sensor should thus ideally have a working range up to 40% and a resolution of about 1%. In addition, strain sensors for on-body monitoring should be linear and have negligible hysteresis.

The performance of knitted strain sensors is affected by two parameters, one is the material type, and the other is the knitting structure. Considering the material type, the effect of elastic or conductive yarns on sensor performance comes to the fore. The embedded structure in a knitted sensor must be highly elastic as it determines the effects of time lag and hysteresis and this elasticity is provided by elastic yarns containing lycra or elastane [13, 14]. A study by Atalay pointed out that the properties of elastomeric yarn had a significant impact on the performance of the sensor [10]. In addition, the use of covered elastic yarn instead of bare elastic yarns has resulted in higher sensitivity [15]. Conductive materials are another important determinant of sensor performance. Metallic yarns such as stainless steel-based conductive yarns showed an unstable performance in many studies which was attributed to shortcuts caused by loose yarn filaments. On the other

hand, yarns consisting of stainless-steel fibers blended with cotton appeared to show improved performance with better sensitivity than sensors knitted with commercial metalized polyamide multifilament yarn due to more stable contact resistance [16]. In contrast to metallic yarns, silver-based nylon yarns show stable electromechanical performance. Although silver-based nylon yarns can produce high sensitivity sensors, the hysteresis values of the sensors can vary from structure to structure and remains a challenge to optimize for reliable sensors. Liang et al. also remark that a promising way to reduce hysteresis is to use Eeontex in the sensor base structure [14]. The resistivities of the currently available conductive yarns vary widely, and the study of Raji et al. [17] seems to suggest that sensors with conductive yarn with a resistance of 77 ohm/cm have an optimum GF in the resistance range of 40 to 120 ohms, but the effect was not studied in detail [18]. The type of knit design is another essential parameter that affects the sensor performance, and many different studies to investigate the effect on sensor performance were reported. One is a single jersey knit strain sensor, developed by adding float and crimp stitches to a structure knit that appears to be suffering from relatively large hysteresis effects [19]. Interlock structures knitted with conductive yarns show a good sensor performance having a gauge factor (GF) value of 3.5 at between a 10–40% working range. In the case of 1x1 rib knitted samples, the effect of the aspect ratio and shape of the sensing region was evaluated by Raji et al. and they concluded that plain rectangular sensors showed higher repeatability and lower noise levels compared to non-rectangular shaped sensors [15]. A 1x1 rib knit design was found to be promising as a strain sensor and presented a sensor with a GF of 1.36 and a working range of 0–21% by Chia et al. [20].

Various materials and methods have been reported for the design of knitted strain sensors, but these sensors have so far lacked reliability, linearity, and low hysteresis. In our effort to develop improved sensors, we use the findings of previous studies—summarized below—as a starting point.

- Stainless steel-based conductive yarns are less suitable for strain sensors because of the relatively high noise levels associated with knitted sensors and silver coated nylon yarns should be preferred accordingly [16, 21].
- Next, the base fabric in which the sensor yarns are embedded needs to be fully elastic. If not, the sensor will not respond elastically and will be prone to show time lag and hysteresis effects [14].
- Rib structures as knit design allow for stretching abilities up to 100% and are therefore potential strong candidates for knitted strain sensors [17].
- Sensors should preferably be rectangular with aspect rations between 24:1 to 77:1 [17].

In the current paper, we take these conclusions as a starting point and report a systematic study on the performance of knitted strain sensors to develop reliable strain sensors with high sensitivity, wide working range and low hysteresis. We do this by manufacturing a series of sensors with the elastic and conductive yarn types as variables, the number of conductive courses, the knit density, and the conductive yarn position in a co-knitted configuration. The electromechanical performance is evaluated by determining the initial resistance, sensitivity, working range and hysteresis for all knitted sensors. Based on these sensor constructions, knitted sensors with minimum hysteresis, maximum sensitivity and working range are selected and evaluated.

2.1 Materials and Methods

Based on the above-mentioned observations from the literature, the following initial choices are made: (i) A rectangular sensor area consisting of a number of parallel conductive courses, (ii) A 1x1 rib knit design, (iii) Silver-coated or plated nylon as the conductive yarn, and (iv) Elastic yarn with as high elastic recovery as possible. As elastic yarns, we used the ones provided by Yeoman (Nm 13, 81% Nylon and 19% Lycra) and Uppingham (Nm 11, 83.26% Nylon and 16.74% Lycra). As conductive yarns, six different silver-coated nylon yarns with various resistivities from Amann Threads UK Ltd. (Ashton-under-Lyne, UK) and Shieldex, Statex Productions- and Sales GmbH (Bremen, Germany) were selected (See the optical images of the conductive yarns in Figure S1 in the Supporting Information). The property details and related coding of these yarns are listed in Table 2.1.

Table 2.1 Conductive yarn details and related properties.

Composition	Coding	Linear Density (Dtex*)	Resistivity (Ω /m)	Manufacturer
Siver-coated polyamide/ polyester hybrid yarn	A1	960	85	Amann
	A2	620	150	
	A3	280	530	
Silver plated polyamide 6 yarn	S1	235	600	Shieldex
	S2	117	1500	
	S3	78	3500	

*The weight per 10000 m (dtex) reflects the yarn thickness

In weft knitted fabrics, the horizontal row of continuously connected loops is called a course, whereas the series of loops that intermeshes vertically is known as wales, as illustrated in Figure 2.1.a. In this study, knitted strain sensors have been produced on a Stoll CMS 530 flatbed knitting machine with a gauge of E8. An 1x1 rib knit structure was chosen for all samples. The conductive yarn is co-knitted with a non-conductive elastic yarn using a yarn carrier with two eyelets as shown in Figure 2.1b. In that way, the position of the conductive yarn with respect to the elastic support yarn is well controlled, resulting in a rib structure in which the conductive yarn is always on the inside or always on the outside. To enhance the elasticity, the base fabric was also manufactured with two parallel elastic yarns. All sensor samples have outer dimensions of approximately 14.5x7 cm. The size of the conductive area changes according to the number of conductive courses, which varied between 1 to 5.

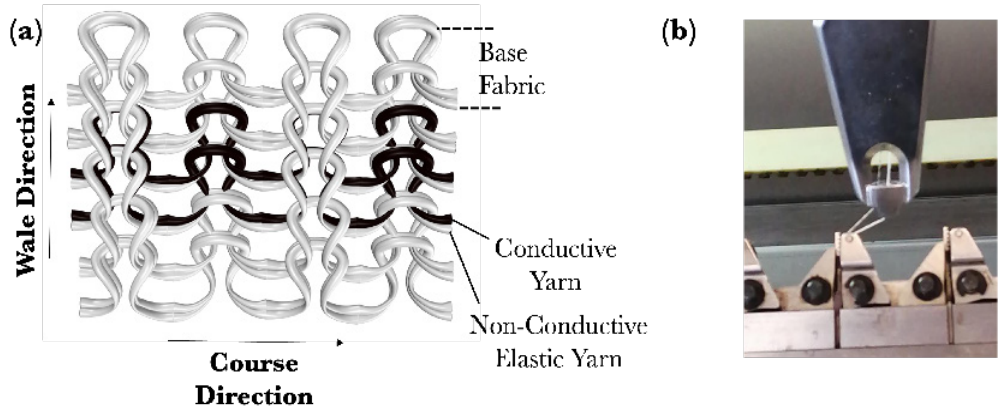


Figure 2.1 (a) Co-knitted 1 × 1 rib structure with two conductive yarn courses (indicated in black) and non-conductive yarns (white), and (b) a yarn carrier containing two parallel yarns.

Knitted strain sensors were prepared with the parameters listed in Table 2.2. The conductive course number was varied between 1 to 5, and knit densities were varied by selecting NP numbers between 6 to 15. The NP value is related to the needle pitch distance. The position of the conductive yarn is referred to as conductive outside (CO) and conductive inside (CI), respectively. This will be discussed in detail later (as shown in Supporting Information Figure S2).

Table 2.2 Parameters of knitted strain sensors tested in the study.

Parameters	Variations
NP number	6, 7, 8, 9, 10, 12 and 15
Conductive yarn type	Shieldex (S1, S2, S3) and Amann (A1, A2, A3)
Elastic yarn type	Yeoman (E1) and Upphingham (E2)
Configuration of the conductive yarn	Inside (CI) and Outside (CO)

In this paper, knitted samples will be coded as $NP_xY_xC_xE_x$ following all the parameters listed in the Table 2.2. As an example, $NP_{10}Y_{S1}C_2E_1$ can be interpreted as the sample knitted with a NP setting of 10 and with two conductive courses using S_1 conductive and E_1 elastic yarns, respectively.

2.2 Resistance-Strain Testing Procedure

The electromechanical properties of the knitted strain sensors were investigated by measuring the changes in resistance during cyclic tensile tests in which the sample was subsequently loaded and unloaded. A custom-made tensile tester with a 1000 N load cell was used to generate a cyclic stretching between 0–40% at a constant speed of 30 mm/min as depicted in Figure 2.2. The samples were stretched in the course direction. Preliminary testing showed that test speed did not have a large effect on the performance in terms of sensitivity and working range in Table S1 (See Supporting Information). The initial length of the samples known as the gauge length was set at 50 mm. All tests were conducted in standard atmospheric conditions. The resistances were measured using a 4-point probe method in which a constant current value of 0.3 mA was applied to the outer red clamps in Figure 2.2. The resulting voltage drop was read from the inner dark green electrodes and stored in a data acquisition system. The resistance values were calculated as the ratio between measured voltage and current values. Mechanical clamps with conductive Velcro tape were used to clamp the samples and provide the electrical connection.

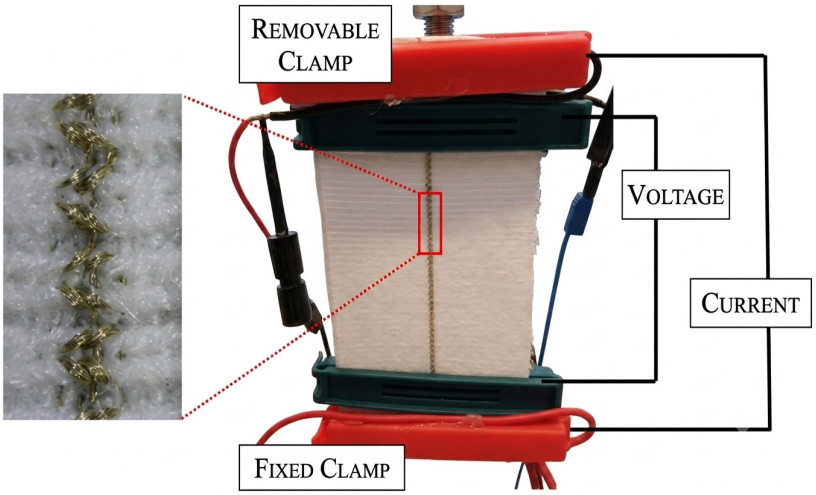


Figure 2.2 Test setup with an attached knitted strain sensor and four-point probe connections.

2.3 Electromechanical Properties

The electromechanical properties such as Gauge Factor (GF), working range (WR) and hysteresis were investigated to analyse the performance of the knitted sensors. During the stretching of sensors, the resistance does not always change monotonically. Thus, not all parts of the recorded resistance changes are suitable to indicate the sensor performance. We define the working range as the region in which the resistance changes monotonically. The onset and end of the working range are referred to and , respectively (see Figure 2.3a. The WR is then defined as (Equation (1));

$$\text{Working Range (WR)} = \varepsilon_{max} - \varepsilon_{min} \quad (1)$$

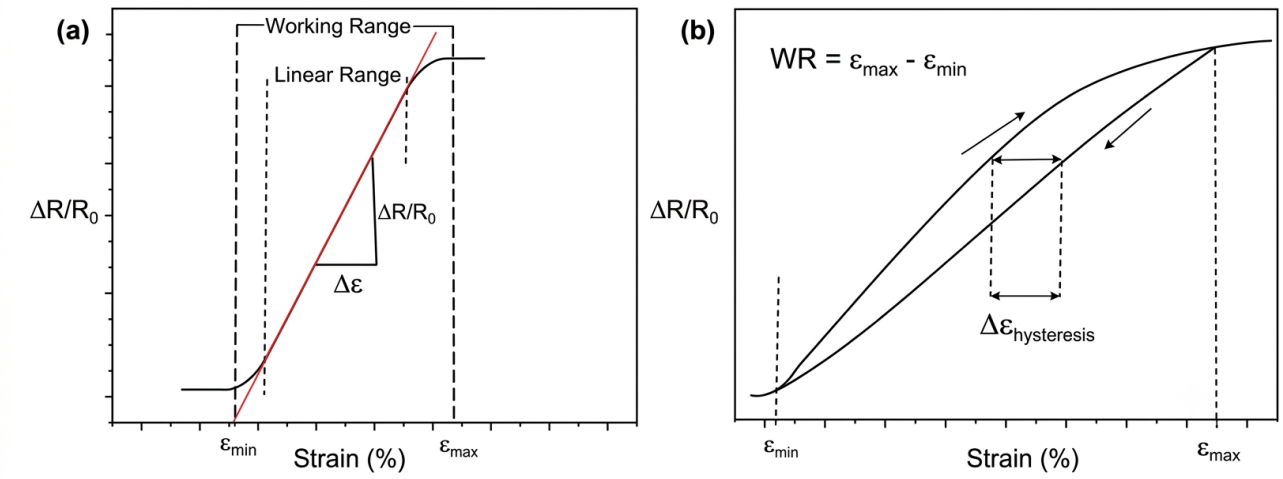


Figure 2.3 (a) A graph showing how to calculate the gauge factor and working range, and (b) A graph showing how to calculate the resistance hysteresis (Black arrows represent the loading and unloading during a cycle)

The GF or sensitivity is defined as the slope of the linear range of the relative resistance change versus the applied strain graph as can be seen in Figure 2.3a. Equation (2) shows the formula for the gauge factor in which $\Delta R = R_{Stretched} - R_0$, R_0 is the initial resistance, and $\Delta\varepsilon$ is the strain change within the linear region of the curve.

$$\text{Gauge Factor (GF)} = ((\Delta R/R_0))/\Delta\varepsilon, \quad (2)$$

Hysteresis values can be calculated along the resistance axis (vertical) or along the strain axis (horizontal), and these values will be referred to as resistance hysteresis and strain hysteresis, respectively [18]. For a strain gauge in an application, the expected errors in the measured strain are of primary concern; thus, as a performance indicator, we prefer to use the strain hysteresis values and not the more commonly reported resistance hysteresis [22, 23]. When the maximum strain in a loading cycle increase, it is evident that the hysteresis also increases. Since we prefer the hysteresis values not to depend too much on the loading conditions, we choose to scale the hysteresis with the working range as shown in Equation (3) and Figure 2.3b. The hysteresis strain, can be defined as the maximum difference between loading and unloading strain as shown in Figure 2.3b.

$$H_\varepsilon = (\Delta\varepsilon_{hysteresis})/WR, \quad (3)$$

2.4 Results

2.4.1 Electromechanical Performance Analysis of a Knitted Strain Sensor

As a first example, we discuss the NP_{10} knitted sample test as shown in Figure 2.4.

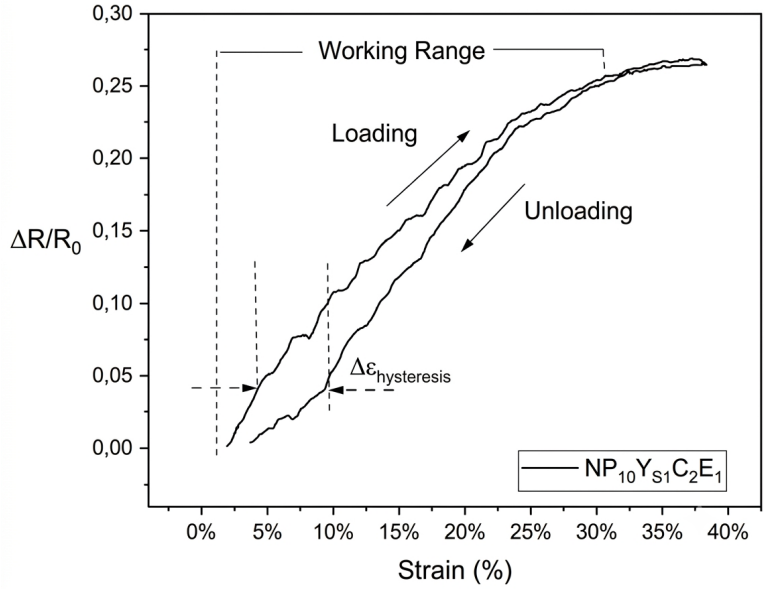


Figure 2.4 Relative resistance change versus strain plot of knitted strain sensor type $NP_{10}Y_{S1}C_2E_1$.

During stretching up to 40%, the relative resistance of the sample changes from 0 to a value of 26%. The last part of the stretching curve shows that the amount of increase in the resistance gradually decreases. During the first part of the unloading curve, the resistance roughly follows the curve of the loading cycle, but deviations start below about a 20% strain, leading to hysteresis. At the end of the unloading cycle, the resistance change approaches nearly its starting value. For this experiment, the working range, gauge factor and hysteresis are determined as WR = 0–27%, GF = 0.89 ± 0.06, and H = 0.07, respectively.

Knitted sensors were fabricated by making conductive/elastic yarn combinations. Knitted sensors without elastic support yarn were also investigated to better understand the effect of using elastic yarn as a co-knit yarn in the sensing region. The results showed that the sample without the co-knitted elastic yarn had a nearly strain-independent resistance where GF was close to 0.1, which is shown in Figure S3 in the Supporting Information. A gauge factor below zero means that the resistance drops when the sample is stretched. Configurations with gauge factors close to zero may prove useful as stretchable interconnects in knitted textile circuits.

2.4.2 The Effect of Knit Density (NP Number) on the Sensor Performance

Knitted densities are determined by the NP numbers. A higher NP number results in less dense fabric structures, while lower NPs result in denser fabrics. Optical images of the $NP_xY_{S1}C_2E_1$ series are shown in Figure 2.5. Areal densities (g/m^2) of the knitted fabrics are calculated using Equation (4) in which YL is the yarn length in a knit design (mm), LD denotes the linear density in Tex, WS is the wale spacing in mm, CS the course spacing in mm, S_h: horizontal size, and S_v: vertical size [24]. The yarn length was determined by unravelling the course of the fabric and measuring the distance when stretched.

$$\text{Areal Density} = (YL \times LD)/(WS \times S \times S_h \times S_v) \quad (4)$$

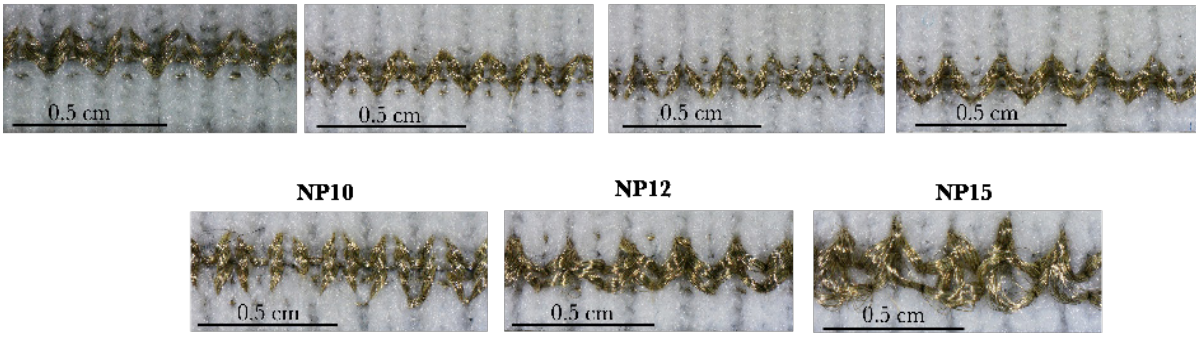


Figure 2.5 The optical images of knitted strain sensors of the series of $NP_xY_{S1}C_2E_1$.

The optical images show that, when the NP number increases, the samples become looser and less dense, an observation which is conformed by the decrease in areal density in relation to the NP numbers as can be seen in Table 2.3. Accordingly, the conductive yarns in the sensing area do not fully integrate into the structure when the NP numbers increase from NP_{10} to NP_{15}, which could play an active role in the sensor performance in terms of the elastic recovery.

Table 2.3 The areal density and elastic modulus of the knitted sample series of $NP_xY_{S1}C_2E_1$.

NPs	Areal Density (g/m^2)	Nominal Thickness (mm)	Elastic Modulus (MPa)
6	796	1.57±0.02	0.26±0.01
7	614	1.57±0.03	0.24±0.02
8	551	1.76±0.01	0.21±0.0005
9	402	1.74±0.01	0.15±0.01
10	331	1.84±0.01	0.12±0.01
12	216	2.27±0.005	0.06±0.005
15	148	2.53±0.005	0.03±0.002

The electromechanical performance of the strain sensors knitted with different NPs changing from NP_6 – NP_{15} is shown in Figure 2.6 along with GFs and working ranges. Tighter structures knitted with the NP numbers 6, 7, and 8 have a working range between 0–10%; above that strain value, the performance of sensors becomes unstable and nonlinear (as shown in Figures S4 and S5 in the Supporting Information). The response curve for the NP_9 sensor showed an initial minimum resistance of 15.5 ohms, hence the effective working range did not start at 0 but at a 6% strain. Like the working range, the gauge factor values are relatively low and range between 0.20 and 0.33. However, for less dense sensors, the gauge factors improve significantly and range from 0.70 to 1.91 as the NP number changes from 9 to 15. When the NP numbers increased from NP_9 to NP_{15}, the working range became broader.

Table 2.3 shows the areal density and measured elastic modulus (E) of the knitted samples with several NP numbers. Nominal thickness values were calculated by following the standard of BS 2544:1954—determination of thickness of the textile fabric [24]. By using the Heidenhain length gauge, fabric samples were placed between two glass plates and fabric thicknesses were calculated by subtracting the total thickness from the previously measured glass plate thickness. The elastic modulus values were calculated by averaging over three tests. The results show that the areal density values decrease with the increase in the NP number. With an increase in NP number from 6 to 15, the areal density decreases with a factor 5.4, the fabric thickness increases 1.6 times and the modulus decreased with a factor 8.7. It demonstrates that, with higher NP numbers, we obtain more open

structures with a lower areal density and a lower elastic modulus and, as seen in Figure 2.6, an increased working range and gauge factor.

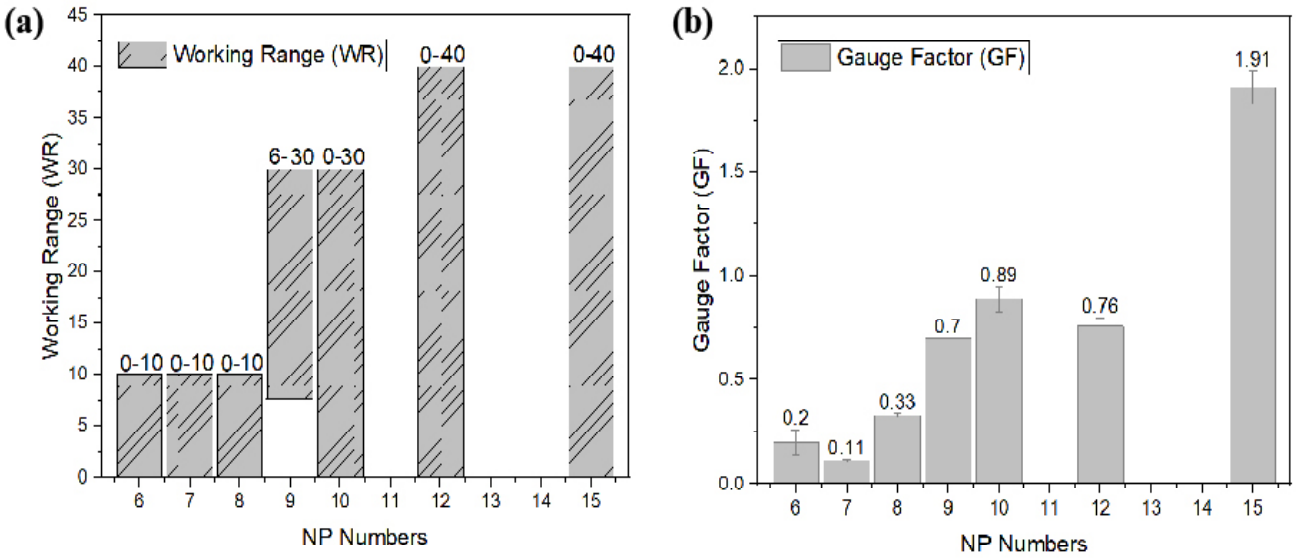


Figure 2.6 The effect of NP values on the sensor performance for the series of $NP_xY_{S1}C_2E_1$ (a) working range, and (b) gauge factor.

2.4.3 The Effect of an Elastic Yarn Type on Sensor Performance

The hysteresis of knitted strain sensors is known to be directly related to the ability of mechanical recovery of the sample. Therefore, in this section, we investigate the effect of elastic yarn type on sensor performance by separately comparing the performance of sensors with elastic yarns of type E_1 and E_2. The test results are summarized in Figure 2.7. Although both yarns still have hysteresis, the samples knitted with E_1 yarn appear to be more promising for each NP numbers except NP_8. Due to their higher elastic recovery performance and relatively lower hysteresis values in comparison with the E_2 yarn, for all next samples, the E_1 type yarn was used. In addition, we choose to select the NP_9 as the preferred density setting in all subsequent tests. Even though the sensor knitted with NP_7 and NP_{10} show the lowest hysteresis, a larger improvement in hysteresis was achieved for the NP_9 sample with the manufacturing technique we used for low-hysteresis sensors and the NP_9 sample seems to be more promising. This will be discussed at later stages in more detail.

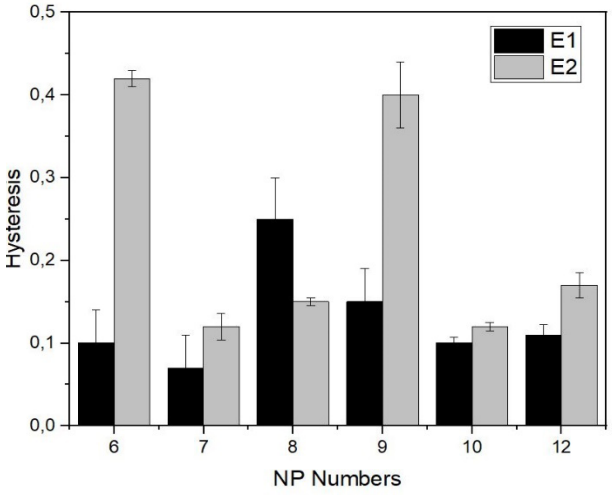


Figure 2.7 The effect of elastic yarn type (E_1 and E_2) on hysteresis for the series of $NP_xY_{S1}C_2E_1$ and $NPxY_{S1}C_2E_2$ (Hysteresis is calculated according to Equation (3)).

2.4.4 The Effect of Conductive Yarn Configuration on the Sensor Performance

The conductive yarns were knitted together using an elastic support yarn. By switching the position of elastic and conductive yarns in the yarn carrier, we can control whether the conductive yarn always ends up on top or below the elastic yarn (see Figure S6 at Supporting Information). For a standard jersey knit, this would result in one fabric surface with mainly conductive yarn and one with a mainly elastic yarn. The 1x1 rib structure that we use in this study, however, creates a more complex structure in which, in an unstretched state, the conductive yarns end up either at the inside or the outside of the fabric. In this section, we will investigate how that positioning affects the sensor performance. The conductive yarn has been positioned inside (CI) or outside (CO). Examples are shown in Figure 2.8.

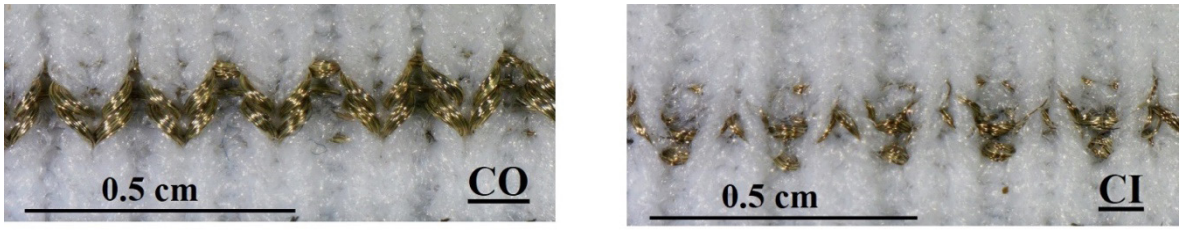


Figure 2.8 The yarn configuration of two samples (a) $NP_9Y_{S1}C_2E_1CO$ and (b) $NP_9Y_{S1}C_2E_1CI$.

The comparison of $NP_9Y_{S1}C_2E_1CO$ and $NP_9Y_{S1}C_2E_1CI$ samples in terms of electromechanical performance is illustrated in Figure 2.9. Preliminary experiments showed that, for all knitted samples, the first resistance cycle always deviated significantly which was attributed to an initial rearrangement of the knitted structure. Therefore, in all subsequent graphs, the first cycle will be omitted. In Figure 2.9, the resistance change graphs of both a sample with the conductive yarns outside (CO, Figure 2.9a) and one with the yarn inside (CI, Figure 2.9b) are presented. This clearly shows that the CI sample performs significantly better regarding hysteresis and linearity. The working range changes from 4–32% for the CO sample to 0–40% for the CI variant. In addition, the resistance increases almost linearly over the full working range for the CI sample, whereas the resistance change flattens out above about 28% in the case of the CO sample. Additionally, the GF of the CI sample,1.19 ± 0.04, is higher than that of the CO knitted sensor with a value of 0.70 ± 0.002. The most significant difference was observed in the hysteresis values, which shows a sharp decline from 0.15 to 0.03 of CO and CI, respectively. The graphs show data from four subsequent cycles (cycles 2 to 5), which can be seen to be nicely overlapping indicating that at least during these initial tests the gauges showed negligible drift.

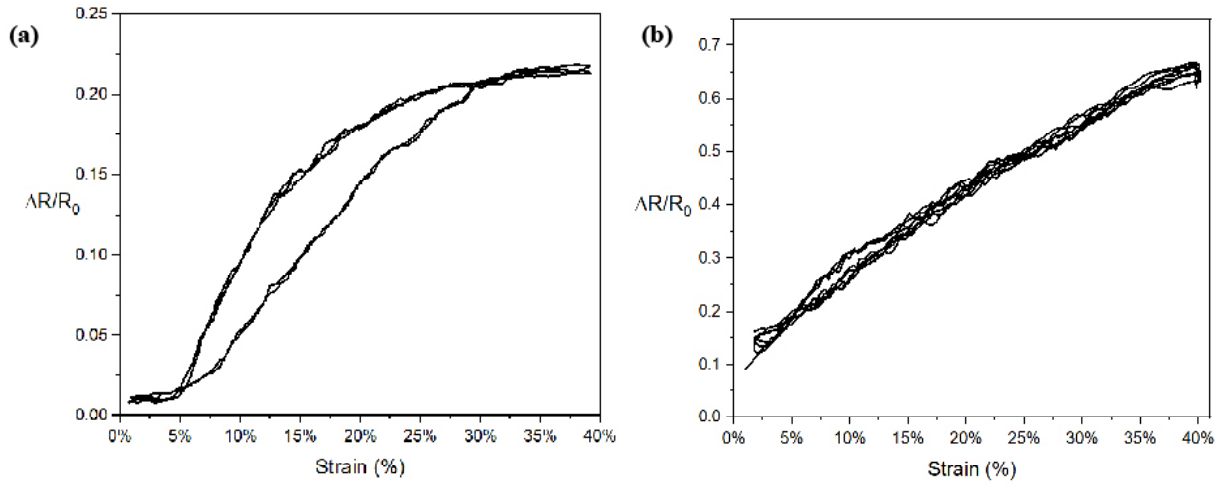


Figure 2.9 The two different results of samples knitted with conductive outside (a) $NP_9Y_{S1}C_2E_1CO$ and conductive inside (b) $NP_9Y_{S1}C_2E_1CI$.

The electromechanical performance of the $NP_9Y_{S1}C_2E_1CI$ and $NP_9Y_{S1}C_2E_1CO$ sensors at high strain values was also investigated and compared by testing the sample up to 70% strain to determine the maximum of the working range. The resistance versus strain graph is depicted in Figure 2.10. Figure 2.10a shows that the resistance change levels-off between strain values 40% and 70%, indicating an overall working range of 0–40% when the conductive yarn is inserted inside. Figure 2.10b shows the nonlinear behaviour of the CO sample with a higher hysteresis when the deformation is applied.

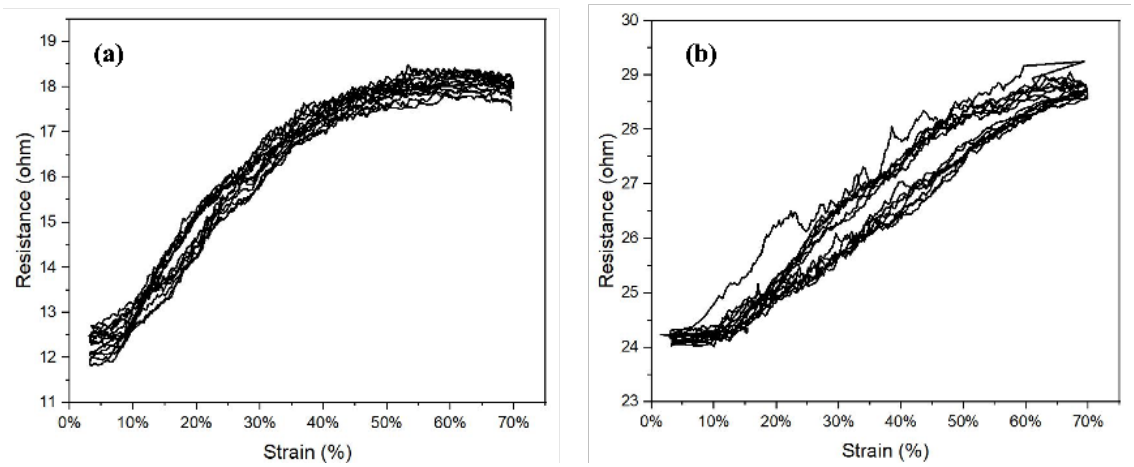


Figure 2.10 The electromechanical behaviour of the (a) $NP_9Y_{S1}C_2E_1CI$ and (b) $NP_9Y_{S1}C_2E_1CO$ sensor sample at a 70% strain value over eight applied cycles.

2.4.5 The Effect of Conductive Yarn Type and Conductive Course Number on Sensor Performance

Knitted strain sensors were produced using Shieldex (S) yarns with conductive course numbers ranging from 1 to 5 with a fixed NP_9 setting and both conductive inside (CI) and outside (CO) structures. The results of both S1 and S2 samples were illustrated in Figure 2.11 with gauge factor and hysteresis values. The average and corresponding error bars are presented to indicate the spread in data. For 1-course samples of S_2, only a single measurement was available, and consequently no error value was reported. In Figure 2.11a, c, the gauge factor is plotted versus the number of conductive courses using conductive yarn type S_1 and S_2, respectively. In all cases, the conductive inside (CI, grey bars) configuration resulted in the highest gauge factor values, with the effect being largest for the S_2 yarn (Figure 2.11c). For both yarn types, 4-course samples appear to be the optimum, resulting in GF values of 1.92 ± 0.24 and 2.10 ± 0.22 for S_1 and S_2, respectively.

The corresponding hysteresis values are plotted in Figure 2.11b, d. Once again, the conductive inside configuration produces the best results with lowest hysteresis values. For S_1 yarn, the change from CO to CI results in a drop in hysteresis from about 0.14 on average for the CO samples to about 0.06 for the CI samples. The lowest hysteresis values are close to $H\varepsilon = 0.04$ and are observed for a 2-course sample (S_1 yarn, CI) and 3- or 4- course samples (S_2 yarn, CI). Note that these values are scaled to the working range, according to our definition in Equation (3). As a result, the configuration in which the conductive inside improves the performance not only for the specific knitted sample, but also for different conductive yarns and course numbers.

By comparing Figure 2.11b, d, it shows that the hysteresis value is not much affected by the number of con-

ductive courses and always stays at a relatively high value of around 0.16 for CO samples with the S_1 yarn and around 0.20 for the S_2 yarn.

After evaluating the effect of yarn positioning on sensor performance for the S_1 and S_2 yarns of Shieldex for both CI and CO samples, the question was to explore if the conductive course numbers of influence CI samples knitted with Amann yarns. Samples were prepared and compared with six different conductive yarns with the yarn specifications listed in Figure 2.11. For the comparison, only 1- and 2-conductive course numbers were prepared with CI samples and all samples, were knitted with the NP_9 setting. The gauge factor versus initial resistance plots is shown in Figure 2.12.

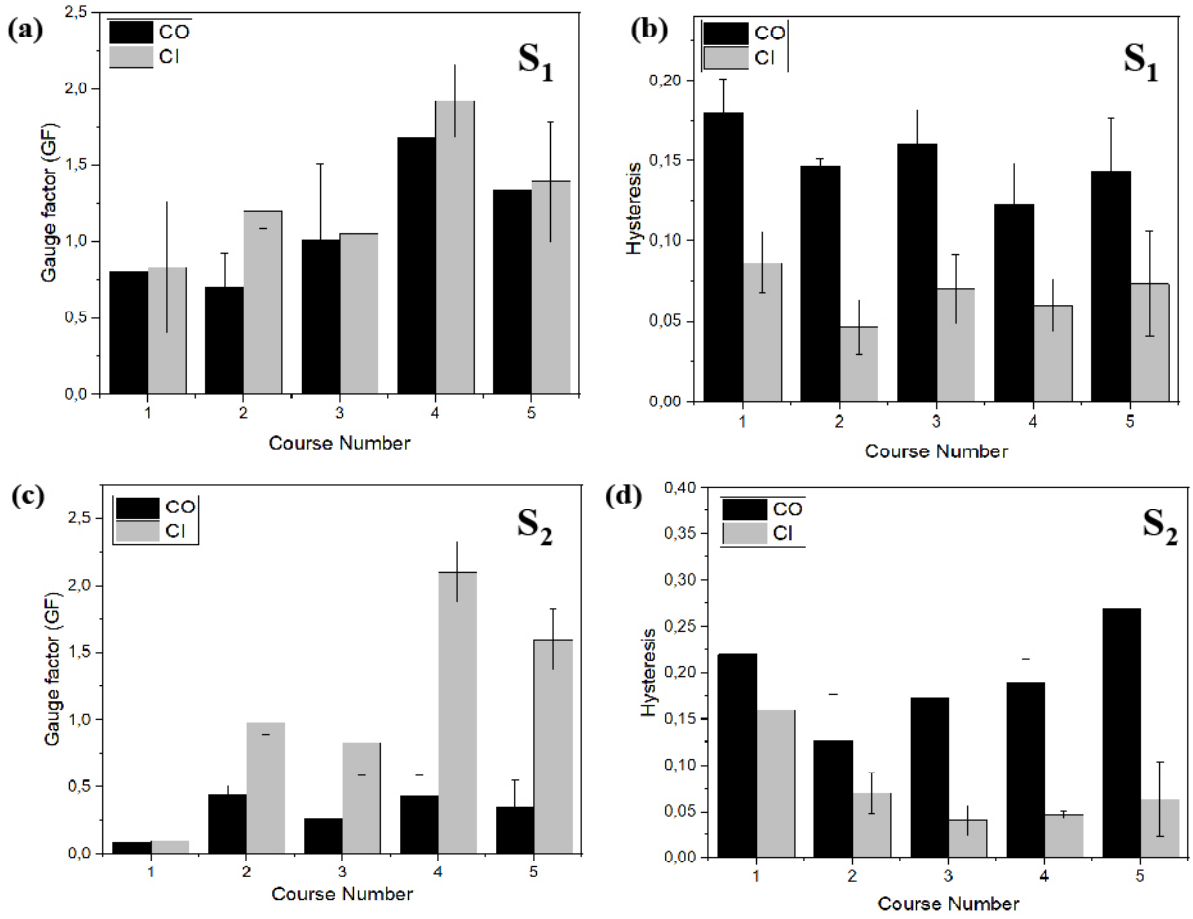


Figure 2.11 Effect of course number and yarn position S_1 yarn and S_2 yarn, respectively; (a) Gauge factor vs course number, (b) Hysteresis vs course number, (c) Gauge factor vs course number, and (d) Hysteresis vs course number.

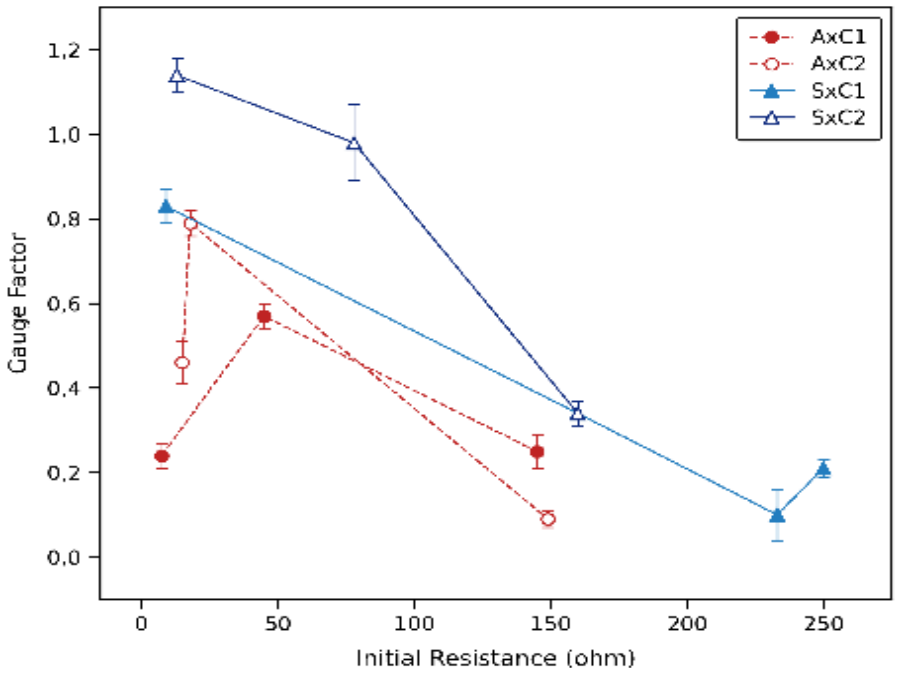


Figure 2.12 Gauge factor versus initial sensor resistance plots of sensors knitted with conductive yarn inside (CI) and NP_9; Sensors knitted with Shieldex yarns (S_1, S_2 and S_3) are indicated with blue straight lines, and Amann yarns (A_1, A_2 and A_3) with red dashed lines.

The general trend is that the gauge factor decreases with increasing the initial resistance (R_0). The major deviation from this trend is for the A_1 yarn, which shows a relatively low GF at low initial resistances for both 1- and 2- conductive course samples. It should be noted that yarn A_1 is much thicker than the support elastic yarn E_1, which has a thickness of 0.39 ± 0.02 mm, and this may have affected the stability of the configuration during co-knitting (see Figure S7 and Table 2.4).

Table 2.4 The yarn thicknesses and electromechanical performance of sensors knitted with NP_9 and CI/CO configurations.

Yarn Type	Yarn Thickness (mm)	Gauge Factor	
		CO	CI
A1	0.49	0.24	0.46
A2	0.33	0.57	0.79
A3	0.27	0.25	0.09
S1	0.32	0.70	1.19
S2	0.19	0.44	0.98
S3	0.16	0.21	0.33

Overall, 2-course samples showed better sensitivity in comparison with the 1-course samples. Thinner yarns with high resistivity such as S_2 and S_3 show a relatively poor sensing performance with GF values below 0.4. The highest GF observed is that for the 2-course configuration of the S_1 yarn around 1.19 and A_2 around 0.79. Note that low initial resistances result in higher power consumption, which can be important in practical applications for smart textiles [13].

2.5 Discussion

The electromechanical performance of knitted strain sensors was studied for different knitting densities, elastic/conductive yarn types, course number and elastic/conductive co-knit configurations. The sensing performance of the knitted strain sensors was evaluated with the focus on gauge factor and hysteresis. As it can be seen from Figure 2.13, by varying the NP number (knitting density), we have control over the sensitivity while still being able to keep the hysteresis low.

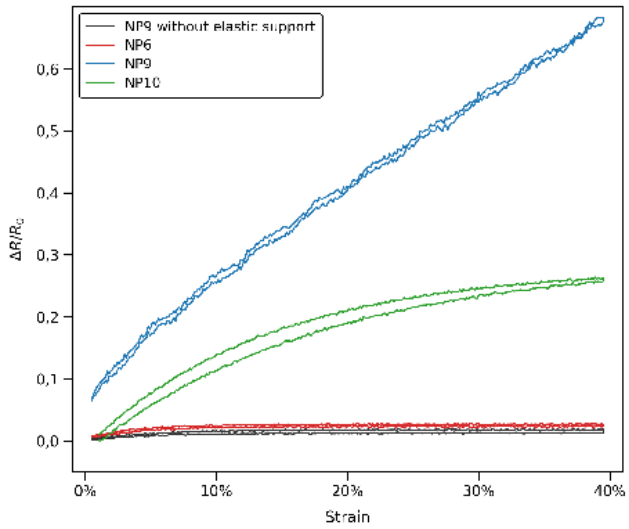


Figure 2.13 Different graphs showing high and low hysteresis knitted samples: $NP_9Y_{S1}C_2$—without E_1, with NP_6, NP_9 and NP_{10}.

The gauge factors corresponding to the curves for NP_6, NP_9 and NP_{10} are 0.20 ± 0.06, 1.19 ± 0.04 and 0.89 ± 0.06, respectively. Note that knitted conductive yarn structures with gauge factors close to zero could be of large practical importance as a basis for stretchable interconnections between sensors and data processing units in a smart garment application. The ability to control the strain sensitivity as shown in Figure 2.13 thus would enable future researchers to knit a garment with a network of connected sensor elements in one go and on one machine. Note that a stretchable conducting line with zero-gauge factor could also be obtained by omitting the elastic support yarn in the co-knit structure (see the black line in Figure 2.13).

The role of the elastic support yarn below the conductive component is therefore probably to provide enough contact pressure between overlapping loop segments. If this pressure is absent and overlapping loops do not act as shortcuts in the electrical path, the mechanism of sliding contacts and changing path lengths is no longer applicable, and no resistance changes are observed. Considering our interpretation that the sliding of overlapping loop contacts is responsible for obtaining resistance changes, we could interpret the observed knit density effects by realizing that in closer knitted structures the sliding may be partially impaired by adjacent yarns. The larger the NP, the more space for contact point sliding and, consequently, the larger resistance change and gauge factor [25].

The hysteresis values are affected not only by the NP number but also by the position of the conductive yarn. To understand the reasoning behind achieving less hysteresis sensors by positioning conductive yarn inside the structure, we need to understand the loop structure under deformation. Resistance changes due to stretching a knitted structure can in principle be due to both the deformation of the structure and to the stretching of the conductive yarns itself. However, due to the large loops in the structure and the relatively high stiffness of

the conductive yarns, the structural deformation will be the dominant part. Only at extremely large deformations (above 70%), the loop lengths are sufficiently straightened up to allow the loading and stretching of the conductive yarns. Note that this type of loading may cause cracks and decrease the adhesion between silver and polyamide in the silver coating and thus compromises the long-term sensor reliability [26]. The fact that this type of yarn stretching in our 1x1 rib structure only occurs at extremely high deformations is therefore highly beneficial for the sensor reliability.

In Figure 2.14, we depict how the co-knitting of a conductive yarn on top of a non- conductive one can result in a structure in which the conductive yarns end up on the inside. Note that this type of configuration is typical for the 1x1 rib structure and is not observed for other knitting stitches. When stretched out, the conductive parts of the interlaced loops make contact and start to slide relative to each other which causes the resistance change responsible for the sensor function [27]. In general, when the fabric is stretched, the intra-yarn contact points are pulled apart resulting in increased resistance, whereas the inter-yarn contact points are pulled together leading to reduced resistance.



Figure 2.14 (a) The illustration of the knitted sample which conductive yarn inserted inside, and elastic yarn positioned outside (CI), (b) Representation of the unfolded loops in a course which shows the relative position of the conductive (black line) and elastic (grey line) yarns.

Knitted sensors with a variety of conductive yarns show different sensor performances. Since the elastic and conductive yarn is inserted into the structure together, the yarn thickness can be another parameter that affects the performance. All yarn thicknesses were estimated using an image analysis program and the thickness of the elastic yarn E_1, as well as the six conductive yarns, are listed in Table 2.4. From this, we can conclude that the highest sensitivity values can be achieved when the conductive yarns have comparable thickness compared to the elastic yarn. Note that the difference between the Shieldex yarns and Amann yarns is that Shieldex yarns consist of only silver coated nylon filaments, whereas Amann yarns are hybrid filaments with polyester fibers.

In the results presented until now, the best performing sensor was the one with a gauge factor and hysteresis of 1.19 and 0.03, respectively. Our developed sensor can be compared with other research in literature as shown in Table 2.5. In addition, these types of sensors are suitable with high signal integrity required applications such as a respiration sensor or finger monitoring applications [28]. Higher gauge factors were observed for the series, as seen in Figure 2.6 at around 1.91 and for the series with four courses at around 2.10 (see Figure 2.11). Knitted textile sensors with high sensitivity, linearity and low hysteresis are suitable for wearable applications that monitor body movements, including activities that involve dynamic motion, as demonstrated by Liang et al [14].

Table 2.5 The performance comparison of previous literature studies and this study.

Ref.	Knit Type	Conductive Material	Non-Conductive Material	GF	Hysteresis
Atalay (2013) [10]	Interlock	235 dtex Silver-Nylon	800 dtex elastic yarn	3.75	0.10
Atalay (2014) [29]	Interlock	Silver-Nylon	800 dtex elastic yarn	3.44	0.08
Tognetti (2014) [30]	Intarsia	Carbon filled nylon	Lycra	6.70	0.14
Raji (2018) [15]	1 × 1 Rib	Silver-Nylon	Nylon covered spandex	1.25	-
Raji (2018) [15]	1 × 2 Rib	Silver-Nylon	Nylon covered spandex	1.50	-
Raji (2018) [15]	1 × 3 Rib	Silver-Nylon	Nylon covered spandex	1.60	-
Oks (2014) [31]	Plain	Silver-Nylon	Elastane, Pes, Cotton	10	0.10
Chia (2021) [20]	1 × 1 Rib	235 dtex Silver-Nylon	Spandex yarn	1.36	-
Yang (2009) [32]	1 × 1 Rib	Bare SS	-	-1.1	-
Our Study (2022) [33]	1 × 1 Rib	235 dtex Sil-Ny, 600 Ω/m	Nylon-Lycra	1.19	0.03
Atalay (2013) [10]	Interlock	235 dtex Silver-Nylon	800 dtex elastic yarn	3.75	0.10
Atalay (2014) [29]	Interlock	Silver-Nylon	800 dtex elastic yarn	3.44	0.08

2.6 Conclusions

This paper investigates the effect of structure and process parameters on knitted strain sensor performance by conducting a systematic study. Knitted strain sensors have the potential to be used in various applications for body movement monitoring and therefore they should have specific features in terms of sensitivity and stability.

The findings of this study can be summarized in several points:

- The separation of the loops within the knitted structure produced with lower NPs such as 6, 7 and 8 cannot be achieved directly because of the tightness of the samples.
- A manufacturing technique in which the sensor properties, especially the hysteresis values, can be reduced and controlled in knitted sensors has been reported for the first time. By positioning the conductive yarns inside the 1x1 rib structure, a knitted strain sensor with linear performance and a gauge factor of 1.19 and negligible hysteresis of 0.03 was developed.
- The effect of yarn positioning on different types of conductive yarns in terms of hysteresis was also proved. For both S_1 and S_2 yarns, the hysteresis values have decreased for different conductive course numbers. The lowest hysteresis values were achieved for a 2-course sample of S_1 yarn and 3- or 4-course samples of S_2 yarn.
- The performance of sensors made with different conductive yarns was evaluated, and those with low-

er initial resistance reported higher gauge factors for Shieldex yarns.

- The highest sensitivity values can be achieved when the conductive yarns have comparable thickness compared to the elastic yarn. Yarns with higher conductivity result in better sensing performance.

In this chapter, a novel textile-based strain sensor is developed. In the following chapter, the developed strain sensor is used to monitor finger joint movements.

References

1. Lee, H.J.H., S.H.; Yoon, H.N.; Lee, W.K.; Park, K.S., Heart rate variability monitoring during sleep based on capacitively coupled textile electrodes on a bed. Sensors, 2015. 15: p. 11295–11311.
2. Niu, B.H., T.; Hu, H.; Xu, B.; Tian, X.; Chan, K.; Chen, S., A highly durable textile-based sensor as a human-worn material interface for long-term multiple mechanical deformation sensing. J. Mater. Chem. C 2019. 7: p. 14651–14663.
3. xMaity, S.C., A., Conductive polymer-based electro-conductive textile composites for electromagnetic interference shielding: A review. J. Ind. Text. , 2018. 47: p. 2228–2252.
4. Amjadi, M.K., K.U.; Park, I.; Sitti, M., Stretchable, skin-mountable, and wearable strain sensors and their potential applications: a review. Adv. Funct. Mater. , 2016: p. 1678–1698.
5. Ma, R.L., J.; Choi, D.; Moon, H.; Baik, S., Knitted fabrics made from highly conductive stretchable fibers. Nano Lett. , 2014. 14: p. 1944–1951.
6. Molinaro, N.M., C.; Presti, D.L.; Saccomandi, P.; Di Tomaso, G.; Zollo, L.; Perego, P.; Andreoni, G.; Schena, E., Wearable textile based on silver plated knitted sensor for respiratory rate monitoring. In Proceedings of the 40th Annual International Conference of the IEEE Engineering in Medicine and Biology Society (EMBC), Honolulu, HI, USA, 2018: p. 2865–2868.
7. Park, S.Y.L., J.H., Machine Embroidered Sensors for Limb Joint Movement-Monitoring Smart Clothing. Sensors, 2021. 21: p. 949.
8. Tangsirinaruenart, O.S., G., A novel textile stitch-based strain sensor for wearable end users. 2019. 12: p. 1469.
9. Zhao, K.N., W.; Zhang, S., Highly stretchable, breathable and negative resistance variation textile strain sensor with excellent mechanical stability for wearable electronics. . J. Mater. Sci., 2020. 55: p. 2439–2453.
10. Atalay, O.K., W.R.; Husain, M.D., Textile-based weft knitted strain sensors: Effect of fabric parameters on sensor properties. Sensors, 2013. 13: p. 11114–11127.
11. Larrabee, W.F., Jr., A finite element model of skin deformation. I. Biomechanics of skin and soft tissue: A review. Laryngoscope, 1986. 96: p. 399–405.
12. Gibbs, P.T.A., H., Wearable conductive fiber sensors for multi-axis human joint angle measurements. Neuroeng. Rehabil., 2005. 2: p. 1–18.
13. Atalay, O., Kennon, W. R., & Husain, M. D., Textile-Based Weft Knitted Strain Sensors: Effect of Fabric Parameters on Sensor Properties. Sensors, 2017.
14. Liang, A.S., R.; Bryan-Kinns, N. A, Analysis of sensitivity, linearity, hysteresis, responsiveness, and fatigue of textile knit stretch sensors. Sensors, 2019. 19: p. 3618.
15. Raji, R.K.M., X.; Zhang, S.; Li, Y.; Wan, A., Influence of rib structure and elastic yarn type variations on textile piezoresistive strain sensor characteristics. . Fibres Text. East. Eur. , 2018. 26: p. 24–31.
16. Xie, J.L., H.; Miao, M., High sensitivity knitted fabric strain sensors. Smart Mater. Struct., 2016. 25: p. 105008.
17. Raji, R.K.M., X.; Zhang, S.; Li, Y.; Wan, A.; Boakye, A., Knitted piezoresistive strain sensor performance, impact of conductive area and profile design. J. Ind. Text., 2020. 50: p. 616–634.
18. Jansen, K., Performance evaluation of knitted and stitched textile strain sensors. Sensors, 2020. 20: p. 7236.
19. Isaia, C.M., S.; McNally, D., The effect of washing on the electrical performance of knitted textile strain sensors for quantifying joint motion. J. Ind. Text., 2022. 51: p. 8528S–8548S.

20. Chia, P.Z.G., U.; Tan, Y.Y.; Lau, J.L.; Ahmed, A.; Soh, G.S.; Low, H.Y., Effect of Stitch Pattern on the Electrical Properties of Wale-wise Knitted Strain Sensors and Interconnects. In Proceedings of the IEEE Sensors, 2021: p. 1-4.

21. Li, Y.M., X.; Chen, J.Y.; Jiang, G.; Liu, Q. , Sensing performance of knitted strain sensor on two-dimensional and three-dimensional surfaces. Mater. Des., 2021. 197: p. 109273.

22. Dupler, E.D., L.E., Effects of the textile-sensor interface on stitched strain sensor performance. Proceedings of the 23rd International Symposium on Wearable Computers, 2019: p. 45–53.

23. Xie, J.L., H., Investigation on the relation between structure parameters and sensing properties of knitted strain sensor under strip biaxial elongation. J. Eng. Fibers Fabr., 2015. 10: p. 166–178.

24. Standards, B., Determination of thickness of textile fabric.

25. Tohidi, S.D.Z., A.; Catarino, A.P.; Rocha, A.M., Effects of base fabric parameters on the electro-mechanical behavior of piezoresistive knitted sensors. IEEE Sensors, 2018. 18: p. 4529–4535.

26. Ankhili, A., Tao, X., Cochrane, C., Koncar, V., Coulon, D., & Tarlet, J. M., Comparative study on conductive knitted fabric electrodes for long-term electrocardiography monitoring: silver-plated and PEDOT: PSS coated fabrics. Sensors, 2018. 18(11): p. 3890.

27. Li, L.L., S.; Ding, F.; Hua, T.; Au, W.M.; Wong, K.S., Electromechanical analysis of length-related resistance and contact resistance of conductive knitted fabrics. Text. Res. J., 201282: p. 2062–2070.

28. Ryu, H.P., S.; Park, J.J.; Bae, J., A knitted glove sensing system with compression strain for finger movements. Smart Mater. Struct., 2018. 27: p. 055016.

29. Atalay, O.K., W.R.; Demirok, E., Weft-knitted strain sensor for monitoring respiratory rate and its electro-mechanical modeling. IEEE Sensors J., 2014. 15: p. 110–122.

30. Tognetti, A.L., F.; Mura, G.D.; Carbonaro, N.; Pacelli, M.; Paradiso, R.; Rossi, D.D. , New generation of wearable goniometers for motion capture systems. J. Neuroeng. Rehabil., 2014. 11: p. 1–17.

31. Oks, A.K., A.; Litvak, J., Knitted resistive fabric: properties and applications. Mater. Sci. Text. Cloth. Technol., 2014. 9: p. 28–33.

32. Yang, K.S., G.l.; Zhang, L.; Li, L.W., Modelling the electrical property of 1 x 1 rib knitted fabrics made from conductive yarns. In Proceedings of the Second International Conference on Information and Computing Science, 2009. 4: p. 382–385.

33. Bozali, B., Ghodrat, S., Plaude, L., van Dam, J. J., & Jansen, K. M., Development of low hysteresis, linear weft-knitted strain sensors for smart textile applications. Sensors, 2022. 22(19): p. 7688.

Chapter 2 - Supporting Information

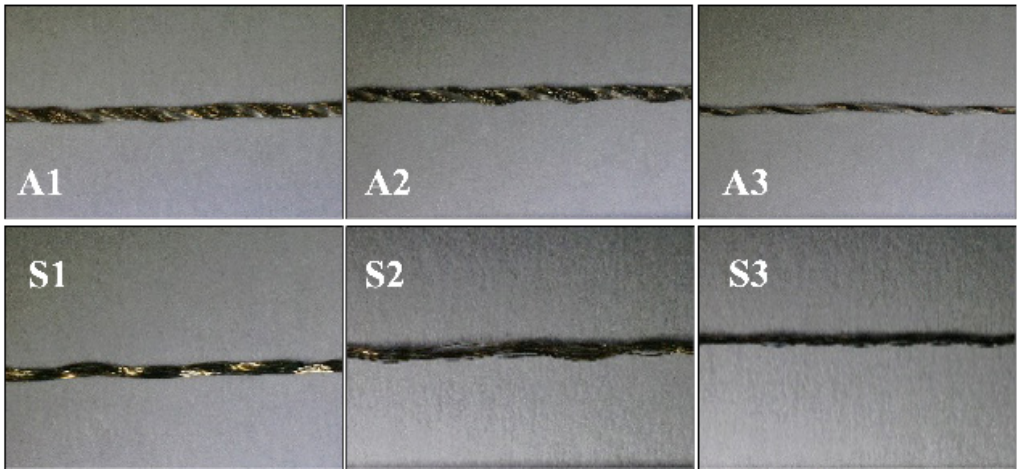


Figure S1. Optical images of conductive yarns in which 'S' refers to the Shieldex yarn (Material: Polyamide 6.6 filament, Metal Plated: 99 % Pure silver) and 'A' refers to Amann yarn (Silver coated Polyamide/Polyester hybrid thread).

	Amann (A)			**Shieldex (S)**		
Resistivity (ohm)	A1	A2	A3	S1	S2	S3
	Tex 28	Tex 62	Tex 96	Dtex 235	Dtex 117	Dtex 78
	< 530 Ω/m	<150 Ω/m	<85 Ω/m	600 Ω/m	< 1.5 kΩ/m	< 3.5 kΩ/m

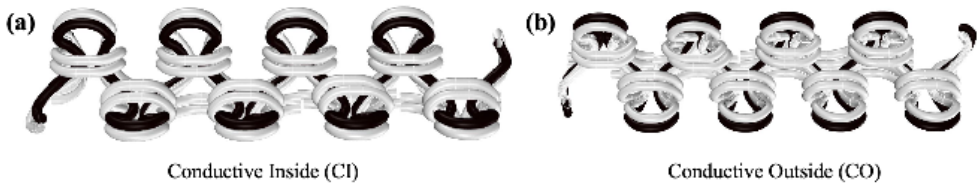


Figure S2. The position of conductive yarn within the co-knit yarn configuration: (a) Conductive yarn (black yarn) positioned inside, and (b) Elastic yarn (white yarn) positioned inside.

Table S2. The effect of test speed on electromechanical performance of the knitted strain sensors of $NP_9Y_{S1}C_2E_1$, $NP_{10}Y_{S1}C_2E_1$ and $NP_{10}Y_{S1}C_3E_1$.

Samples	**Test Speed (mm/min)**	**Initial Resistance (Ω)**	**Gauge Factor (GF)**	**Working Range (%)**	**Hysteresis**
$NP_9Y_{S1}C_2E_1$	30	17.33	1.60	0-22	0.07
	40	17.19	1.80	0-20	0.07
	50	17.22	1.80	0-22	0.07
$NP_{10}Y_{S1}C_2E_1$	30	23.40	1.14	0-23	0.07
	40	23.60	1.11	0-24	0.05
	50	23.03	1.40	0-25	0.07

$NP_{10}Y_{S1}C_3E_1$	30	7.13	0.23	0-36	0.25
	40	7.21	0.37	0-17	0.30
	50	7.21	0.52	0-17	0.27

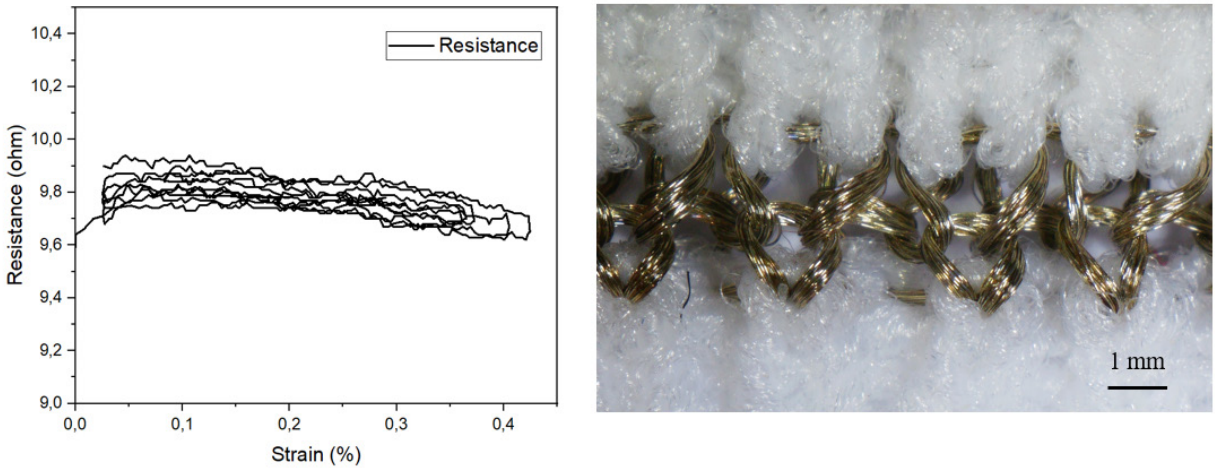
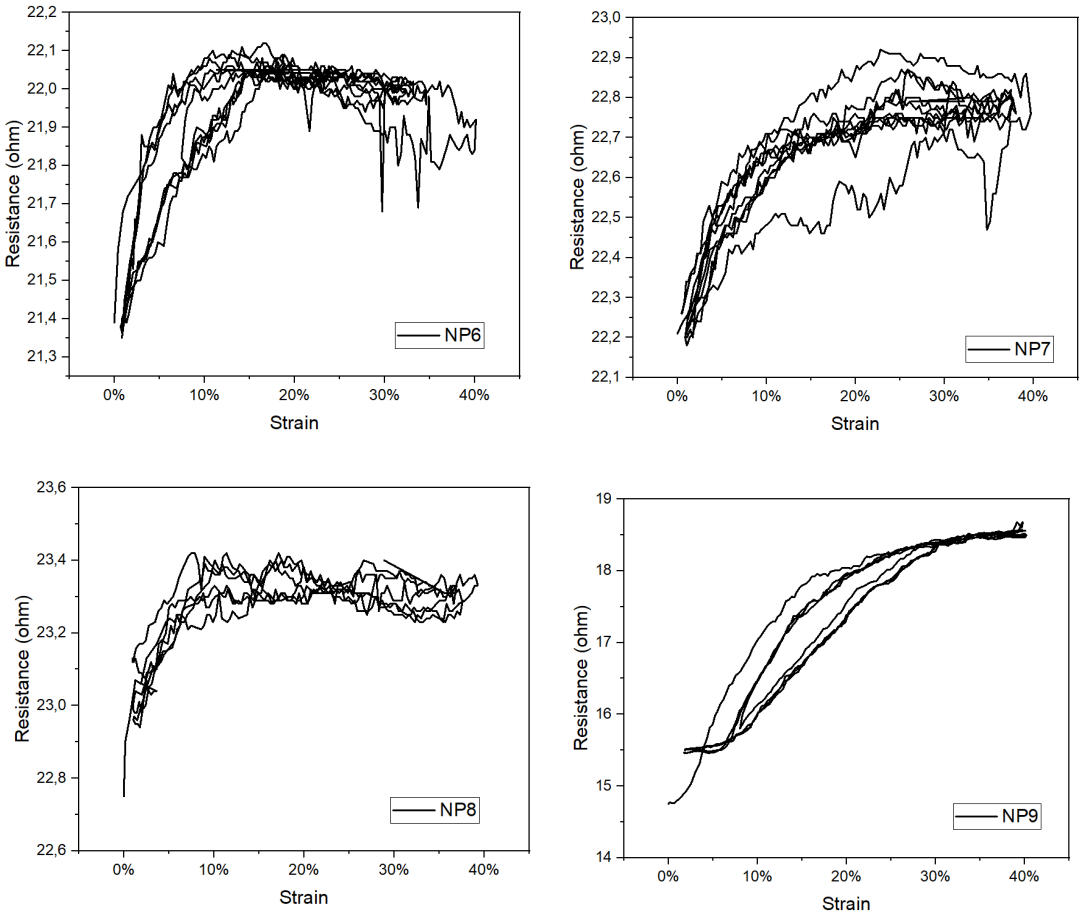


Figure S3. The resistance versus strain graph without E_1 plating/elastic yarn as a co-knit material for the $NP_9Y_{S1}C_2$ sample (left) – Optical image of the $NP_9Y_{S1}C_2$ sample without elastic plating yarn.



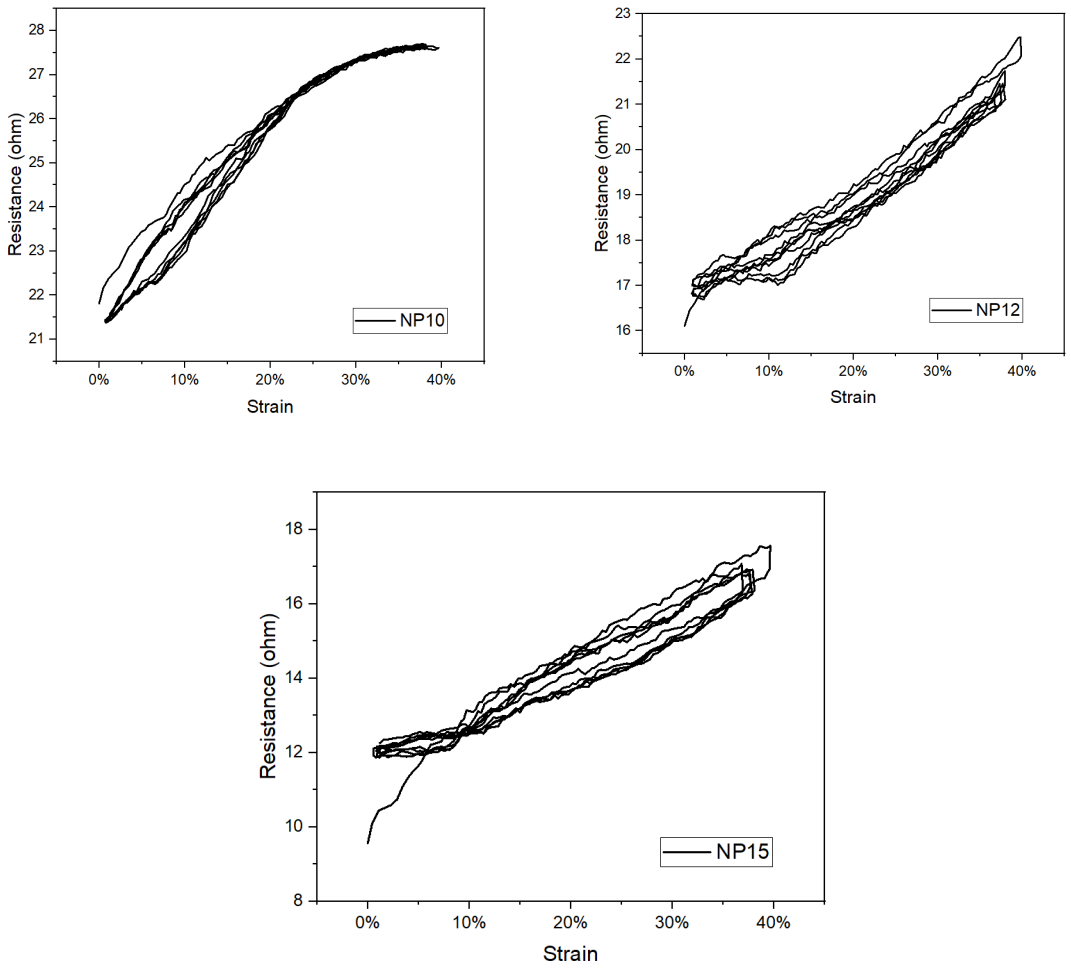
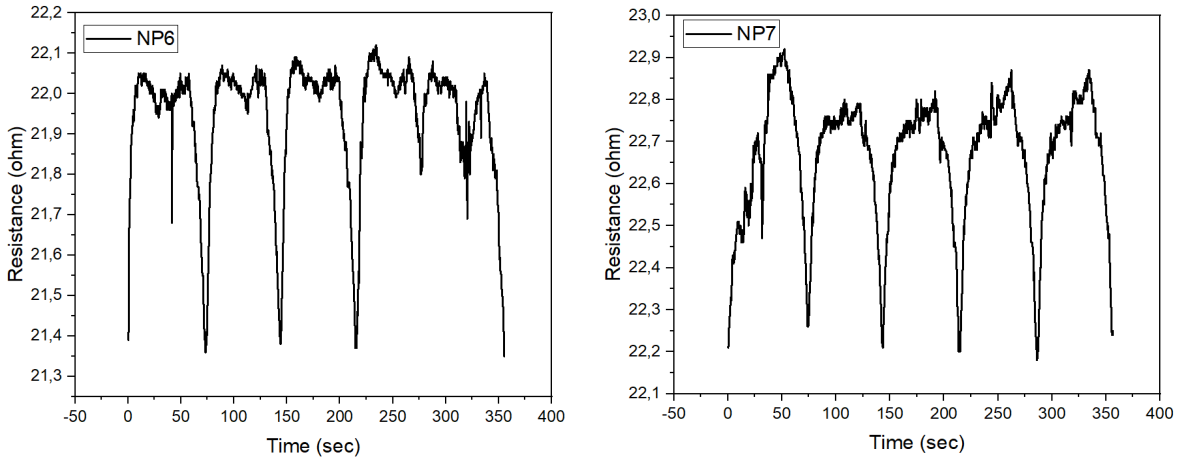


Figure S4. Examples of irregular and regular cyclic patterns: NP_6, NP_7, NP_8, NP_9, NP_{10}, NP_{12}, NP_{15}. Resistance versus strain graphs for the series of $NP_xY_{S1}C_2E_1$.



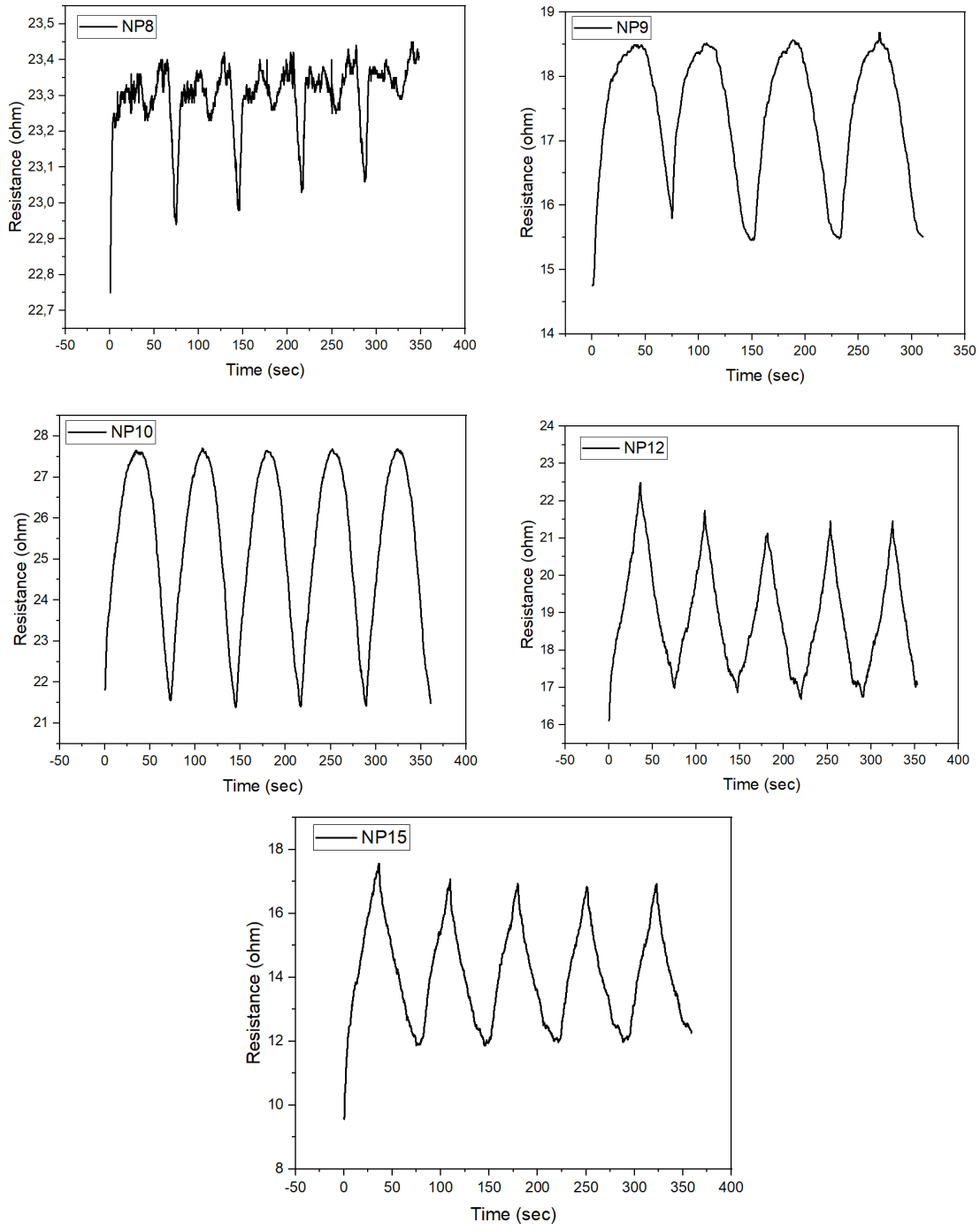


Figure S5. Examples of irregular and regular cyclic patterns: NP_6, NP_7, NP_8, NP_9, NP_{10}, NP_{12}, NP_{15}. Resistance versus time graphs for the series of $NP_xY_{S1}C_2E_1$.

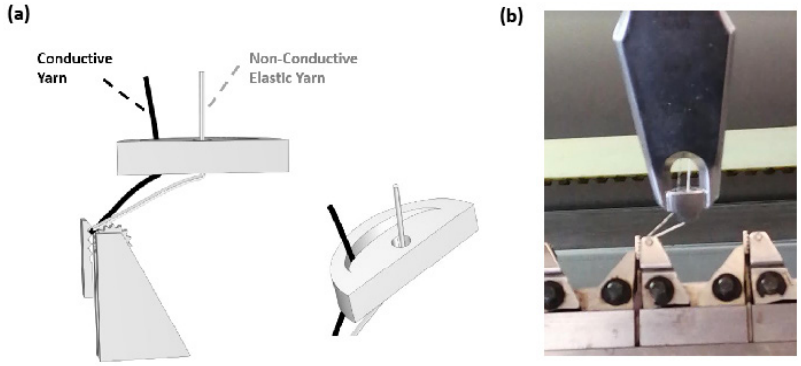


Figure S6. The schematic of yarn carrier (a), and picture of plated yarn carrier with 2 yarns consisting of conductive yarn and non-conductive elastic yarn.

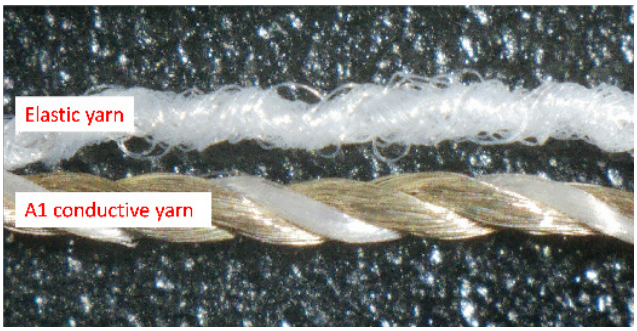


Figure S7. Optical image of plating elastic yarn (white) and A1 conductive yarn (white and silver)

Chapter 3

3. Application of knitted strain sensors

While Chapter 2 discussed knitted strain sensors, this chapter focuses on their use for rehabilitation and health monitoring. It examines their integration into finger-worn devices, evaluates their performance in tracking finger movements and joint angles and investigates the impact of spacer layer thickness.[2]

As an emerging technology, smart textiles have attracted attention for rehabilitation purposes or to monitor heart rate, blood pressure, breathing rate, body posture, as well as limb movements. Traditional sensors do not provide comfort, flexibility and adaptability, whereas textile-based sensors do not cause any discomfort to the body and therefore ensure good biocompatibility and skin-friendliness. In this study, knitted strain sensors that are linear up to 40% strain with a sensitivity of 1.19 and a low hysteresis characteristic were integrated into different versions of wearable finger sensors for rehabilitation purposes. The results showed that the different finger sensor versions have accurate responses to different angles of the index finger at relaxation, 45° and 90°. Also, the effect of layer thickness between the finger and sensor was investigated.

2 *This chapter is based on the following publication: Bozali, B., Ghodrat, S., and K. M. Jansen, "Design of wearable finger sensors for rehabilitation applications," Micromachines, vol. 14, no. 4, p. 710, 2023.*

Introduction

Flexible and wearable sensors have attracted attention in recent years for a variety of applications, including human-device interfaces and health monitoring such as respiration rate, heart rate, and body position [1-3]. Traditional sensors are often integrated into garments as an external element or attached to the surface and create discomfort for the user due to the bulky and rigid nature of electronic devices such as inertial measurement units (IMUs) [4]. Moreover, these systems are not always well-suited for long-term use or home-based applications, particularly during movement. Moreover, rigid to soft transitions are vulnerable to failures due to fatigue during wearing and washing [5]. For future generations, it is desirable if wearable sensors would be flexible and stretchable such that they conform to the body contours as well as being breathable and washable. As an example, textile-based sensors offer a new possibility for fully integrated monitoring of body-related parameters such as heart rate or local strains. They are easy to wear, flexible and washable, and can be used for numerous health monitoring applications, making them a good alternative to traditional bulky sensors [6].

Knitted strain sensors are obtained by embedding conductive yarns in the knit structures and can be manufactured with commercially available conductive yarns and existing standard textile manufacturing equipment. They are completely integrated into the textile and can measure strains up to 40%. This makes them suitable candidates for unobtrusive monitoring of body posture and movement of hands, arms, legs and fingers as they provide a good integration into garments. And they can apply this to measure limb movement during a therapy session and give feedback to the patient and therapists [7]. In literature, textile strain sensors have been produced either (i) by inserting stretchable sensor yarns produced at laboratory conditions, (ii) by coating an existing knitted structure with conductive materials such as graphene [8-10], PEDOT: PSS [9, 10] or nanosilver [11], (iii) by introducing commercially conductive yarns in the knit structure during the knitting process. Although strain sensors with conductive materials have good stability, high sensitivity and fast response, they lack flexibility, which hinders their stretchability under conditions of large deformation. This is because the conductive component may have structural damage because of high friction. And also, their mechanical incompatibility with textiles subsequently causes the electrical properties of the sensors to deteriorate and they are difficult to scale up [12, 13]. As an alternative, these challenges can be realized by using conductive yarns in knitted strain sensors.

Knitted strain sensors are three-dimensional textile structures in which deformation of conductive yarn loops leads to measurable changes in electrical resistance. The sensor mechanism in knitted structures is related to contact resistance between the conductive yarns under deformation. While the interlocked loops are separated from each other, contact resistance between successive knitted loops of conducting yarn changes which results in a decrease or increase in resistance [14].

Knitted strain sensors are quite suitable for rehabilitation applications, and many studies have been reported so far. Ryu et al. investigated the performance of the knitted strain sensor in a glove by using silver-plated yarns to distinguish the finger movements and the electrical responses of the compressive strain demonstrated strong stability and linearity through various finger rolling angles [15]. Different hand motions were also detected by the knitted sensor developed by Han et al., but the electrical resistance change was not high enough to monitor the overall movements of the fingers [1]. A previous study examined the performance of the sensor in gloves for recognizing gestures and concluded that elasticity of the fabric affects the effective detection range of knit-

ted sensors, the size of the sensor has a significant influence on sensitivity, and appropriate glove size helps to avoid nonlinear sensing phenomenon [16]. Lee et al. also concluded that the developed glove might be useful to amputees as a tool that allows them to rehabilitate or regulate the myoelectric prosthesis by putting the sensing elements into the glove and producing the whole garment knitting technique for ease of commercialization [17]. Isaia et al. evaluated the performance of strain sensors knitted with various conductive yarns in terms of sensing properties, hysteresis and comfort for joint motion tracking applications during repetitive flexion-extension cycles [18, 19].

Although it is feasible to produce knitted strain sensors with different designs using conductive yarns, performance is not always optimal resulting in a limited working range, non-linearity and hysteresis. That results in poor sensing performance, and they are currently not commonly integrated into practical applications. To be able to apply the knitted strain sensors in practical applications, first, the sensor itself must have a suitable working range, good linearity and high sensitivity [20]. In addition, it should be realized that the textile structures in which the sensor performance is integrated are also affected by thickness, elasticity and slipping of the fabric.

In this study, we focus on the application of a knitted strain sensor into a finger sensor for movement detection. We previously developed a knitted strain sensor with a working range of 40% and sensitivity of 1.19±0.03 GF and low hysteresis of 0.03 (smaller than 1%) [21]. And the knitted strain sensor is integrated into different versions of wearable finger sensors. Several finger sensor designs will be considered, and their sensor performance will be evaluated on a finger movement sensor and its use.

3.1 Materials and Methods

In a previous study [21], a textile-based strain sensor and its electromechanical performance were analysed, and in the current study, this newly developed strain sensor was integrated into a finger sensor for the detection of movement. The strain sensor was knitted on a Stoll CMS 530 machine with a 1x1 rib design by using conductive yarn from Shieldex with a yarn count of dtex 235 and initial resistance of ≤600 Ω/ m and elastic yarn from Yeoman of Nm 15 as illustrated in Figure 3.1. The plating technique was used to position the conductive yarn inside and the elastic yarn outside in the sensing region (See. Figure 3.1 b and Figure 3.1 c). The conductive yarn is knitted together with a non-conductive elastic yarn using the two eyes of the plating carrier. Thus, the position of the conductive yarn relative to the elastic support yarn is well controlled, resulting in a rib structure in which the conductive yarn is positioned always inside. During stretching, conductive loops inside slide over each other resulting in a measurable resistance change.

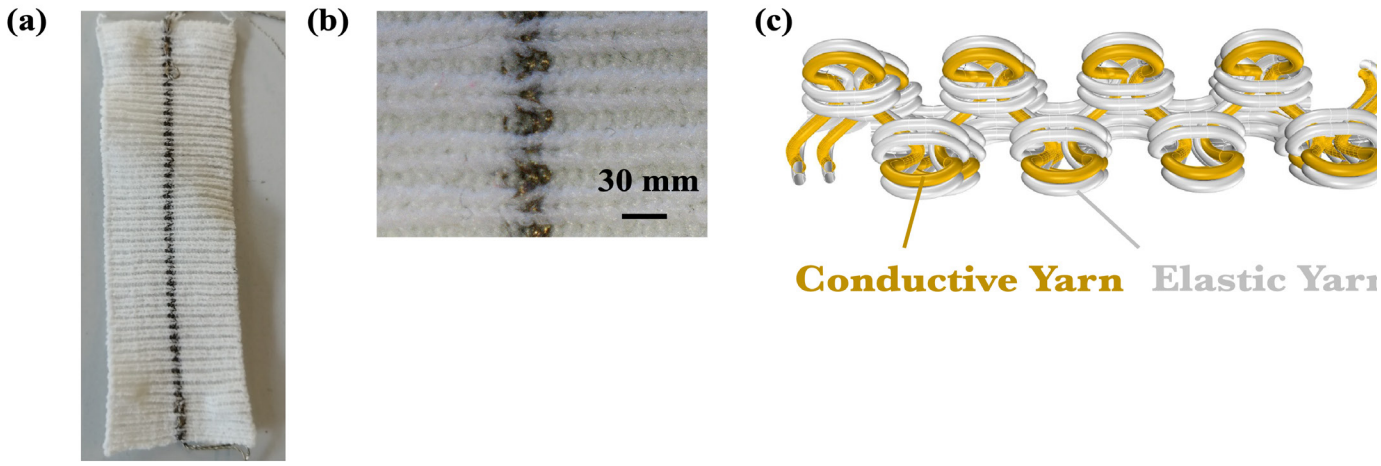


Figure 3.1 a) The developed knitted strain sensor, (b) Optical images of the sensing region which shows the conductive yarns (yellow) positioned inside and elastic yarns outside (white), and (c) Illustration of the conductive and elastic yarn positioning within the sensing region.

The knitted strain sensor is integrated into different versions of wearable finger sensors as shown in Figure 3.2. Version 1 is the knitted sensor strip attached to a nonwoven tube fabric as shown in Figure 3.2a, whereas Version 2 is the knitted sensor strip attached between the fingertip and wrist. We expect that because of the small pre-stress in the version 2 sensor, the slack is reduced during operation. In the version 1 sensor, we add a spacer layer of different thicknesses, and we expect this to increase the sensor stretching and thus a measured signal. The advantages and disadvantages of the different versions are listed in

Table 3.1. The length and width of the knitted strain sensor were set to 8 cm and 2 cm, respectively. Apart from the knitted sensor, the design includes an Arduino Nano BLE and a power supply with an integrated USB connector.

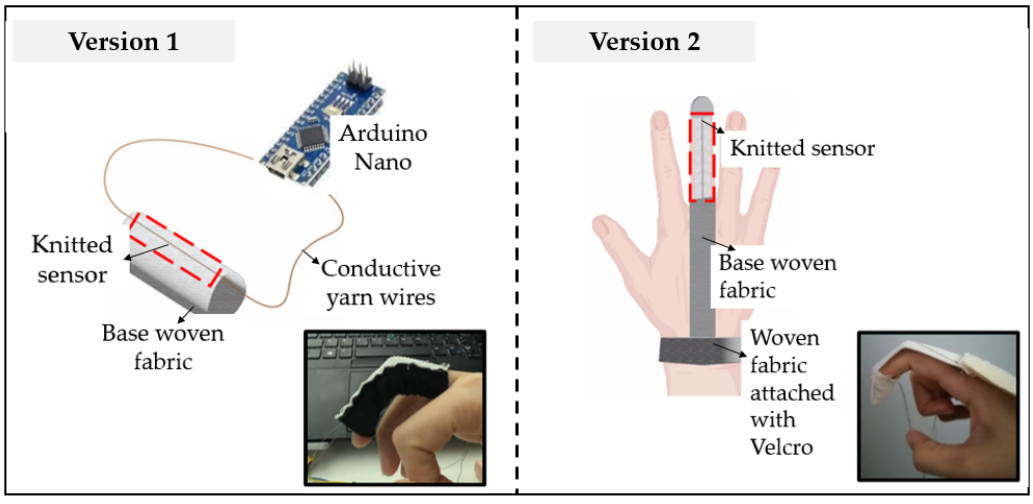


Figure 3.2 Different versions of wearable finger sensors: (a) Version 1, and (b) Version 2.

Before the application of the strain sensor into a finger wearable demonstrator, the characteristics of the knitted strain sensor strips were tested in the course-wise direction by performing four test cycles at 30 mm/min, using a custom-made tensile tester and the resistance response during tensile extension-relaxation tests was assessed. The gauge length was set as 50 mm in the customized tensile tester. The tests were done up to 40% strain considering the finger deformation is less than 20 mm extension [22]. To evaluate the electromechanical performance of finger

sensors at different angles, resistance and time values are recorded using a Bluetooth accelerometer plotter according to the finger movements. The actual angles of finger were obtained using the Kinovea – 0.9.5 program.

3.2 Results

3.2.1 Electromechanical performance of the knitted strain sensor

The electromechanical performance of the knitted strain sensor is investigated, and various tensile tests are carried out to investigate the strain sensing properties as illustrated in Figure 3.3. In Figure 3.3a and 3c, the sensor is stretched five times to the range of 40% and the relative resistance change of the sensor is measured for 5 cycles, where R_0 and R represent the initial and real-time resistances, respectively. The first cycle always deviates which was attributed to the first reorganization of the knitted structure and is therefore omitted. The relative resistance changes of the sample show a linear characteristic (R_2 = 0.98) with the gauge factor (GF) and hysteresis value of 1.19±0.03 and 0.03, respectively. The stability of the sensor is investigated by cycling up to 70 times as shown in Figure 3.3b. It turns out to be the linearity is maintained and but GF drops from 1.19±0.03 to 1.05±0.02 at the 70th cycle.

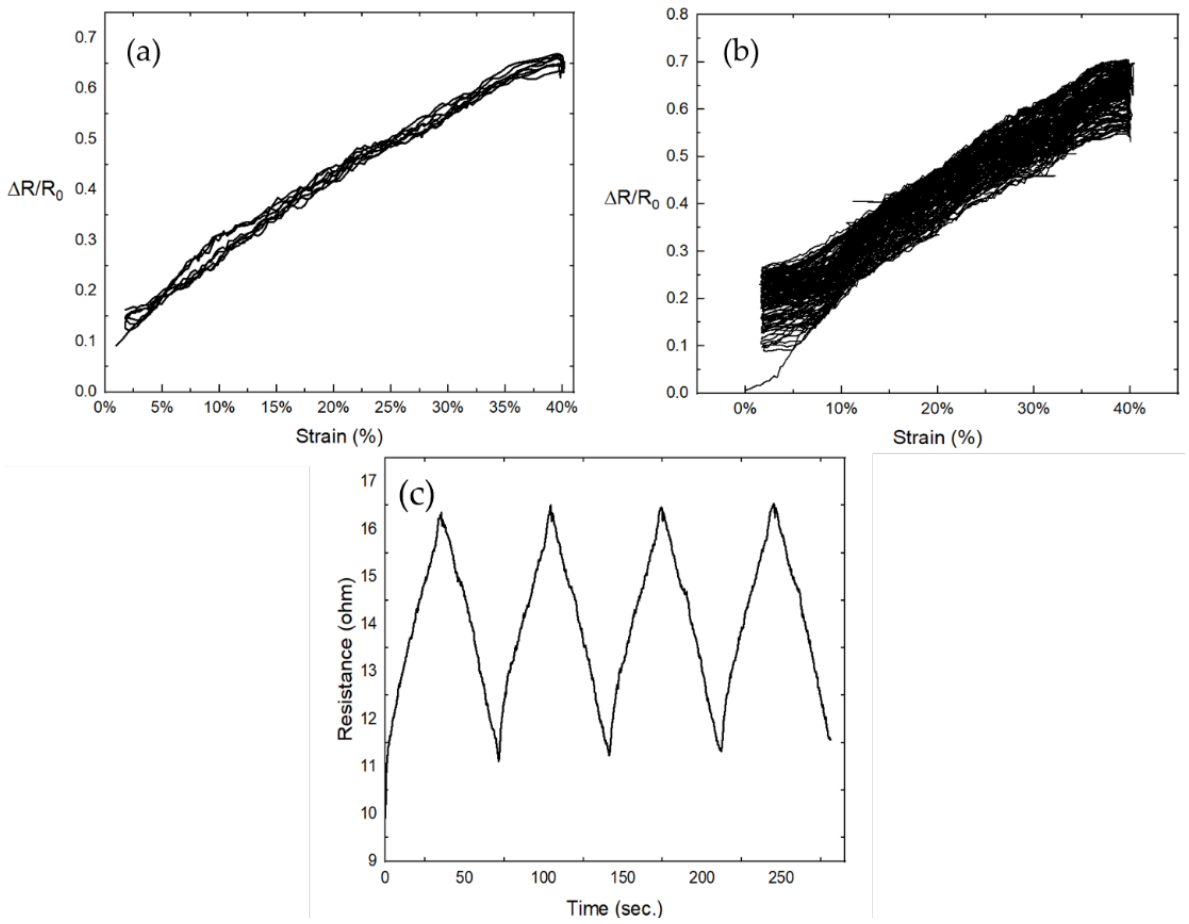


Figure 3.3 The developed knitted strain sensor graphs under four cyclic tests, (a) Relative resistance change versus strain, (b) Relative resistance change versus strain for 70 repetitive cycles, (c) Resistance changes versus time at a strain 40% under 4 cycles.

The static-hold strains during the cycles of the loading and unloading test are measured to demonstrate the retention property of the knitted strain sensor in Figure 3.4a. In the cycles, the strain was increased with a speed of 30 mm/min to the maximal value and held for 10s; then it was released to 0% and held again for

another 10s. The fourth cycle of the hold test was selected and illustrated in Figure 3.4b. During the holding phase, the resistance drops by 4.9 percent (-0.008 percentage point (pp)) which is attributed to the knitting sensor structure. After a full cycle, the resistance can be seen to return to its original value.

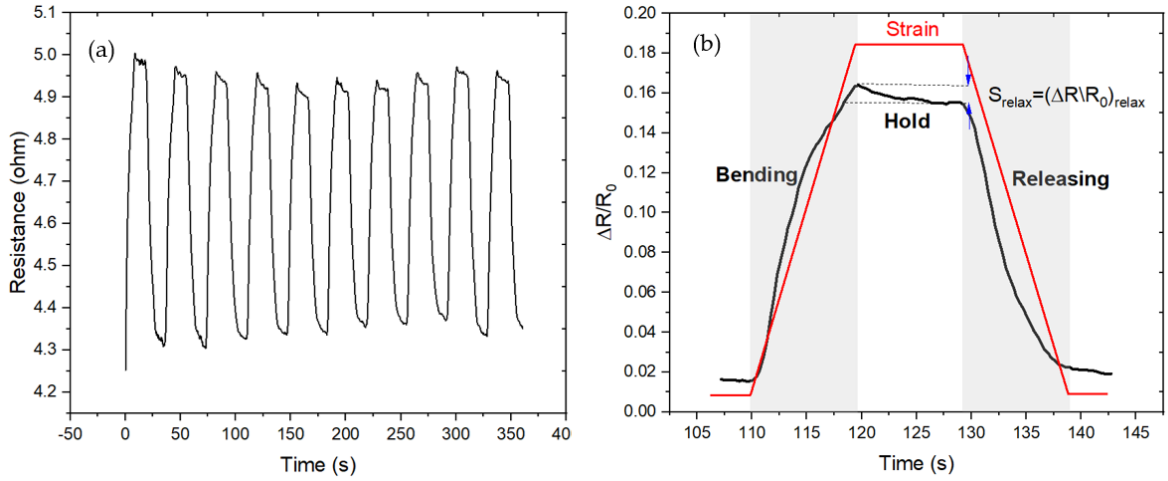


Figure 3.4 The cyclic hold test of knitted strain sensor: (a) Resistance versus time graph when the hold time was set as 10 s, and (b) Relaxation during the holding phase.

3.2.2 Application of knitted strain sensor for rehabilitation purposes

The Version 1 and Version 2 sensor designs were first tested on different fingers. The pink finger was considered too small for the present sensor versions and was not included in the measurements. And the results are summarized in Table 3.1. The tests were applied to each finger 4 times and their mean, standard deviations, and coefficients of variation (CV) were listed. The lower the CV value, which means less variability around the mean, the more precise and reproducible the results. The index shows the highest resistance change with the lowest variations, and subsequent tests focused on the use of the index finger for sensor performance evaluation.

Table 3.1 Variability of demonstrator measurements for repeatability.

Finger	Version 1			Version 2		
	Relative Resistance Change (ΔR/R0)					
	Mean	SD	CV (%)	Mean	SD	CV (%)
Thumb	0.30	0.01	0.05	0.44	0.07	0.16
Index	0.31	0.02	0.06	0.53	0.05	0.09
Middle	0.21	0.04	0.18	0.42	0.06	0.14
Ring	0.25	0.04	0.17	0.42	0.07	0.17

The sensor performance was evaluated by collecting the electrical resistance and time values at different angles of the finger. For both designs as illustrated in Figure 3.2, the effect of various angles on resistance change during finger bending and holding was investigated, and results are shown in Figure 3.5. It illustrates the dynamic resistance response of both sensor versions at different bending angles, highlighting differences in signal amplitude, peak behavior, and stability during holding phases. The response of the sensor to the dynamic bending at positions of 45° and 90° is accurate for both demonstrators. A sharp peak in resistance was always observed directly after bending for each version. Where the Version 1 design shows resistance changes of 0.17 to 0.18, respectively, the Version 2 sensor shows resistance changes of 0.05 and 0.04 when the angles change

from 0 to 45 and 45 to 90 degrees as shown in Figure 3.5b and Figure 3.5d. These measurements were made based on the resistance after the first peak at each angle. The relative resistance changes between the two design versions can be observed to be 3.4 to 4.5 times higher for Version 2 in comparison to Version 1, respectively. For both versions, the peaks are followed by a gradual decrease during holding. In different studies, it is common to see that resistance cannot sustain its value for textile-based sensors when the sensor is held [23]. The signal noises during holding can be explained by small muscles or joint twitching [24].

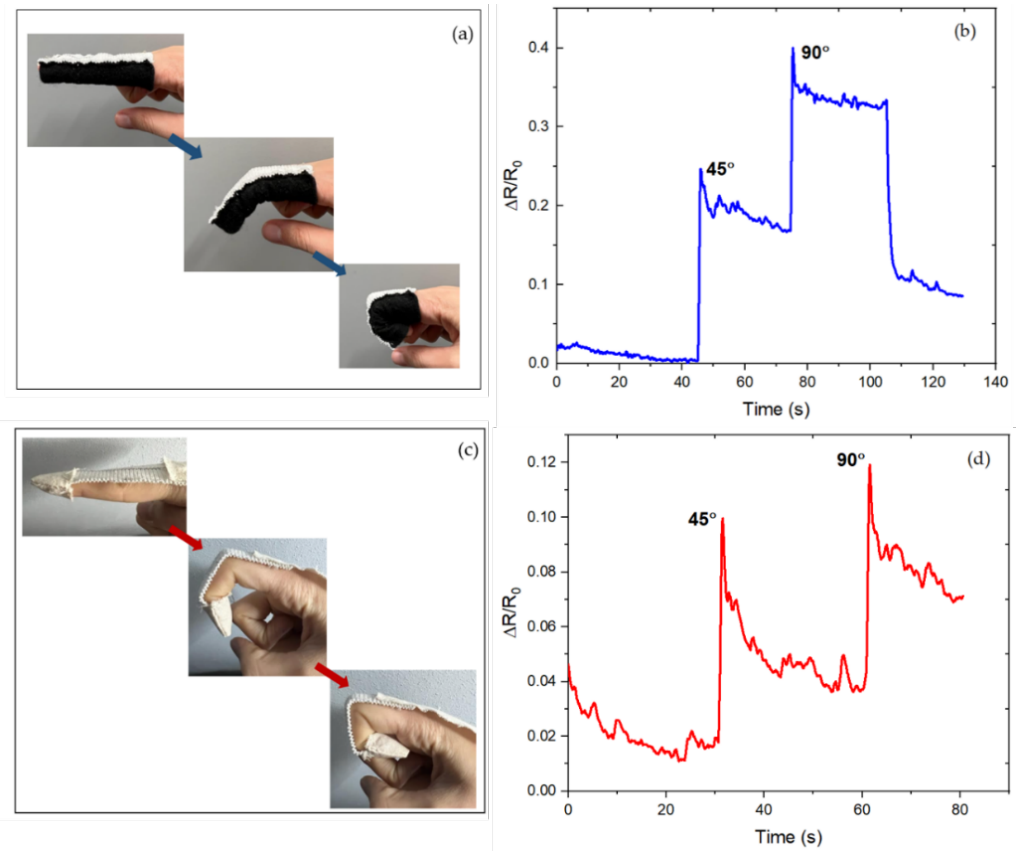


Figure 3.5 The relative resistance change versus time for Version 1 and Version 2 at various positions: relaxation, 45° and 90°; (a) The positions of fully fashioned sensors at different angles, (b) Relative resistance changes versus time of fully-fashioned sensor (c) The positions of the semi-covered sensor at different angles and (d) Relative resistance changes versus time of the semi-covered sensor.

The effect of different angles and layer thickness on finger movement of demonstrator performance

Further tests were applied to Version 1, and the repeated 0-45-90 degrees finger movements were measured for four trials and illustrated in Figure 3.6. With the increase in the bending angle of the finger joint from 0° to 45° and then to 90°, the change of the relative resistance value gradually increases, and it can be tracked with three different signals. The repetitive signals showed that the Version 1 finger sensor can distinguish the finger movements while establishing a trend in each finger move. While all tests give distinguishable and similar signals in the 4 trials, after the first bending cycle, the bandwidth between the lower and upper peaks remains reasonably constant for tests 1 and 3. This was not observed in the rest of the tests.

Apart from the repeated tests on Version 1, a further test was also carried out by increasing the layer thickness between the sensor and the finger to observe the effect of the layers on whether the sensor is tightly wrapped with the finger during movement. This will be explained by the formula as shown in Equation 1 and Figure 3.7, where R represents the distance from the point where the finger is bent and D represents the finger thickness. The h_{layer} is the thickness of the layer that is added in between the finger and the sensor.

$$\varepsilon_{stretch} = (D/2+h_{layer})/R, \quad (1)$$

In the first Version 1 sensor design, the thickness of the substrate fabric was 0.1 cm, and the test was carried out by adjusting this thickness up to 0.4 cm by changing the layer number in between. The tests were done at an angle of 45 and the results are shown in Table 3.2.

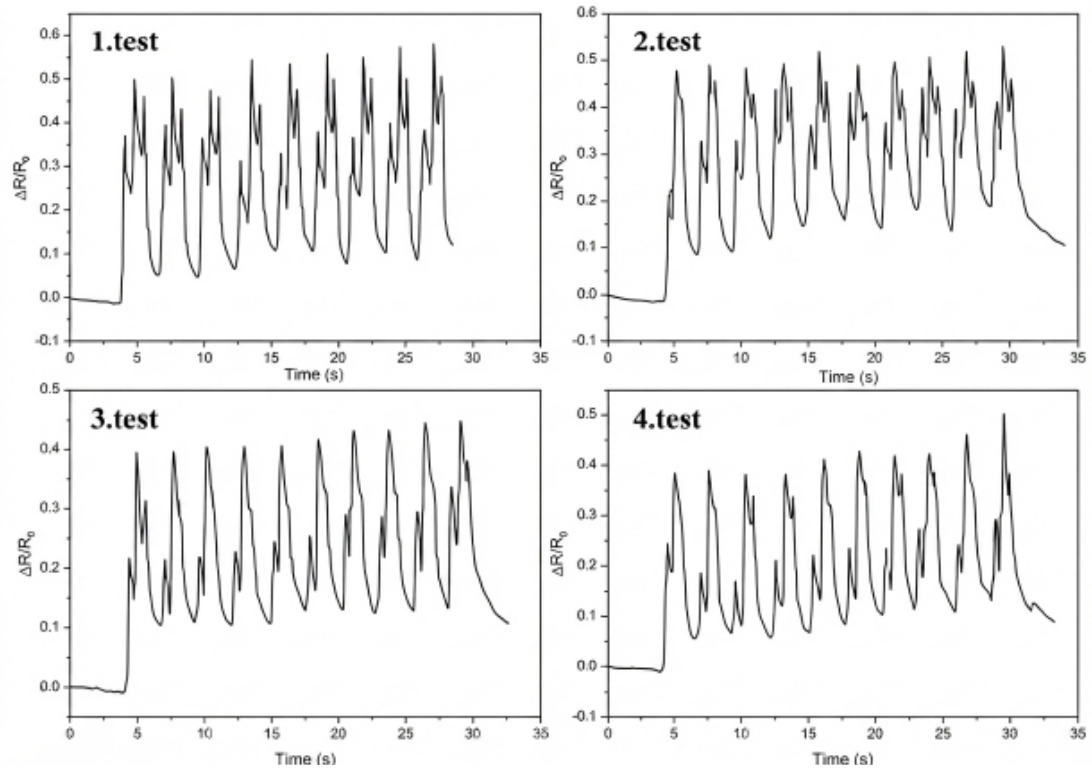


Figure 3.6 The performance of the fully formed sensor (Version 1) in four different trials with repeated finger movements 0-45-90 degrees.

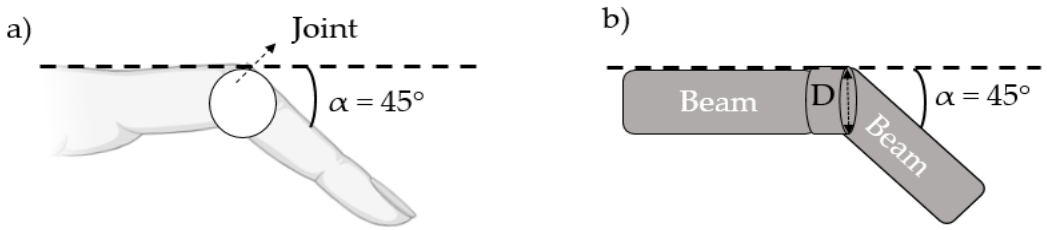


Figure 3.7 (a) The schematic illustration of the bent finger, and (b) Side view of the relaxed finger.

When the number of layers is increased up to 2, the resistance change tends to increase, while when it is above 4, the resistance decreases. Increasing the number of spacer layers initially enhances resistance change; however, beyond a certain thickness, the response decreases due to restricted finger mobility. In addition, the resistance change when the number of layers is 2 was found to be 0.40. This is equal to the value obtained at a 90-degree angle during the normal repetitive test as illustrated in Figure 3.3b.

Table 3.2 The effect of layer thickness on resistance changes at an angle of 45°.

Angle	Layer number	εstretch	$\Delta R/R_0$
45	0	0.25	0.18±0.01
45	1	0.28	0.28±0.02

45	2	0.31	0.41±0.02
45	4	0.38	0.19±0.01

3.3 Discussion

Knitted strain sensors integrated into the finger show a change in resistance due to a deformation caused by the finger's inclination at various angles. This resistance change is due to the elongation of the conductive yarn in the knitted structure, and the contact points between the successive knitted loops of the conductive yarn are separated, causing the sensor to change its resistance [25].

Different sensor designs cause differences in resistance changes. The Version 1 sensor is better than Version 2 in distinguishing different angles at 45 and 90 degrees. This can be explained by the full coverage of the sensor on the finger because of the tubular form. The slackness seen in version 2 causes the deformation during finger movement not to be fully achieved, which can be a reason for the lower resistance change. When examining the effect of layer thickness, it is known that there is a space between the finger and the sensor in the lower layers such as for 0 and 1 layers. As the number of layers increased, the gap between the sensor and the finger decreased, allowing the sensor to fully conform to the finger's surface. Also, the layers between the sensor and finger increase the distance to the neutral plane thus the amount of sensor stretches. That results in an increase in resistance change up to an $\varepsilon_{stretch}$ of 0.31. However, as the number of layers increases, the ease of finger movement decreases, and this increase in resistance is not observed. Overall, it means that the sensor design must be optimized so that it does not create slackness.

3.4 Conclusion

We produced finger sensor designs for rehabilitation applications. The previously developed knitted strain sensor [21] is integrated into a finger, and the performance of the integrated sensor is tested at different bending angles of the finger.

- The index finger shows the highest resistance change with the lowest variations for different finger sensor versions; thus, all tests were followed on the index finger.
- The response of the sensor to the dynamic bending at positions of 45° and 90° is accurate for both demonstrators. However, the resistance change is higher in Version 1 in comparison to Version 2. For both versions, the peaks are followed by a gradual decrease during holding.
- As the number of layers increases, the change in resistance tends to increase, while as the number of layers increases, the change in resistance tends to decrease. This is because finger movement gradually decreases as the number of layers increases.

Despite these promising results, the evaluation of the proposed finger sensor is primarily limited to technical performance under controlled laboratory conditions. Comprehensive validation, including user studies and real-world deployment, is beyond the scope of this study and is identified as future work.

References

1. Zhang, L., et al., A self-protective, reproducible textile sensor with high performance towards human–machine interactions. Journal of Materials Chemistry A, 2019. 7(46): p. 26631-26640.
2. Li, B., et al., A flexible humidity sensor based on silk fabrics for human respiration monitoring. Journal of Materials Chemistry C, 2018. 6(16): p. 4549-4554.
3. Massaroni, C., et al., Smart Textile Based on Piezoresistive Sensing Elements for Respiratory Monitoring. IEEE Sensors Journal, 2019. 17: p. 7718-7725.
4. Lin, B.S., et al., Design of an Inertial-Sensor-Based Data Glove for Hand Function Evaluation. Sensors, 2018. 18(5).
5. Locher, I.a.A.G.S., Joining technologies for smart textiles. in Multidisciplinary Know-How for Smart-Textiles Developers, 2013: p. 285-305.
6. Hatamie, A., et al., Review—Textile Based Chemical and Physical Sensors for Healthcare Monitoring. Journal of The Electrochemical Society,, 2020. 167(3).
7. Coyle, S.a.D.D., Medical applications of smart textiles. in Advances in Smart Medical Textiles., 2016: p. 215-237.
8. Reddy K, R., S. Gandla, and D. Gupta, , Highly Sensitive, Rugged, and Wearable Fabric Strain Sensor Based on Graphene Clad Polyester Knitted Elastic Band for Human Motion Monitoring. Advanced Materials Interfaces, 2019. 6(16).
9. Tian, M., et al., Stretchable and Designable Textile Pattern Strain Sensors Based on Graphene Decorated Conductive Nylon Filaments. Macromolecular Materials and Engineering, 2019. 304(10).
10. Lee, H., et al., Preparation of fabric strain sensor based on graphene for human motion monitoring. Journal of Materials Science, 2018. 53(12): p. 9026-9033.
11. Seyedin, S., et al., Knitted Strain Sensor Textiles of Highly Conductive All-Polymeric Fibers. ACS Appl Mater Interfaces, 2015. 7(38): p. 21150-8.
12. Morteza Amjadi, A.P., Sangjun Lee, Seunghwa Ryu, and Inkyu Park,, Highly Stretchable and Sensitive Strain Sensor Based on Silver Nanowire Elastomer Nanocomposite. . ACS Nano, 2014. 8.
13. Lu, B., et al., , Ultra-flexible Piezoelectric Devices Integrated with Heart to Harvest the Biomechanical Energy. Biomechanical Energy. Sci Rep, 2015. 5: p. 16065.
14. Ryu, H.P., S.; Park, J.J.; Bae, J. A knitted glove sensing system with compression strain for finger movements. Smart Mater. Struct., 2018. 27: p. 055016.
15. Han, X., et al., Research on finger movement sensing performance of conductive gloves. Journal of Engineered Fibers and Fabrics, 2019. 14.
16. Han, X., et al., A Fabric-Based Integrated Sensor Glove System Recognizing Hand Gesture. Autex Research Journal, 2021.
17. Lee, S., et al., A Knitted Sensing Glove for Human Hand Postures Pattern Recognition. Sensors (Basel), 2021. 21(4). A Knitted Sensing Glove for Human Hand Postures Pattern Recognition. Sensors, 2021. 21(4).
18. Isaia, C.M., S.; McNally, D., The effect of washing on the electrical performance of knitted textile strain sensors for quantifying joint motion. J. Ind. Text., 2022. 51: p. 8528S–8548S.
19. Jansen, K.M., Performance evaluation of knitted and stitched textile strain sensors. Sensors, 2020. 20(24): p. 7236.
20. Jansen, K., Performance evaluation of knitted and stitched textile strain sensors. Sensors, 2020. 20: p.

7236.

21. Bozali, B., Ghodrat, S., Plaude, L., van Dam, J. J., & Jansen, K. M. , Development of low hysteresis, linear weft-knitted strain sensors for smart textile applications. Sensors, 2022. 22(19): p. 7688.

22. Lu, S., et al., A 3-D finger motion measurement system via soft strain sensors for hand rehabilitation. Sensors and Actuators A: Physical, 2019. 285: p. 700-711.

23. Huang, F., et al., High-linearity, ultralow-detection-limit, and rapid-response strain sensing yarn for data gloves. . Journal of Industrial Textiles, 2022. 51: p. 4554S-4570S.

24. Li, Y.M., X.; Chen, J.Y.; Jiang, G.; Liu, Q. , Sensing performance of knitted strain sensor on two-dimensional and three-dimensional surfaces. Mater. Des., 2021. 197: p. 109273.

25. Atalay, O.K., W.R.; Demirok, E. , Weft-knitted strain sensor for monitoring respiratory rate and its electro-mechanical modeling. IEEE Sensors J., 2014. 15: p. 110–122.

26. Li, Y., et al., Sensing performance of knitted strain sensor on two-dimensional and three-dimensional surfaces. Materials & Design, 2021. 197.

27. Takamatsu, S., et al., Wearable Keyboard Using Conducting Polymer Electrodes on Textiles. Adv Mater,, 2016. 28(22): p. 4485-8.

Chapter 4

4. Development of knitted pressure sensors

While Chapter 3 focuses on applications of knitted strain sensors in wearable devices for rehabilitation and health monitoring, Chapter 4 addresses developments in knitted pressure sensors. [3]

As an emerging technology, smart textiles attract a lot of interest in various fields in healthcare, sports, entertainment, etc. The new trend in smart textiles is to design sensor elements that are entirely textile-based consisting of conductive and non-conductive yarns which make the traditional sensor systems more comfortable and available for everyday use. In this study, stretchable knitted pressure sensors with different configurations and designs were produced by using commercial conductive yarns. By controlling the knit structure, the overall resistance can also be fine-tuned for practical pressure sensor applications. The impact of different knit densities and knit designs on the pressure sensing performance is investigated for tactile sensing and force distribution applications for flat-knitted and dome-like knitted sensors. Initial studies showed that the flat structures knitted less densely and, in more stretchers, knit designs result in better sensor performance with a sensitivity of 0.71 kPa^{-1} and within the pressure ranges of 0 to 0.71 kPa and a sensitivity of 0.13 kPa^{-1} within a pressure range of 0.70 to 2.5 kPa. This pressure sensor is knitted with the rib 3x3 design and with a stitch length of 3 mm, and the response time of the sensor is measured as 220 msec. For dome-like pressure sensors, rib 3x3 showed a relatively better sensitivity value within a pressure range of 0 to 10 kPa. A practical application of these sensors can be for touch detection in human-computer interaction applications.

3 *This chapter is based on the following publication: Bozali, B., van Dam, J., Ghodrat, S., & Jansen, K. Design of Knitted Pressure Sensors for Tactile Perception Applications.*

Introduction

As an emerging technology, textile-based sensors gained a lot of attention over the years due to their intrinsic softness, flexibility and comfort properties. They can distinguish between various environmental stimuli such as strain, pressure and temperature which enables them to be used in applications such as human-computer interaction [1], health monitoring applications [2], human motion recognition [3], and so on.

Textile-based pressure sensors show high-pressure sensing ability and improved flexibility when compared to traditional pressure sensors. Depending on the application area, textile pressure sensors can be tuned in to have the desired characteristics. Monitoring physiological characteristics such as speaking, aspiration and pulse require low pressure, ranging from 0 to 10 kPa. The medium pressure range (about 10-100 kPa) is suitable for the detection of finger movements like clicking a mouse button, whereas the high-pressure range (100 to 1000 kPa) can be used for pressure sensing in socks and wheelchairs[4]. In addition to the pressure range, other performance indicators are sensitivity, durability, detection range and response time [5].

Textile-based pressure sensors manufactured from commercially available materials have been studied previously by several researchers. Riley, Oliveria, Morris and Dias focused on knitted spacer pressure sensors for monitoring wheelchair users' seat posture [6]. They explored the effect of pressure, applied pressure area and hysteresis of the sensor and found out that knitted sensors could measure up to a pressure of 25 kPa. Baribina, Oks, and Eizentals studied the comparative analysis of the effect of pressure loads on knitted pressure sensors with different shapes and knitted with copper-coated acrylic yarns. They concluded that filled-shaped sensors in rectangular forms show the highest sensitivity at lower pressures [7]. Tian et al. produced a piezoresistive pressure sensor in the form of a composite pillow and noted that the sensor showed a high sensitivity of 3.5 kPa^{-1} and good durability. They also concluded that the change in diameter under pressure results in a big change in sensitivity which proves the importance of the structural design of pressure sensors [8]. Although metallic particle-coated yarns and conductive blended yarns have been used for making knitted pressure sensors [9], there is still a lack of attention on directly implementing conductive yarn into piezoresistive pressure sensors. In this study, we investigate the performance of knitted pressure sensors using commercial conductive yarns and materials. The proposed knitted pressure sensor designs possess the potential to be used in different application areas.

This paper is structured as follows: In Section I, there will be an introduction to textile-based pressure sensors, followed by an experimental section in Section II describing the material and measurement technique. Results and discussion will be summarized in Section III, and the paper is finalized with the conclusion in Section IV.

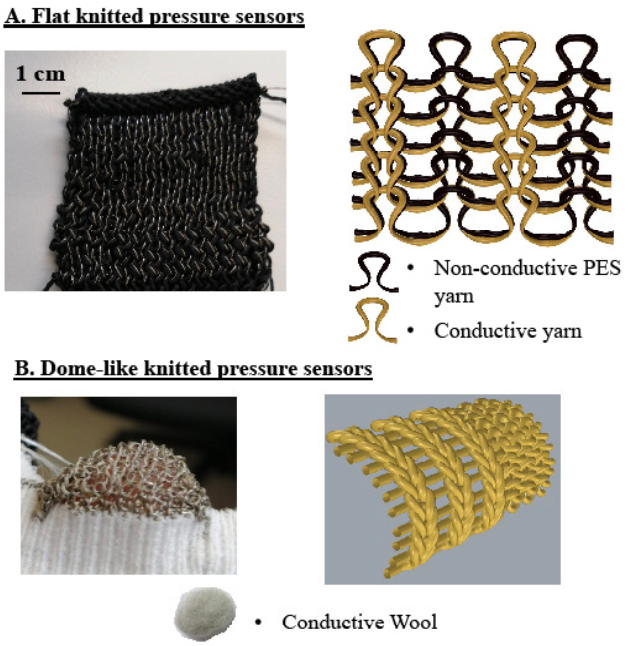


Figure 4.1 Knitted pressure sensors: A: Flat-knitted, B: Dome-like knitted pressure sensors.

4.1 Materials and Methods

In this paper, we conducted a study on the electromechanical performance of knitted pressure sensors in which the material and process parameters were varied systematically. In terms of the materials, silver-plated nylon yarn from Shieldex with a resistivity of ≥600 Ω/m and non-conductive PES yarn with a linear density of dtex 110/32 is used. The stitch density and the knit designs were the two parameters that we changed as knitting parameters for the pressure sensors. As shown in Figure 4.1, two types of designs were produced one of which is rectangular and the other in a dome-like form. These forms were selected to investigate the importance of the structural design on sensing performance. The advantages and disadvantages of two different sensors were compared in Table 4.1.

Table 4.1 Comparison of flat and dome-like knitted pressure sensors.

A&D	Comparison of flat and dome-like sensors	
	Flat knitted sensors	**Dome-like sensors**
Advantages	Easy to produce at one go. Can be directly attached to the skin.	Short response time. Easy to use for tactile perception application-bump form
Disadvantages	Low detection range	Complex sensor design

Rectangular samples were knitted via plating technique in such a way conductive and non-conductive yarn were knitted together. The dimension of the flat knitted sensors is 4 x 4 cm^2. NP number and knit design were changed to examine the sensitivity, detection range and stability performance of the samples. The NP number which refers to the number of pitches directly change the loop length and changes the fabric tightness. In dome-like structures, the sensor part was produced only by using conductive yarn. The diameter (D) of the dome-like pressure sensor is 24 mm, and its area is calculated with the formula of $S=\pi(D/2)^2$. To gather the resistance change values under deformation, conductive wool which was purchased from Bekinox® W12/8 as a filler was inserted inside and optimized. The knitted pressure sensors used in this study have been weft-knitted on a Stoll CMS 530 flat knitting machine with an E8 machine gauge and 0.30 m/s.

Knitted pressure sensors were evaluated in terms of sensitivity, in which P refers to applied pressure while ΔR refers to the resistance change and R_0 is the initial resistance of the sensor.

$$S = (\Delta R/R_0)/P \quad (1)$$

Sensitivity tests were conducted for flat knitted sensors by applying the same size blocks as pressure. And for dome-like knitted pressure sensors, sensitivity tests were conducted by using a rheometer in compression mode. During the test, a digital multimeter was used to record the sensor's resistance by connecting the cables on the sensor's edges, and 2 wire resistance measurement was conducted. The test speed was set as 20 μm/sec. The axial force range is set to be between 0 and 10N.

4.2 Results and Discussion

In this section, the sensor performances of flat-knitted and dome-like pressure sensors will be analysed, and the results will be discussed in terms of sensitivity and detection range.

4.2.1 Analysis of flat knitted pressure sensors

Flat knitted sensors in different knit designs were evaluated in terms of sensitivity and detection range. Resistance changes were collected by loading different weights on top of the sensors and tests were conducted three times per set. Pressure sensors in the forms of rib 1x2, 2x2 and 3x3 were knitted in different NPs of 14 and 15. As can be seen in Table 4.2, the pressure sensitivity of the rib 2x2 and rib 3x3 sensors increases as the loop length increased from NP 14 to NP 15. Fabrics with high stretchability allow the creation of more pressure-sensitive sensors [3]. In addition to that, rib 3x3 sensors have a higher elasticity than the rib 2x2 which can explain the better sensitivity values. Under loading, yarn-to-yarn contacts are adjusted which leads to a change in overall fabric resistance [9]. Response time is another important parameter to minimize delays during application. The rib 3x3 design knitted with NP 15 has a response time of 220 msec with a detection range of 0-0.7 kPa.

Table 4.2 Sensitivity results of flat-knitted pressure sensors.

Knit Design	Electromechanical Properties		
	NP	Sensitivity (kPa^{-1})	Detection Range (kPa)
Rib 1x2	15	0.10±0.06	0-2.6
Rib 1x2	14	0.23±0.01	0-0.7
Rib 2x2	15	0.28±0.02	0-2.0
Rib 2x2	14	0.09±0.004	0-1.3
Rib 3x3	15	0.71±0.01	0-0.7
Rib 3x3	14	0.05±0.03	0-2.0

As a preliminary study, rib 3x3 sensors knitted with NP 15 were tested to explore whether the sensor distinguish the different pressures. Blocks of the same size corresponding to 1.2N are used to investigate the effect of pressure on resistance by applying pressure to the sensor area. As shown in Table 4.2, the rib 3x3 flat knitted sensor has a good ability to distinguish the different loading forces.

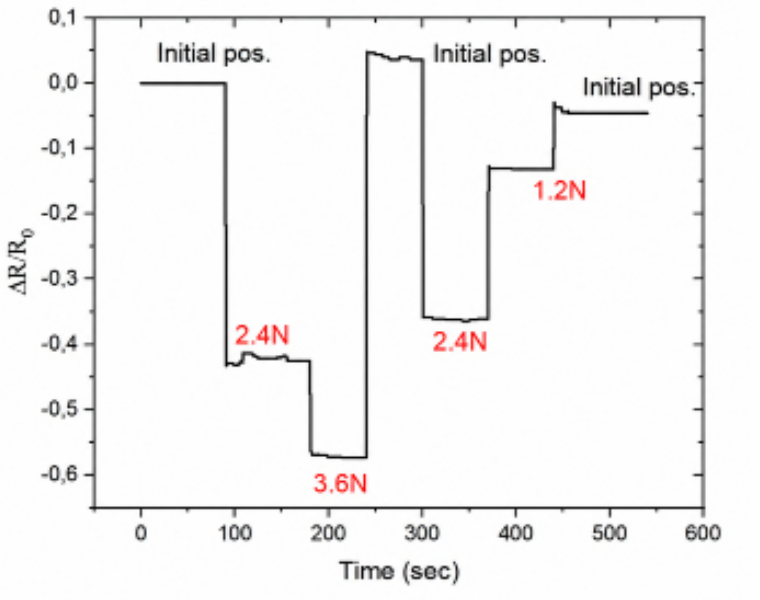


Figure 4.2 The response of the rib 3x3 sensor knitted with NP15 when different pressure is loading and unloading.

4.2.2 Analysis of dome-like knitted pressure sensors

In this section, dome-like knitted pressure sensors were prepared, and the performance was evaluated in terms of sensitivity and detection range. Because of the difficulties in the manufacturing process, samples were not produced with higher NPs like in the flat knitted sensors and were knitted with NP 9. rib 2x2 and rib 3x3 samples were produced. The conductive wool amount is set as 0.046g. The results were depicted in Table 4.3. The Rib 3x3 sensor showed better sensitivity performance than rib 2x2 at a pressure range of 0-10 kPa.

As mentioned in Table 4.1, the detection range of flat-knitted sensors is lower than the dome-like sensors because of the contact areas and the interfaces related to the sensor design. When we think about the tactile perception application, a higher detection range is needed to be efficiently used which makes dome-like structures more promising. And higher sensitivities were observed for flat-knitted sensors at low detection ranges with looser samples. This can be related to the diameter variation in the conductive-filled assembly fibers, sensitivity changes can be obtained [9]. For future studies, dome-like sensors will be produced in a looser form, and the sensitivity range will be compared with the flat knit sensors at lower pressures.

Table 4.3 Sensitivity results of dome-like knitted pressure sensors

Sample Names	Electromechanical Properties		
	Filler (g)	Sensitivity (kPa^{-1})	Detection Range (kPa)
Rib 3x3	0.046	0.020±0.004	0-10
Rib 2x2	0.046	0.015±0.001	0-10

The rib 3x3 dome-like sensor knitted with NP 9 was further investigated to explore its performance during loading and unloading. As shown in Figure 4.3, 4 cycles were applied, and it demonstrates that the sensor responds to the pressure changes. The dome-like knitted sensors have much lower sensitivity than the flat knitted sensors but do react properly when activated by a light finger press.

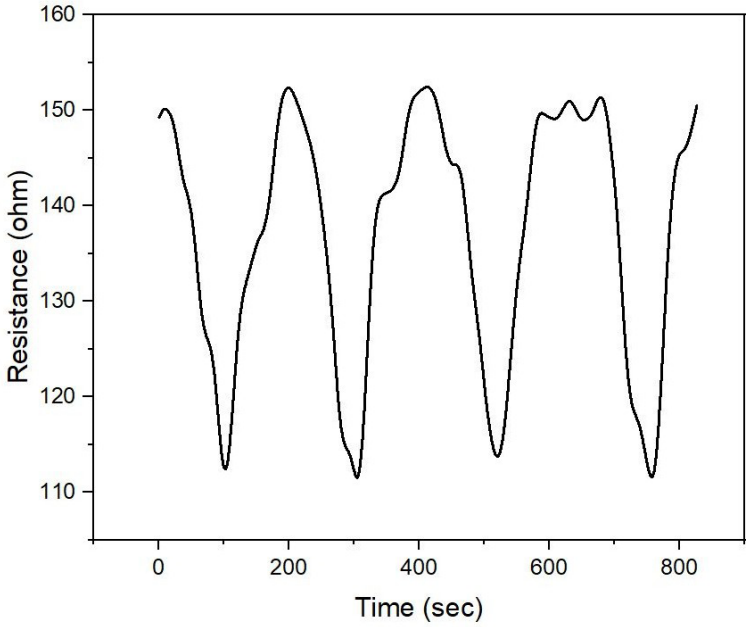


Figure 4.3 Cyclic test of Rib 3x3 dome-like knitted sensor.

4.3 Conclusion

This study demonstrates the importance of the structural design of knitted pressure sensors. Two different types of knit designs were produced, and their sensor performance was evaluated. In the flat knitted form, rib 3x3 with NP 15 possesses a high sensitivity of 0.71±0.01 kPa^{-1}. Apart from flat knitted structures, dome-like pressure sensors in the Rib design were produced and their sensor performance was evaluated. In the flat knitted form, rib 3x3 with NP 15 possesses a high sensitivity of 0.71±0.01 kPa^{-1}. Apart from flat knitted structures, a dome-like pressure sensor in the rib 3x3 form also possesses a potential design with a quick response time and a good sensitivity.

Flat knitted can be directly attached to the skin or large area textiles and be utilized for human-computer interface systems. Dome-like sensors were found to be promising for tactile applications such as the detection of finger movements by pinch or pressure sensing mats for shape or object recognition. Also, the user can perceive the sensors as protrusions by touching them, which provides convenience in the application.

For future studies, dome-like pressure sensors will be evaluated in detail by changing the filler content, type of filler and the shape of the dome. The production of multiple dome-like pressure sensors will be done at one-go and be tested for pressure sensing performance.

References

1. L. Zhang, J.H., Y. Liao, X. Zeng, N. Qiu, Y. Liang, P. Xiao, T. Chen, A self-protective, reproducible textile sensor with high performance towards human-machine interactions. Journal of Materials Chemistry A,, 2019. 46: p. 26631-26640.
2. J. Zhang, T.G.Y., M. A. MJ, S. A. Imam, and A. Zhao, A review of passive RFID tag antenna-based sensors and systems for structural health monitoring applications. Sensors, 2017: p. 265-298.
3. C. Jingyuan, M.S., B. Zhou, M. Hirsch, and P. Lukowicz, Smart-surface: Large scale textile pressure sensors arrays for activity recognition. Pervasive and Mobile Computing, 2016. 30: p. 97-112.
4. L. Possanzini, M.T., L. Mazzocchetti, E. Campari, and B. Fraboni, Impact of fabric properties on textile pressure sensors performance. Sensors, 2019: p. 4686-4701.
5. J. Zhang, Y.Z., L. Yuan-yuan, and P. Wang, Textile-based flexible pressure sensors: A review,. Polymer Reviews, 2022: p. 65-94.
6. T. Hughes-Riley, C.O., R. Morris, and T. Dias, The characterization of a pressure sensor constructed from a knitted spacer structure. Digital Medicine, 2019. 5: p. 22-29.
7. N. Baribina, A.O., I. Baltina, and P. Eizentals, Comparative analysis of knitted pressure sensors. 7th International Scientific Conference, 2018: p. 1599-1604.
8. M. Tian, L.Y., Q. Lijun, S. Zhu, X. Zhang, and S. Chen, A pillow- shaped 3D hierarchical piezoresistive pressure sensor based on con- ductive silver components-coated fabric and random fibers assembly. Industrial Engineering Chemistry Research, 2019. 58: p. 5737–5742.
9. Xie, J.L., H.; Miao, M., High sensitivity knitted fabric strain sensors. Smart Mater. Struct., 2016. 25: p. 105008.

Chapter 5

5. Development of knitted heaters

This chapter introduces the design and optimization of knitted textile heaters for wearable applications. A physics-based model links resistance, power, and temperature distribution to material and structural parameters, validated through experiments. The findings provide design guidelines for uniform, safe, and efficient heating, highlighting the potential of knitted heaters in wearable health, comfort and therapeutic applications.[4]

Knitted heaters have attracted significant interest due to their flexibility and ease of integration into smart textile applications. However, uneven heat distribution remains a major challenge, leading to comfort issues and inefficient energy usage. This study presents an analytical, physics-based model that links the resistance, power distribution, and surface temperature of knitted heaters to key design parameters such as size, configuration, material properties, and knitting structure to establish guidelines for achieving a desired temperature rise over a specified surface area. The model was validated experimentally across a range of heaters (3–12 lines) arranged in ladder and diagonal configurations. Results showed good agreement between predictions and measurements for higher line counts (10–12), while larger deviations occurred in smaller heaters (3–5 lines) due to contact resistance and current losses. A prototype knitted wristband demonstrated physiologically relevant heating (>33 °C) under safe, low-voltage operation. These findings provide a quantitative design framework for optimizing knitted heaters and highlight their potential for scalable integration into wearable and therapeutic applications.

4 *This chapter is based on the following publication: Bozali, B., Ghodrat, S., & Jansen, K. M. (2025). Structural Design and Optimization of Knitted Heaters for Optimized Heat Distribution. Thermo, 5 (4), 54.*

Introduction

Smart textiles have attracted significant attention owing to their potential applications in textile-based antennas [1], energy harvesting [2], electromagnetic shielding [3], and health monitoring [4]. Integrating smart functionalities into garments leverages inherent textile qualities such as comfort, breathability, stretchability, and washability. Consequently, textiles serve as ideal platforms for active temperature regulation applications. Such textile heaters are particularly beneficial for soldiers or workers operating in cold environments, as well as for medical applications aiming to reduce thermal stress [4] and to improve thermal comfort in general. They are especially useful for rehabilitation therapies, such as treating rheumatic arthritis and alleviating muscle spasms and inflammation [5]. They aid in reducing joint stiffness, enhancing blood circulation, and improving the flexibility of collagen tissues, all contributing to pain relief through the therapeutic application of heat. They can also be applied to body joints to promote the effective functioning of bodily components and alleviate discomfort in muscles and joints [6]. Even during surgery, textile- based heaters can be used for an anesthetized patient who can experience significant heat loss during surgery [7]. Furthermore, smart heating insoles and socks such as electrical heating pads can be used to improve the thermal comfort of occupational workers in cold environments [8].

The performance of electrical heating textiles relies predominantly on the type of conductive material used in the structure. As conductive materials, metallic wires are commonly used. Hamdani et al. investigated stainless steel as a heater material and concluded that the temperature distribution is primarily concentrated within the central parts of the heater, resulting in non-uniform heat distribution [9]. Yanyan et al. studied the thermal performance of fine copper wire integrated into interlining fabric. They concluded that the breaking strength and elongation at the break of the copper wires remain relatively unaffected by aging time and temperature, displaying favorable thermo-mechanical properties. However, despite these mechanical advantages, metallic wires present several drawbacks when integrated into textiles, primarily due to their reduced flexibility, increasing rigidity, and hindered moisture extraction [10].

Given the limitations of traditional metallic wires, researchers have explored a variety of alternative conductive materials to enhance heater performance using metallic nano- materials, intrinsic conductive polymers (ICPs), graphene, and carbon nanotubes (CNTs). Metallic nanoparticles coated onto the textile can achieve stable heating performance with high surface temperatures at very low electrical potential [11]. However, toxicity and durability restrict wearable applications. Intrinsic conductive polymers (ICPs) can show superior flexibility, light weight, and good conductivity, but they are inferior in long-term stability. Many researchers have explored the impregnation of materials with CNTs and graphene, which have demonstrated excellent heating performance. However, comprehensive reviews on graphene-enhanced textiles and graphene fibers indicate performance advantages (conductivity, flexibility) but also note scale-up and cost barriers for mass production-a key reason most graphene/CNT heater studies remain at lab scale [12, 13]. Apart from the mentioned conductive materials, it is possible to produce heaters from commercially available conductive yarns to overcome the challenges. These yarns are well suited for mass production using existing knitting machinery [14].

While material choice is fundamental, the manufacturing technique also plays a critical role in heater performance, particularly how the conductive yarns are integrated into textile structures. Common approaches include weaving, knitting, and nonwoven fabrication [15]. Different textile fabrication techniques, such as weaving, knitting, and non-woven production, each present specific trade-offs: woven fabrics offer dimensional stability

but may limit stretchability, whereas non-woven structures can pose challenges for uniform integration of conductive elements [5]. Knitted structures, in contrast, offer stretchability, breathability, and close body fit. Knitting also allows tuning of electrical properties through changes in loop density, knit pattern, and yarn configuration. Maurya et al. compared rib, interlock, and plain knit structures with varying knitting densities and concluded that rib knit samples with a compact structure, and a short loop length showed good heating performance [16]. A study by Hamdani et al., on the other hand, concluded that the interlock structure is particularly favored for heating fabrics, primarily due to its stability. Moreover, it has been observed that the interlock structure can achieve a higher temperature compared to the plain structure when subjected to the same voltage. Additionally, the interlock structure reaches its steady-state temperature in less time when compared to the plain knitted structure [9]. Liu et al. investigated plain, rib, and interlock knit fabrics produced from silver-plated yarn and polyester staple yarn and reported that the fabrics' maximum equilibrium temperature increases proportionally with their power consumption density [17]. Six different knit structures were studied by Kexia et al. [18]. They concluded that the temperature of knitted structures increased proportional to the square of the applied voltage and from their results the maximum surface temperature at 2.4 V increases from the plain knit to rib to interlock structure.

In the studies so far, only relatively small-area heaters have been used. Despite these advances, most studies focus on small heating areas and do not fully address current losses in large wearable heaters. However, for medical applications, there is a need to apply textile heaters to larger areas of the body-such as 50x200 mm-while maintaining close contact with the skin. This need for larger, flexible heaters underlines a gap in current research, which our study aims to address. Knitting is the preferred technique. One possible challenge is the occurrence of current losses along the heater length. Adding extra heater lines can lead to uneven heating, with lower temperatures appearing farther away from the power source. In this study, we demonstrate that the performance of textile-based heaters at a given voltage is primarily governed by the electrical resistance of the heater lines, with yarn and knitting parameters playing a more indirect role. Based on our findings, we propose practical guidelines for optimizing knitted heater designs. Our results indicate that heating performance can be effectively tuned by controlling the heater's resistance, which, in turn, can be adjusted through specific knitting parameters and layout configurations.

5.1 Theory

In the literature reviewed above, conflicting conclusions have been reported regarding heater performance. Maurya [16] found that rib structures outperform interlock and plain knits, Hamdani reported that interlock yields higher peak temperatures, and Sun observed the performance order as interlock > rib > plain knit [9]. Such inconsistencies make it difficult for designers and researchers to make informed decisions when selecting heater designs.

From a heat transfer standpoint, however, the governing principles are relatively straightforward. The maximum attainable temperature is determined predominantly by the balance between the applied electrical power and the heat losses to the environment, rather than by the knit structure itself. The heating rate is governed by the ratio of the fabric's thermal mass (i.e., thickness and density) to the heat transfer coefficient. The main influence of knitting parameters arises through their effect on the electrical resistance of the knitted elements. Heater lines with different knitting structure and yarn conductivity but with the same resistance are expected to exhibit essentially equivalent thermal performance. The objective of this section is to develop a simplified

model that addresses these considerations and provides design guidelines for heaters capable of achieving a specified temperature rise over a defined surface area. The core of the model is to connect the three key aspects of heater design using physical equations. This is accomplished by first deriving the equivalent electrical resistance of the different knitted arrangements, then determining the current and power distribution across the heater lines and lead wires and finally formulating the resulting surface temperature rise driven by power input and moderated by heat loss. This framework supports the rational design of heaters optimized for performance, safety and comfort.

A rectangular area can be covered with heater lines using three fundamental configurations.

1. A serpentine (zigzag) pattern (Figure 5.1a), where the heater line meanders across the surface.
2. A ladder configuration (Figure 5.1b), in which two parallel electrode lines distribute power to interconnecting heater wires with higher resistance that dissipate energy.
3. A diagonal configuration (Figure 5.1c), similar to the ladder setup but arranged diagonally.

The ladder configuration is the simplest and most straightforward. However, if the equivalent heater resistance R_{eq} is too high, it can present challenges. Since the heater is designed for applications near human skin, the operating voltage should remain below 50 V to prevent skin irritation [19]. To ensure safety, we limit the maximum voltage to 12 V and the current to approximately 500 mA, allowing for a maximum power output of 6 Watt with a resistance of 24 Ω.

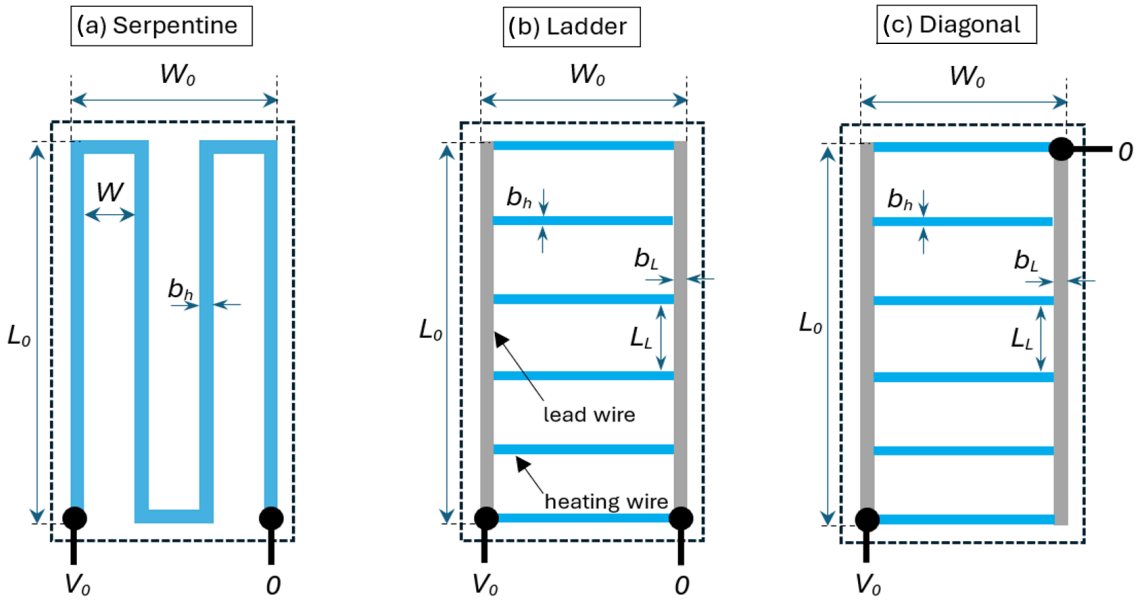


Figure 5.1 Layout and geometrical parameters of a serpentine (a), ladder (b), and diagonal (c) configuration. The power is applied via the connection points, indicated as black circles.

As shown in the experimental section, knitted heater lines typically have resistances exceeding 1 Ω/cm. For example, a heater measuring 15 cm in length and 5 cm in width, arranged in a serpentine pattern with four lines, would have a resistance of approximately 65 Ω. Such a setup would generate only 2.2 Watt, which may be insufficient for adequate heating. To address this, low-resistance lead wires or electrode lines are used to distribute the power to a series of parallel higher-resistance heating elements (Figure 5.1b,c). The ladder configuration benefits from power connection points placed in proximity but suffers from heat loss in wires positioned farther from the power source. In contrast, the diagonal configuration distributes power more evenly across the surface, mitigating this issue.

The equivalent resistance of the serpentine configuration is given as (see Figure 5.1a)

$$R_{eq}^{S} = \rho_L (nL_0 + W_0) \quad (1)$$

in which is the resistance per unit length of the heater wire and n denotes the number of longitudinal heater lines. For ideal lead wires with zero resistance, the equivalent resistances of both the ladder and diagonal configuration would be given as $R_{eq} = R_h/n$, in which R_h denotes the heating wire resistance. In practice, the lead wire segments between the heating wires have a small but finite resistance. As demonstrated by Jansen [20], the expression for the equivalent resistances of the ladder configurations can then be written as

$$R_{eq}^{L} = R_h (1-\sinh[(n-1)\sqrt{\varepsilon}]/\sinh[n\sqrt{\varepsilon}]), \qquad \varepsilon=(2R_L)/R_h \quad (2)$$

and for the diagonal configuration as

$$R_{eq}^{D} = R_h(1/2 \coth[n/2\sqrt{\varepsilon}]\sinh[\sqrt{\varepsilon}] + 1/4(n-2)\varepsilon) \quad (3)$$

where is the ratio between twice the lead wire resistance, R_L, and the heater resistance R_h. With these expressions we can immediately estimate the overall resistance and thus the total power that can be generated by the heaters.

$$P_{tot} = V_0^2/R_{eq} \quad (4)$$

As mentioned before, this power is not evenly distributed over the heater surface, so, as a next step we would like to calculate the local power p in the heater wires and lead wire parts. For this, we need the local currents and :

$$p_h = i_h^2 R_h \qquad p_L = i_L 2R_L \quad (5)$$

where subscripts h and L stand for the heater and lead wire, respectively. By using the finite difference method, Jansen [20] derived the following closed-form expressions for the current distributions in ladder resistor networks.

$$i_{(A,k)} = I_0(\sinh[(n-k)\sqrt{\varepsilon}])/\sinh[n\sqrt{\varepsilon}],\ i_{(h,k)} = V_0/R_h(\cosh[(n-k+1/2)\sqrt{\varepsilon}])/(\cosh[(n-1/2)\sqrt{\varepsilon}]),\ I_0=V_0/R_{eq} \quad (6)$$

whereas for the diagonal configuration, they are given as

$$i_{(A,k)} = 1/2\ I_0(1-(\sinh[(k-n/2)\sqrt{\varepsilon}])/\sinh[n/2\sqrt{\varepsilon}]), \qquad i_{(h,k)} = (I(_0)\sinh[\sqrt{\varepsilon}/2])/\sinh[n/2\sqrt{\varepsilon}]\ \cosh[(k-(n+1)/2)\sqrt{\varepsilon}] \quad (7)$$

Here k is the heater wire index, ranging from 1 close to the power source to n at the far end. All these equations depend on three parameters: the heater and lead wire segment resistances and (expressed as the resistance ratio ε) and the number of heater lines n. The resistances can be manipulated by, e.g., changing the line width or length, the knit structure, or choosing a yarn with different conductivity. For the present study, we focus on the geometrical parameters and use the following relation for the resistance of a knitted or embroidered conductive line with length L and width W:

$$R = C_R L/W \quad (8)$$

Here, C_R is the knit structure resistivity that depends on the resistivity of the conductive yarn, as well as the knitting structure and stitch density. This constant can be determined experimentally by measuring the resistance of several knitted lines with varying dimensions. Alternatively, it can be estimated through numerical simulations of the knit structure. Note that in practice, it may be more effective to express length and width in terms of the number of course and wale stitches rather than using standard length measurements.

When a knitted surface is heated, its temperature increases in proportion to the applied heating power until the generated Joule heat balances the heat loss to the environment. As demonstrated by Zhang et al. [21], this behav-

ior can be modeled using a simple exponential relationship.

$$T = T_0 + p_h/hA\ (1\text{-}e^{-t/\tau}), \qquad \tau = h/(\rho_m c_p d) \tag{9}$$

where T_0 is the initial temperature and p_h is the local heating power, h the heat transfer coefficient and A the surface area. The parameter τ is a time constant that depends on the density, heat capacity, and thickness d of the knit structure. In the current paper, we focus on the steady-state temperature rise and rewrite this as

$$\Delta T_{max} = C_H p_h \tag{10}$$

where $C_H = 1/hA$ is a coefficient that can be determined experimentally.

5.2 Materials and Methods

Knitted heaters were fabricated using a combination of knitting and stitching, as illustrated in Figure 5.2. Initially, double-jersey knit samples were produced with varying numbers of heater lines: 2, 3, 5, 10, and 12. The heater lines were formed using silver-plated nylon yarns integrated into the double-jersey base structure, primarily made from cotton. Double jersey was selected to allow the heating yarns to be situated on a single surface of the fabric and to have the back side as an insulation layer. The heaters were produced with an NP11 setting for the knitting density. The fabric structure had a total width of 100 rows, of which 70 rows were for the heater lines. For the heating elements, Shieldex® 235/36 dtex Z 130 HC + B yarn (Statex Produktions und Vertriebs GmbH, Bremen, Germany) was selected due to its relatively high resistivity of approximately 768 Ω/m. Lead wires were fabricated using Shieldex® 235/36 dtex 2-ply HC + B yarn, chosen for its lower resistivity of 50 Ω/m. Modern industrial knitting machines like the Stoll ADF series can produce high-resistivity heater lines and the perpendicular low-resistivity lead wires in a single process. The Stoll CMS 530 flatbed weft knitting machine (Karl Mayer Stoll GmbH & Co., Reutlingen, Germany) used in this study, however, can knit conductive yarns only horizontally in the course direction and lacks independent yarn carrier movement in both directions. Therefore, for the samples used to validate the theoretical section, heater lines were knitted first, and vertical lead wires were subsequently added via embroidery.

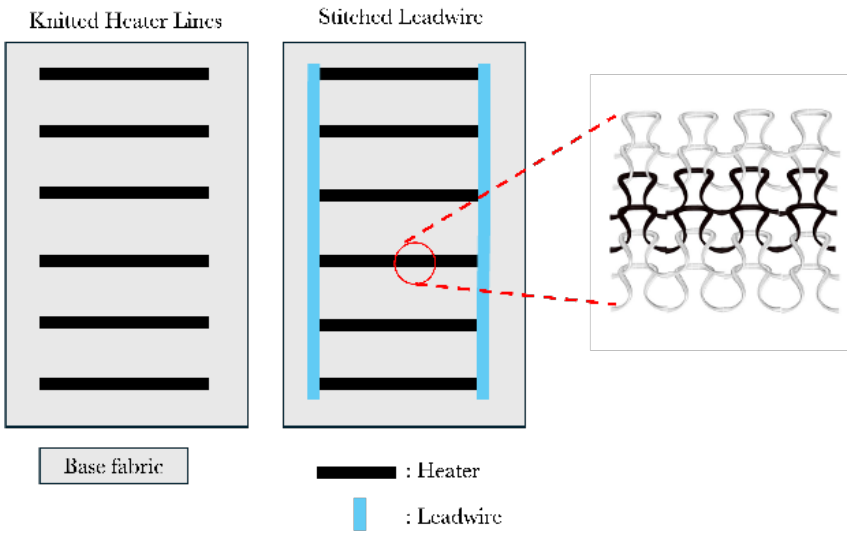


Figure 5.2 Production process of knitted heaters starting with initial knitting followed by stitching of the lead wires.

Two different yarns were used for stitching: a non-conductive yarn positioned on the back and a conductive yarn placed at the desired location on the front. To ensure proper production of the embroidered conductive lead wire on the knitted heater, a layer of Stitch & Tear® (Weinheim, Germany), a stabilizing backing material, was added to support and stabilize the embroidery process. This layer was removed after stitching.

The resistance measurements were carried out using a FLUKE 110 digital multimeter (Everett, WA, USA). The power for the heating tests was supplied by a N6705B DC power analyzer from Agilent Technologies (Santa Clara, CA, USA), and the temperatures were measured using a FLIR E60 thermal camera (Wilsonville, OR, USA) mounted on a tripod. All thermal images were analyzed with Thermal FLIR software (product version: 2.0.37). The knitted samples were clamped onto a frame and placed in free air, as shown in Figure 5.3. The thermal camera consistently recorded the highest temperature within the selected region of interest. For the thermal images' validation, the average temperature of each heater line was determined by drawing a line across each heating element and average temperature using the FLIR Thermal Studio program (product version: 2.0.37).



Figure 5.3 Experimental setup for thermal imaging measurements. A FLIR infrared camera is mounted on a tripod at a fixed distance of 80 cm from the sample, which is secured using a custom clamp to ensure stability during imaging.

5.3 Results

5.3.1 Heater Line Knit Structures

To determine the resistance parameter of Equation (8), samples were knitted with the Shieldex 235/36 dtex-1 ply yarn containing conductive lines with 2, 3, 5, 10, and 12 courses width and 100 wale stitches long. Optical images are shown in Figure 5.4. As the number of courses increases, the coverage of conductive yarn within the fabric becomes noticeably denser reducing the visible gaps between loops. At two and three courses, the conductive yarn is sparsely visible, with significant gaps between loops. With five courses, the structure becomes more uniform. A close-up image of the different courses is shown in Figure 5.5. It also demonstrates that the double-jersey structure, with its different front and back sides, helps produce insulated textile heaters. The stitch densities in the course and wale directions were calculated as 4.72 courses/cm and 10 wales/cm, respectively (see Supporting Information-Figure S2).

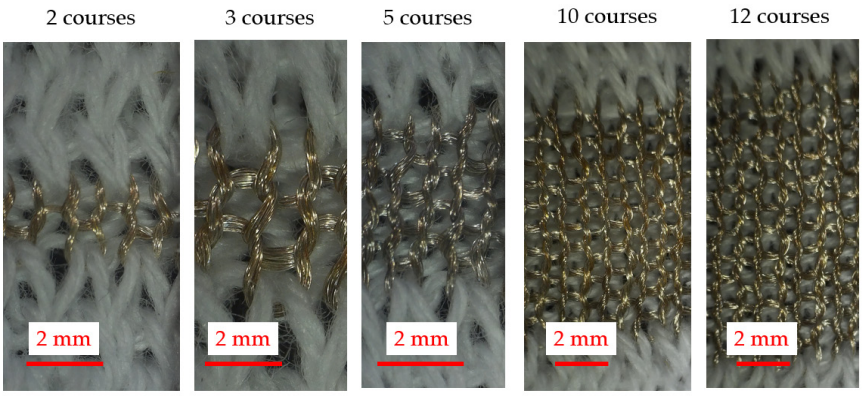


Figure 5.4 Optical images of knitted heaters with different numbers of lines.

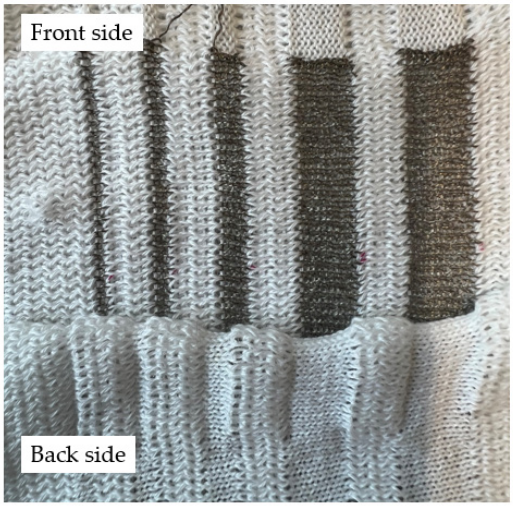


Figure 5.5 Heater lines with 12, 10, 5, 3, and 2 courses at the front side (upper part) and the insulated back side (lower part).

5.3.2 Equivalent Resistances of Knitted Heaters

The overall heater resistances predicted by Equations (2) and (3) are compared with the measured values in Figure 5.6. The comparison reveals that the equivalent resistance decreases as the number of heater lines increases. In both graphs, the measured values closely follow the calculated values, indicating that the theoretical or modeled calculations align well with the experimental measurements. The largest drop in resistance occurs between one and three heater lines, and the curves tend to flatten as the number of lines in-creases, suggesting diminishing changes in R_{eq} for higher numbers of heater lines. The similarity of the deviations observed in both configurations indicates that the model captures the physical behavior of the system, while opportunities for refinement remain.

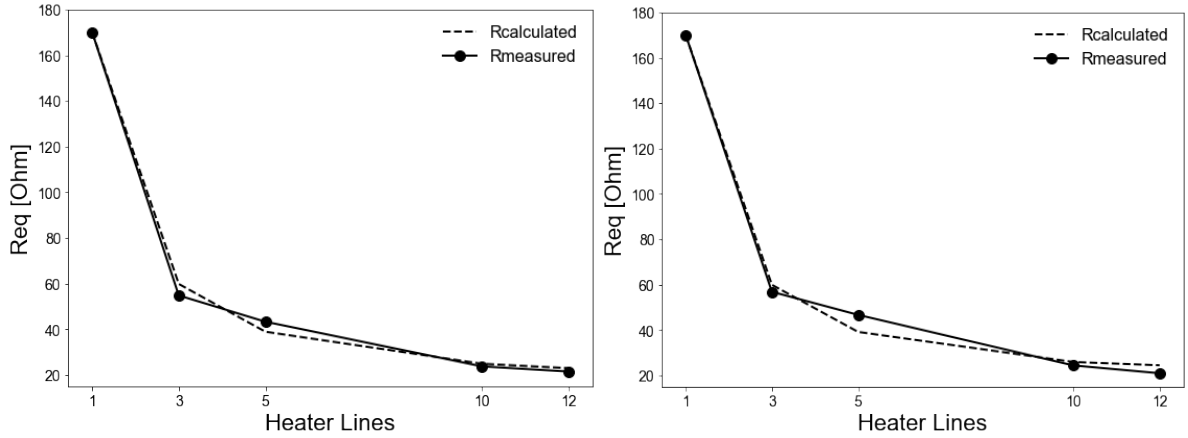


Figure 5.6 Equivalent resistances of knitted heaters with 1, 3, 5, 10, and 12 lines in ladder (left) and diagonal (right) configurations. The plotted values show both the predicted (calculated from Equations (2) and (3)) and measured resistances.

5.3.3 Resistance Characterization of the Heater Lines

For the L/W (length to width ratio), the ratio of the number of courses to wales was used instead of the actual measured length and width. Figure 5.7 shows the relationship between resistance (in Ω) and the L/W ratio for a knitted heater, with multiple data series represented by different colors. The lines show a linear trend, as expected, and the overall slope C_R is determined from a fit through all data points and is calculated to be 2.78 ± 0.07 Ω.

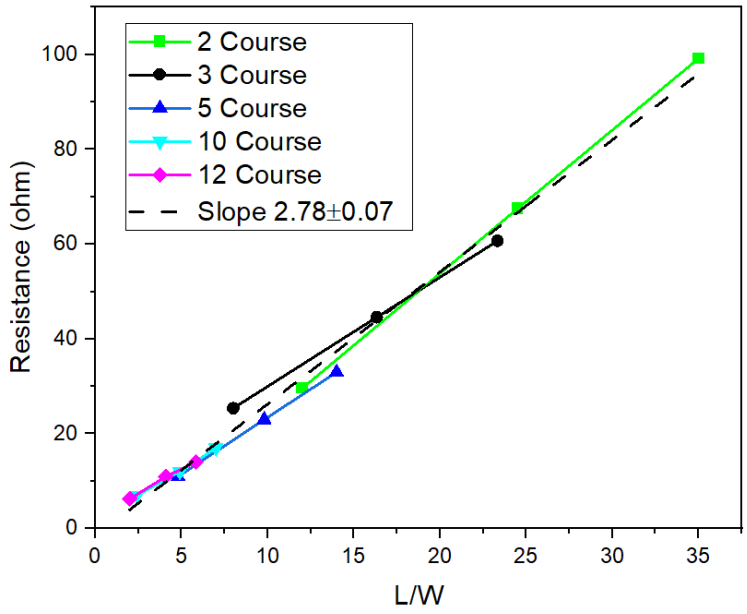


Figure 5.7 Resistance versus L/W for heaters with 2, 3, 5, 10, and 12 courses.

The temperature change (ΔT) versus power (P) graph is shown in Figure 5.8. All curves exhibit a linear trend, indicating that ΔT is proportional to the applied power. The slopes of the lines for the 3, 5, 10, and 12 course lines are, respectively, 20.95, 23.98, 27.70, and 26 °C/Watt. The corresponding mean absolute error (MAE) and root mean square error (RMSE) values are low across all configurations, indicating that the linear model accurately represents the measured data (see Supporting Information Figure S1). The results of the two-course sample deviate significantly from this trend. To verify this deviation, two additional measurements were performed, resulting in an average slope for the two lines of 45.96 ± 1.28 °C /Watt (see Supporting Information Figure S3). The resistance coefficient Cl for the 0.2 cm wide lead wires was determined to be 0.67 ± 0.03 Ω by

plotting the resistance of lead wires versus L/W (see Supporting Information Figure S4).

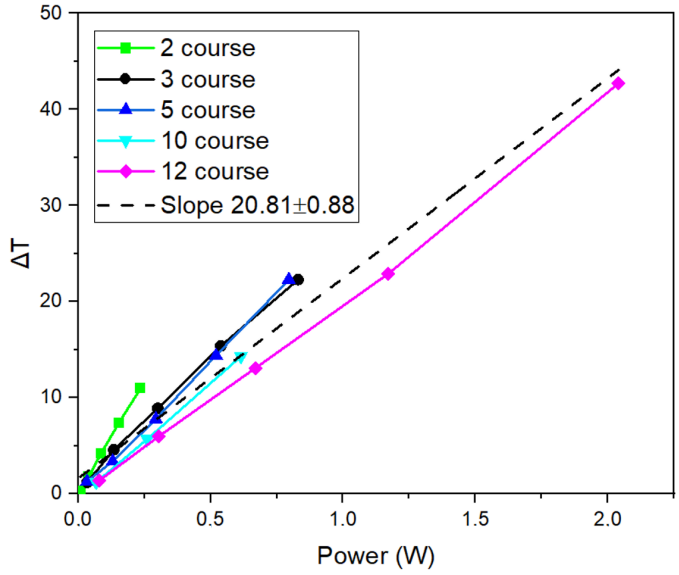


Figure 5.8 Temperature change versus power graph of different heater lines.

5.3.4 Validation of Measured and Predicted Temperature Profiles

In this section, we evaluate the performance of heaters composed of multiple heater lines of a width of two courses, connected by stitched lead wires of 0.2 cm width. Thermal images of samples with 3, 5, 10, and 12 heater lines arranged in a ladder configuration are shown in Figure 5.9. Across all configurations, the heaters exhibit a clear decrease in heating power for heater lines further away from the power source and this effect becomes more pronounced as the number of heater lines increases. The three-heater sample has a maximum temperature at the left line of 33.9 °C and 25.1 °C for the last heater line. The five-line sample recorded a peak temperature of 39.8 °C, with the first and last heater lines measuring 25.4 °C and 37.4 °C, respectively. The sample with 10 heaters shows a more substantial heat output, reaching a maximum temperature of 59.2 °C. The 12-course configuration demonstrates a rather large temperature non-uniformity. The maximum temperature (79.6 °C) is in the lead wires near the power source and the heating wires at the end of the sample are hardly increasing in temperature. Thermal images of the heaters in diagonal configurations are provided in Supporting Information Figure S5. They show a more uniform temperature distribution from left to right heater line and increased thermal dissipation in the lead wire elements near the power source connections.

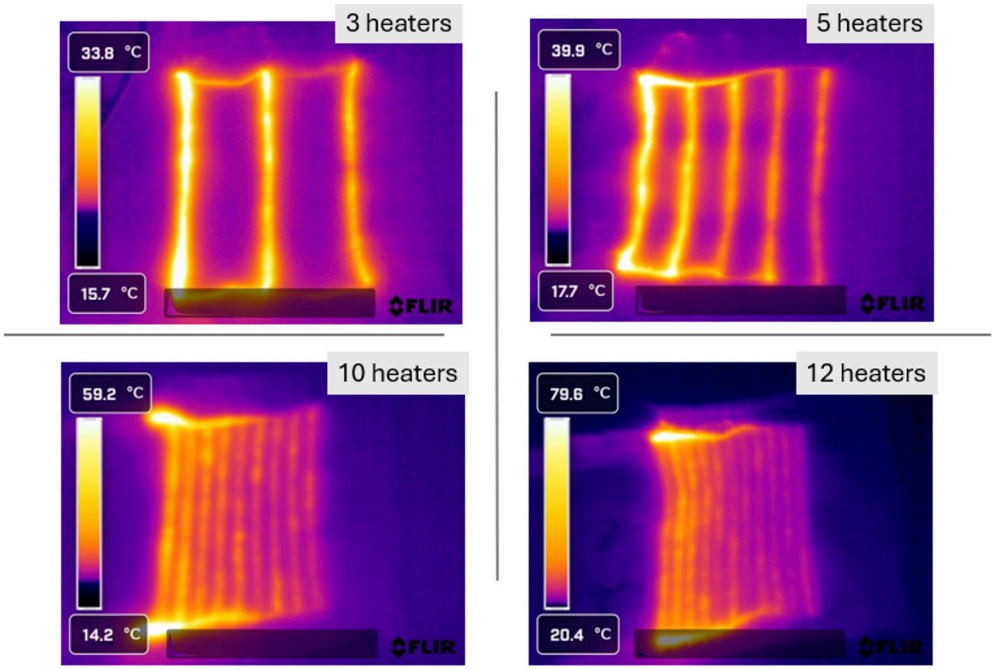


Figure 5.9 Different heater samples and their thermal images. The power is applied at the two left corners (ladder configuration).

The measured temperature differences along the heater lines in the ladder configurations are compared with predictions from Equations (5) and (6), as shown in Figure 5.10. For the predictions, we used the previously determined heat transfer coefficient of 45.96 ± 1.28 C/Watt and resistance coefficients of 2.78 ± 0.07 Ω and 0.67 ± 0.03 Ω for the heater line and the lead wires, respectively. For ladder configurations, the model predictions capture the general trend of decreasing temperature with increasing distance from the power source, although they exhibit an overprediction that becomes more pronounced in heaters with fewer lines. This overprediction is most pronounced for the three-line heater ranging 2 to 6 °C. For the 5-, 10-, and 12-line heaters, this gap is smaller, ranging from ap-proximately 0.4 to 2 °C. The overall trend shows that prediction accuracy improves as the number of heater lines increase. Also, the three- and five-line heater configurations exhibit a more rapid temperature drop along the heater lines compared to the 10- and 12-line configurations.

Figure 5.11 shows the corresponding results for the diagonal configuration. Unlike the ladder configuration, both the predicted and observed values display a non-monotonic trend, with a minimum temperature in the middle. For the three- and five-line heater configurations the observed and predicted values diverge more significantly, ranging approximately from 3.5 to 5 °C and from 3.6 to 5.3 °C, respectively. In contrast, the 10- and 12-heater configurations exhibit a smoother, more consistent temperature profile and better agreement between predicted and observed temperatures (within ~1 to 2 °C).

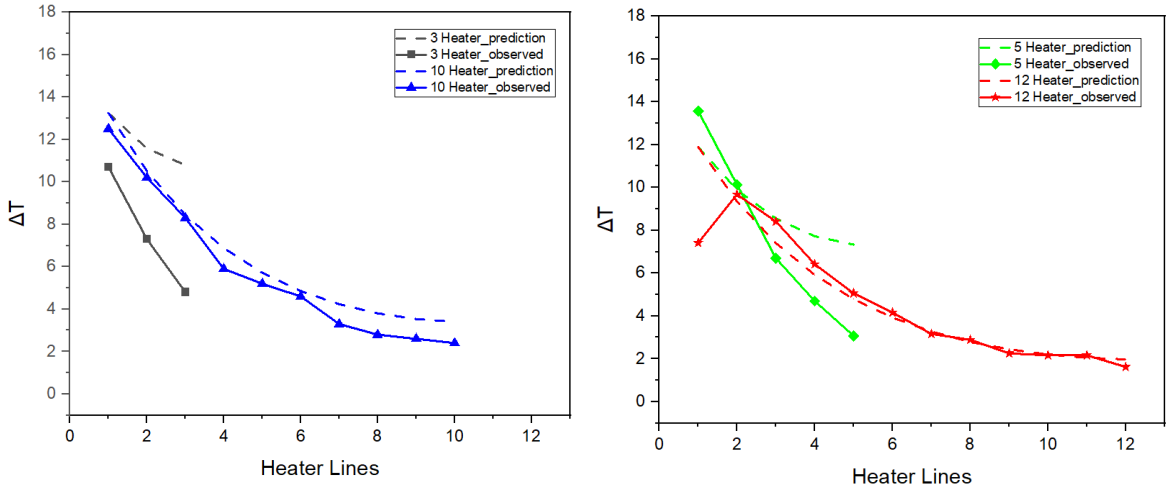


Figure 5.10 The observed (full lines with symbols) and calculated (Equations (5) and (6), dashed lines) temperatures for knitted heaters in ladder configuration with 3 and 10 heater lines (left) and 5 and 12 heater lines (right).

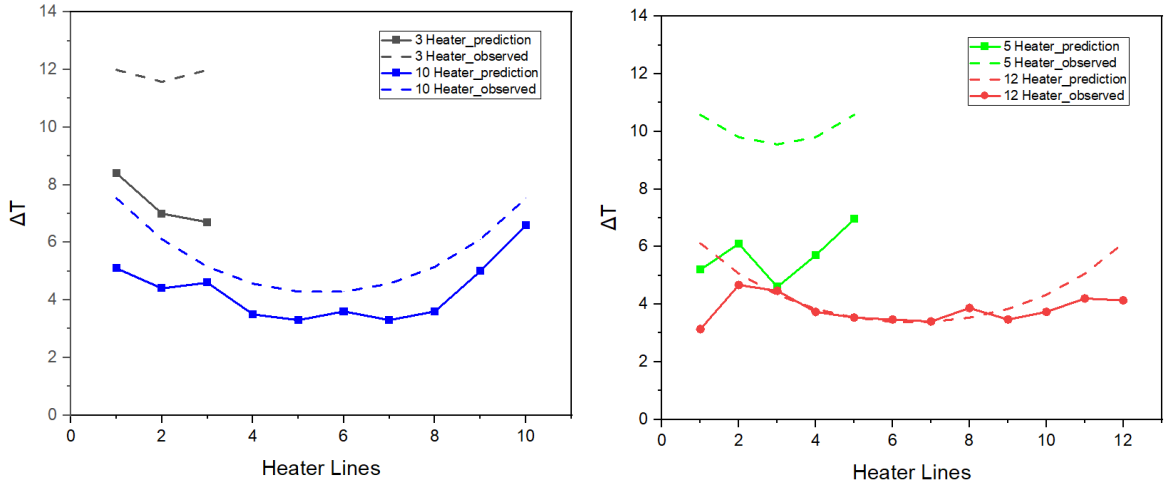


Figure 5.11 The observed (full lines with symbols) and calculated (Equations (5) and (7), dashed lines) temperatures for knitted heaters in diagonal configuration with 3 and 10 heater lines (left) and 5 and 12 heater lines (right).

The average absolute deviations between predicted and measured for both ladder and diagonal configurations are illustrated in Figure 5.12. In both configurations, the largest differences are observed for the samples with three and five heater lines, while the predictions and measurements show much closer agreement for higher heater line counts (10 and 12 samples).

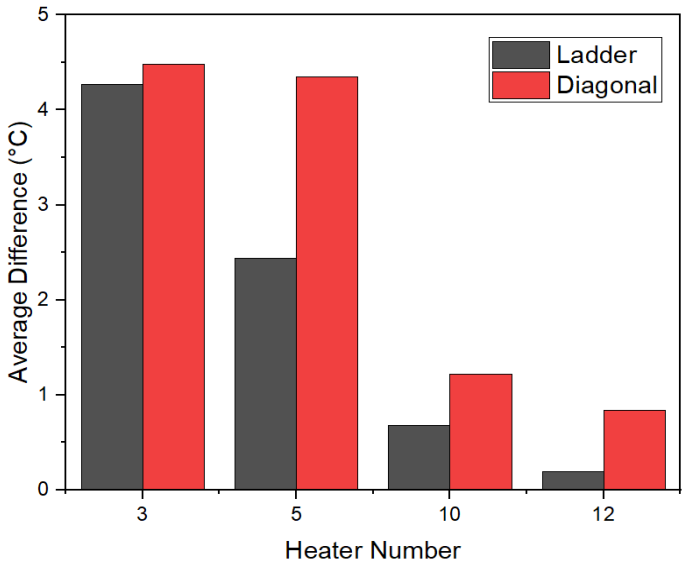


Figure 5.12 Average difference between predicted and observed data versus heaters with different courses.

5.4 Discussion

We analysed the thermal performance of a knitted heater composed of a chosen number of parallel heater lines interconnected by two lead wire lines. The thermal performance model consists of three verifiable components.

- Prediction of the equivalent resistance of a heater consisting of several heater lines and two interconnecting lead wires.
- Prediction of the resistance and heating capacity of knitted conductive lines of a given length and widths.
- Prediction of the temperature variations across the heater lines based on the current distribution for a given overall power input.

In our experimental series, the total heater length was kept constant, while the number of heater lines was varied from three to twelve. Consequently, the lengths of the lead wire segments differed, resulting in resistance ratio parameters ranging from $\varepsilon = 0.023$ to $\varepsilon = 0.006$. As shown in Figure 5.6, the close agreement between predictions and measurements indicate that these effects are well captured by the model, allowing accurate prediction of the overall heater resistance.

The assumption that the resistance of a knitted line increases linearly with the line length and decreases linearly with its width (Equation (8)) is confirmed by the results as shown in Figure 5.7. The proportionality constant in this study was determined to be $2.78 \pm 0.07\ \Omega$. A knitted line 100 wales long and two courses wide will thus have a resistance of about 115 Ω. In general, the resistance parameter depends on the stitch type, knitting parameters, and the resistivity and type of conductive yarn used. In Table 5.1, resistivity values for other conductive yarns and knit structures are listed. The resistivity values vary depending on both the knit structure and the conductive yarn type. Double-jersey structures exhibit lower resistivity than single-jersey samples due to their denser configuration which enhances electrical pathways. Similarly, resistivity tends to decrease with increasing course and wale numbers, indicating the effect of higher stitch density on conductivity. These results indicate that the majority of line resistivity values fall within the range of $C_R = 2$ to 6.

Table 5.1 Resistivity values of different conductive yarn types and knit structures.

Yarn Type	Course/Wale Number	Knit Type	C_R Value
Shieldex® 235/36 dtex Z 130 HC + B ((768 Ω/m)	2 Courses/70 Wales	Double Jersey *	2.78
	3 Courses/70 Wales		2.68
	5 Courses/70 Wales		2.34
	10 Courses /70 Wales		2.54
	12 Courses /70 Wales		2.47
	95 Courses /3 Wales	Single Jersey **	5.66
	95 C Courses 6 Wales	Single Jersey	5.50
	95 Courses /9 Wales	Single Jersey	2.83
	95 Courses /2 Wales	Double-Jersey Plated Sandwich **	2.20
	95 Courses /4 Wales	Double-Jersey Plated Sandwich	2.80
	95 Courses /6 Wales	Double-Jersey Plated Sandwich	2.63

* Double-jersey samples are knitted with a STOLL CMS 530;

** Single-jersey structures were knitted on a STOLL ADF 530-32 W machine, while double-jersey plated sandwich structures were knitted on the same machine using plating combined with intarsia technique.

In addition, we evaluated the heat generated by applying a voltage to the various knitted lines. As expected, our measurements confirmed a linear relationship between the temperature rise and the applied power, as shown in Figure 5.9. Contrary to our expectations, however, the heater line performance showed a clear dependence on the line width. Lines two courses wide have a much higher proportionality constant compared to those with three or more courses (Figure 5.13). For widths between 3 and 12 courses, a consistent but much slower decrease is observed. The deviation of the two course structures can probably be attributed to the much looser knit structure (Figure 5.4, left picture). The slower overall decrease can be explained by the surface effect. Broader lines have larger surface area and thus an increasing heat loss to the surroundings.

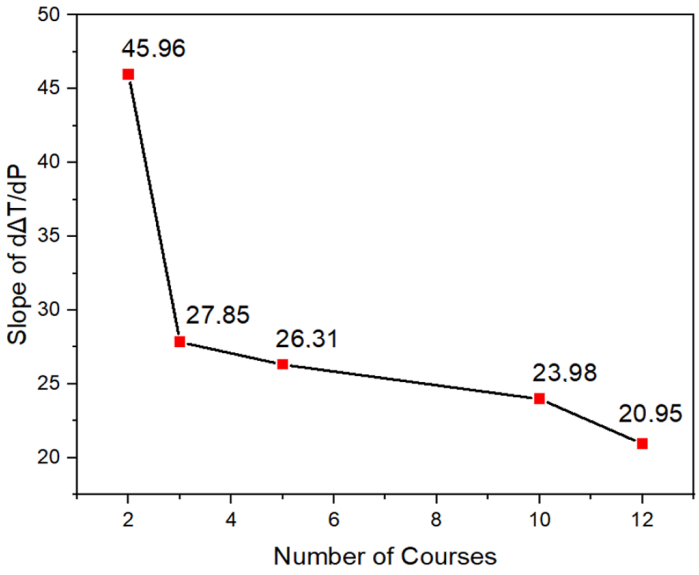


Figure 5.13 Effect of line width on generated temperature increase per unit of applied power.

As explained in the introduction, lead wires with non-zero resistance cause progressively lower currents in

subsequent heater lines. In the present examples, the lead wire resistance is substantial (0.67 $\Omega.cm^{-1}$), leading to significant voltage drops and corresponding reductions in current. As shown in Figure 5.9 these effects manifest as poor heating performance at locations distant from the power input points. While such pronounced non-uniformities in heating should be avoided in practical applications, they are valuable here for validating the proposed model.

Our measurements show that, for heaters with a larger number of heater lines (10 and 12), the predicted temperature distributions agree with the experimental data within 1–2 °C. In contrast, heaters with only three or five heater lines exhibited much larger deviations, up to 5 °C. These unexpectedly large discrepancies cannot be attributed to inaccuracies in the resistance and current distribution predictions (Equations (2)-(7)), as these are exact and in full agreement with simulations [20]. It is also unlikely that the deviations result from errors in the determined heat transfer parameter C_H, since the thermal boundary conditions of a heater line in a three- or five-line heater are comparable to those in a heater with 10 or 12 lines. We therefore attribute the discrepancies to variations in the contact resistance between the lead wire and the heater line in heaters with fewer lines. Such variations may occur when the stitched lead wires do not fully cover the ends of the heating wires.

Lateral conduction in the 10–12-line heaters naturally equalize temperature variations, whereas heaters with only 3–5 lines lack sufficient lateral conduction, making them more sensitive to local contact resistance. Limited lateral conduction makes the heater more sensitive to local variations, such as contact resistance, temperature drops, or localized hotspots near the lead wires.

The heatmaps illustrate the impact of heater arrangement and quantity on relative error.

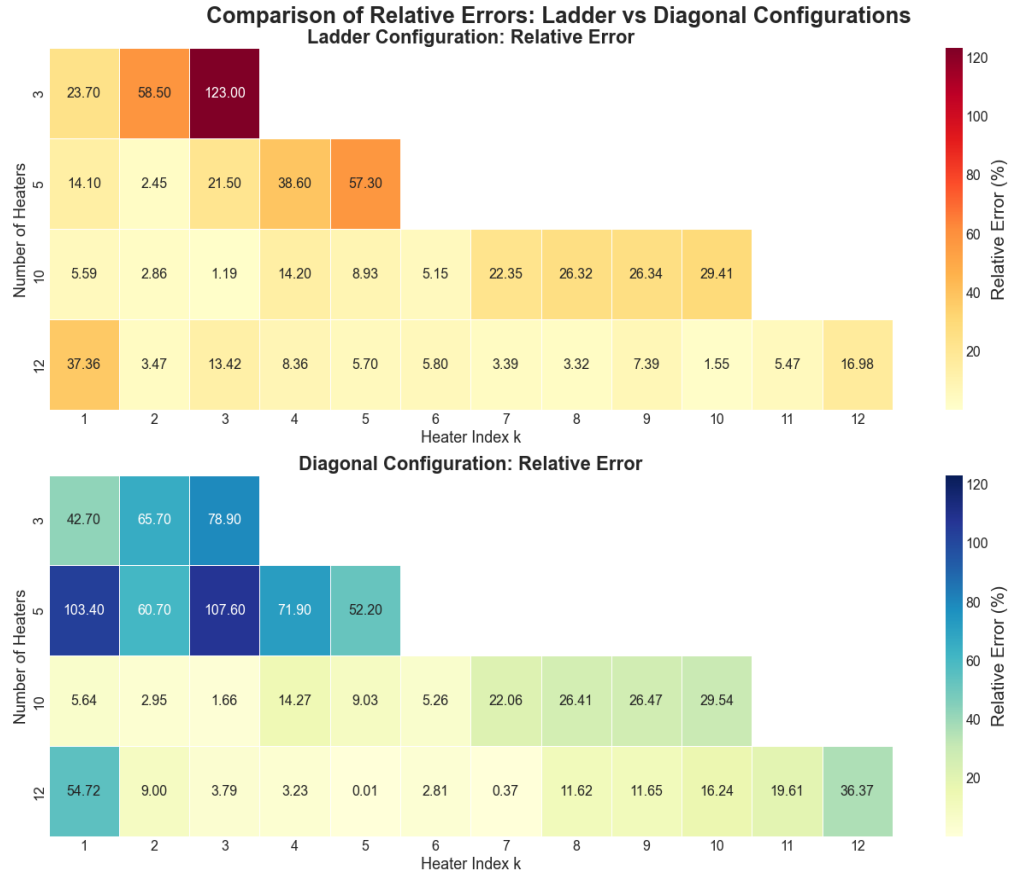


Figure 5.14 Comparison of relative errors (%) for ladder and diagonal heater configurations with a different number of heater lines. The heater index k corresponds to the heater line numbering de-fined in Equation (6).

A knitted heater with 10 lines, each course wide, is integrated into a wearable wristband configuration. As shown in the thermal image (Figure 5.15), the heater rapidly reaches surface temperatures above 33 °C demonstrating active heating while conforming comfortably to the shape of the hand. It is worth noting that, in practical applications requiring heating over larger surface areas, heaters typically incorporate between 10 and 30 heater lines. Consequently, our finding that the model accurately predicts performance for heaters with a larger number of heater lines supports its applicability for the design of large-area, textile-based heaters. Surface temperatures around 33 °C are considered physiologically supportive, for example, in wound healing, as identified by Lugoda et al. in their wearable textile thermograph study [22]. The heater highlights its potential for integration into smart textiles and personal thermal therapy.

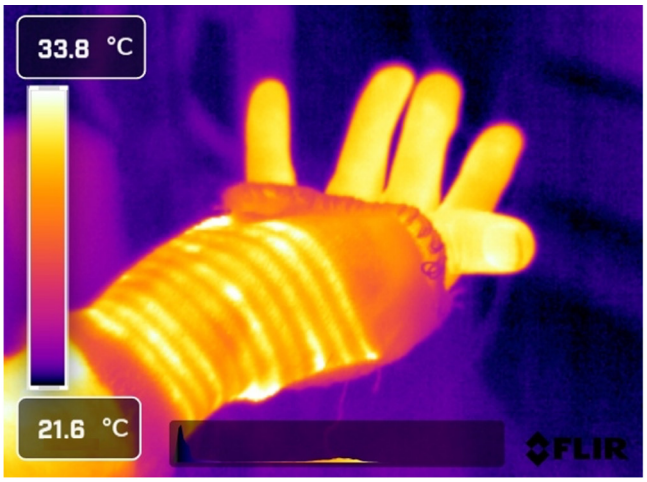


Figure 5.15 Thermal image of a wearable wristband with 10 heater lines, each 2 stitches wide, showing the conformability to the body shape.

5.5 Conclusions

This study discusses the design space of fully textile-based and stretchable knitted heaters. Heated garments may incorporate multiple heating units, each supplied independently. Using a conservative operating limit of 12 V and 500 mA per unit provides a maximum power output of 6 W and an associated target resistance of approximately 24 Ω per heater. We derived a simple model that (1) relates the heater line resistance to the heater layout, knit line structure, geometry, and conductive yarn resistance, (2) relates the heater layout to heater line currents, and (3) relates the heater line currents to the steady-state temperature. Experimental results confirmed the predictive accuracy of the model, particularly for heaters with higher line counts (≥10), which closely matched theoretical expectations. Remaining discrepancies suggest that lead wire resistance and contact resistance variations are critical factors that need to be further optimized. Overall, the findings provide practical design guidelines for integrating low voltage knitted heaters into wearable applications, with strong potential for scalable manufacturing using existing textile technologies. This study was the demonstration and characterization of the heated prototype, without conducting user trials to assess thermal comfort or safety under real-world conditions. Future work will focus on performing actual wearing tests to evaluate these aspects and validate the practical performance of the developed system.

References

1. Asha Banu, S.M.M.A.J., K. Textile based antenna design for breast cancer detection. Mater. Today Proc. 2022, 62, 4814-4820, Textile based antenna design for breast cancer detection. Mater. Today Proc., 2022. 62: p. 4814-4820.

2. White, P.B., D.; Moshrefi-Torbati, M.; Beeby, S., The Energy Harvesting Performance of a Flexible Triboelectric-Based Electrospun PTFE/PVDF Fibre. Eng. Proc., 2023. 30(8).

3. Verma, S.D., M.; Paul, S.; Chaturvedi, K.; Khan, M.A.; Srivastava, A.K. , Recent Advances for Fabricating Smart Electromagnetic Interference Shielding Textile: A Comprehensive Review. Electron. Mater. Lett., 2022. 18: p. 331-344.

4. Hatamie, A., et al., Review—Textile Based Chemical and Physical Sensors for Healthcare Monitoring. Journal of The Electrochemical Society,, 2020. 167(3).

5. Stoppa, M., & Chiolerio, A, Wearable Electronics and Smart Textiles: A Critical Review. Sensors, 2014. 14: p. 11957–11992.

6. Cochrane, C.H., C.; Schwarz-Pfeiffer, A., Smart textiles in health. In Smart Textiles and Their Applications; , 2016: p. 9-32.

7. Mohring, U.S., D.; Hanus, S. Textiles for patient heat preservation during operations. In Handbook of Medical Textiles; Woodhead Publishing, 2011: p. 434-442.

8. Chen, Z.L., J.; Song, W.; Lu, Y.; Cao, B., Smart Wireless Charging Heating Insoles: Improving Body Thermal Comfort of Young Males in an Extremely Cold Environment. Cloth. Text. Res. J., 2020. 40: p. 220-234.

9. Hamdani, S.T.A.F., A.; Maqsood, M., Thermo-mechanical behavior of stainless steel knitted structures. Heat Mass Transf. , 2015. 52: p. 1861-1870.

10. Bai, Y.L., H.; Gan, S.; Li, Y.; Liu, H.; Chen, L., Flexible heating fabrics with temperature perception based on fine copper wire and fusible interlining fabrics. Measurement, 2018. 122: p. 192-200.

11. Cai, L.S., A.Y.; Wu, P.; Hsu, P.C.; Peng, Y.; Chen, J.; Liu, C.; Catrysse, P.B.; Liu, Y.; Yang, A.; et al. , Warming up human body by nanoporous metallized polyethylene textile. Nat. Commun., 2017. 8: p. 496.

12. Park, H.K.K., S.M.; Lee, J.S.; Park, J.-H.; Hong, Y.-K.; Hong, C.H.; Kim, K.K., Flexible plane heater: Graphite and carbon nanotube hybrid nanocomposite. Synth. Met., 2015. 203: p. 127-134.

13. Aznar, P.R.D.J., H.L.O., Advances and Applications of Graphene-Enhanced Textiles: A 10-Year Review of Functionalization Strategies and Smart Fabric Technologies. Textiles, 2025. 5: p. 28.

14. Thilagavathi, G.M., N.; Kannaian, T., Development and Characterization of Electric Heating Fabric Based on Silver Coated Nylon Yarn. J. Text. Eng. Fash. Technol., 2017. 1: p. 224-226.

15. Tseghai, G.B.M., B.; Fante, K.A.; Nigusse, A.B.; Van Langenhove, L., Integration of Conductive Materials with Textile Structures, an Overview. Sensors, 2020. 20: p. 6910.

16. Maurya, S.K.D., A.; Kumar, B., Optimization of Heating Performance of the Rib-Knitted Wearable

Heating Pad. In Proceedings of the E-Textiles 2022.

17. Liu, H.L., J.; Chen, L.; Liu, L.; Li, Y.; Li, X.; Li, X.; Yang, H., Thermal-electronic behaviors investigation of knitted heating fabrics based on silver plating compound yarns, Text. Res. J., 2015. 86: p. 1398-1412.

18. Kexia, S.L., S.; Hairu, L. , Structural Parameters Affecting Electrothermal Properties of Woolen Knitted Fabrics Integrated with Silver-Coated Yarns. Polymers, 2019. 11: p. 1709.

19. NFPA. NFPA 70E: Standard for Electrical Safety in the Workplace; NFPA: Quincy, M., USA, 2004. 2004.

20. Jansen, K.M.B., Closed-Form Solutions for Current Distribution in Ladder-Type Textile Heaters. Thermo, 2024. 4: p. 433-444.

21. Zhang, L.B., M.; Andrew, T.L., Transforming Commercial Textiles and Threads into Sewable and Weavable Electric Heaters. ACS Appl. Mater. Interfaces 2017. 9: p. 32299-32307.

22. Lugoda, P.H.-R., T.; Morris, R.; Dias, T. A Wearable Textile Thermograph. Sensors, 2018. 18: p. 2369.

Chapter 5 - Supporting Information

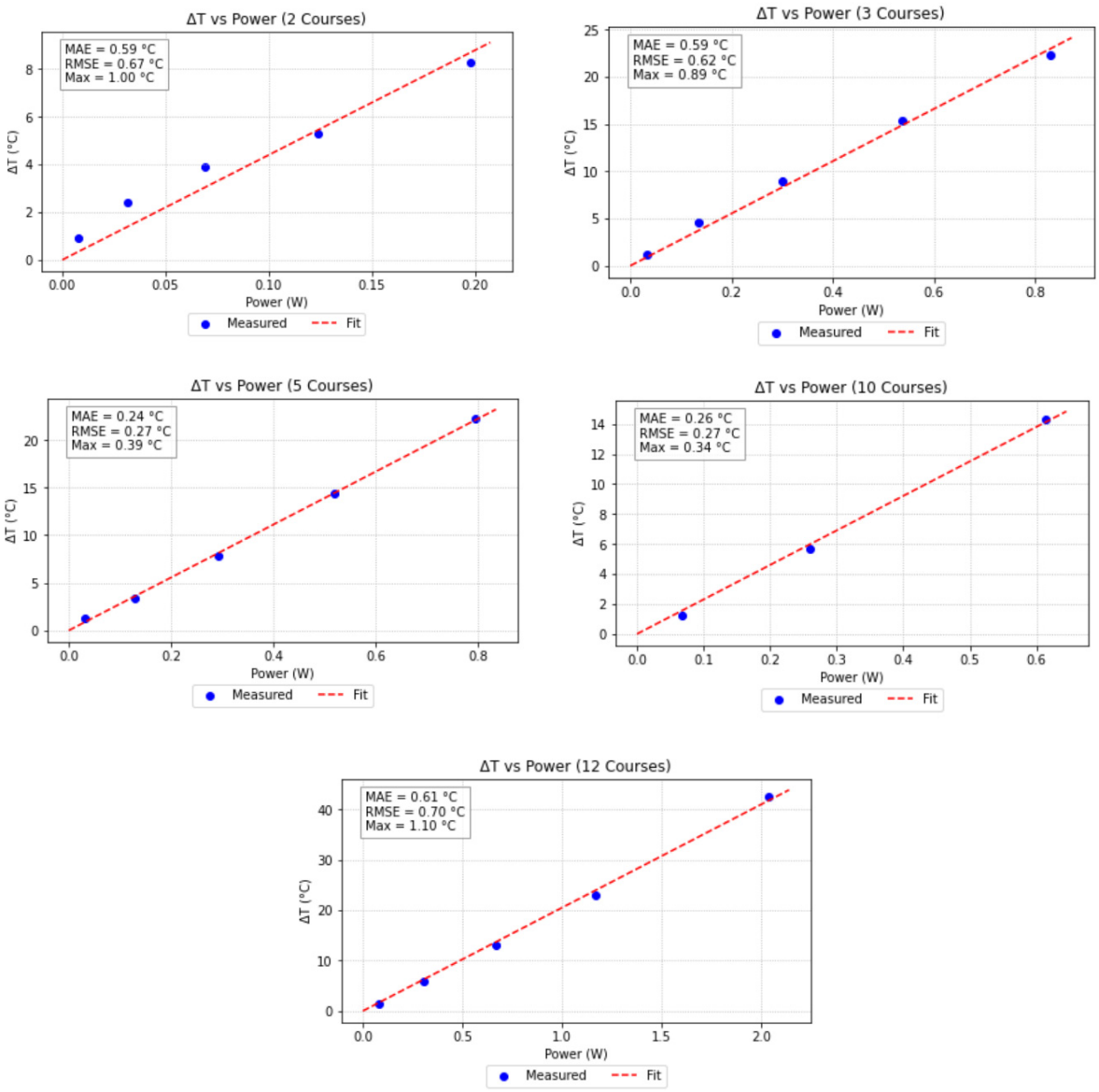


Figure S1. Relationship between power input and ΔT for a knitted heater. Blue markers indicate measured data; red dashed line shows the linear fit through the origin. Fitted slope (°C/W), MAE, RMSE, and Max error are shown in the inset box.

Chapter 6

6. Conclusions, Limitations and Future Perspectives

This final chapter provides a summary of the research objectives and questions of the thesis and outlines the contribution to the field by addressing these questions. The study aimed to develop knitted textile sensors and heaters and to investigate the potential applications of knitted textile structures. The conclusions are structured to progress from material selection and architectural knit design to physics-based modeling and practical wearable applications.

Knitted functional textiles for sensing and thermal regulation remain a developing research area. The focus of this thesis was to investigate how knitting can be utilized as both a manufacturing technique and a design methodology for wearable sensing and heating components. Consequently, this thesis was guided by three research questions:

- The first research question investigated how knitted textile structures can be engineered to serve as functional sensors and actuators.
- The second research question examined the fundamental structure–property–performance relationships defining knitted sensing and heating behavior.
- The third research question explored the potential applications of knitted textile sensors.

6.1 Answering the research questions

RQ1: How can knitted textile structures be engineered to make functional sensors and actuators?

I intended to investigate how knitted textile structures can be engineered to integrate sensing and heating functions directly into fabrics while preserving comfort and flexibility. By modifying knit architecture, material combinations and conductive layouts, the goal was to explore the electromechanical and thermal performance of the textile-based structures for wearable applications.

For the strain sensor (Ch.2), a 1×1 rib structure was selected because of its high stretchability and the presence of overlapping loops. In this design, I co-knitted the conductive yarn together with elastic yarn to provide an effective elastic restoring force during repeated deformation. The elastic yarns also create vertical compression which helps keep the sliding loops consistently in contact throughout stretching and relaxation. In addition, the conductive yarn was deliberately positioned on the inside to ensure more stable electrical behavior.

Through this study, I clearly demonstrated that by modifying the knitted structure, precise control over the sensor performance can be achieved. In this way, both strain insensitive and strain sensitive structures can be integrated in a single garment as elements with different functionality. The strain insensitive structures can for example serve as conductive tracks that interconnect the strain sensors. Conversely, the sensitive knitted strain sensor had a linear working range of at least 40%, a gauge factor of about 1.2, and negligible hysteresis which can be used in different wearable applications.

In another part of the study (Ch.4), I developed fully textile-based knitted pressure sensors composed of conductive and non-conductive yarns for wearable and tactile applications. Compared to conventional rigid or thin film pressure sensors, these textile-based structures provide intrinsic softness, flexibility and comfort, making them a good alternative for healthcare monitoring and human–computer interaction systems. Stretchable pressure sensors were produced using commercial conductive yarns and non-conductive PES yarns, and their electromechanical performance was systematically investigated by varying knit design and stitch density. By carefully controlling these structural parameters, the overall resistance and sensing behavior could be adjusted. Two different geometries were designed: flat rectangular sensors produced by plating technique and dome-like sensors formed in a three-dimensional structure to evaluate the influence of structural geometry on pressure sensing performance.

The final designs of the pressure sensors showed that the structural design plays an important role in determining sensitivity and detection range. For flat-knitted sensors, different Rib structures were analyzed and increasing loop length improved sensitivity due to enhanced elasticity and more significant yarn-to-yarn contact changes under loading. Among the tested samples, the Rib 3×3 structure knitted with NP 15 exhibited the highest sensitivity in the low-pressure range and a fast response time, while distinguishing different loading forces. In contrast, the dome-like sensors showed lower sensitivity but offered a much wider detection range, making them more suitable for applications requiring broader pressure monitoring. Overall, these findings confirm that by modifying knit pattern, loop length and sensor geometry, the performance of knitted pressure sensors can be tailored to obtain either highly sensitive structures for low-pressure detection or more robust designs for wider-range tactile applications.

In the third part of the study, fully textile-based knitted heaters were developed, addressing challenges in uniform heating and efficient power use. In this part, a model-based study was conducted to investigate the uniformity of temperature in knitted textiles. Integrating silver-plated nylon yarn into double-jersey fabrics, heaters with varying numbers of heating lines were fabricated, and their electrical and thermal performance was systematically analyzed. A physics-based model was developed to link heater resistance, current distribution and resulting surface temperature, accounting for lead wire effects and heat losses. Experiments showed that heater resistance decreases with more lines, while temperature rise is approximately linear with applied power. Narrower heater lines generated higher temperature per unit power due to looser knit and reduced heat dissipation, whereas wider lines showed more stable heating but slightly lower temperature change per watt. Ladder and diagonal layouts were tested, with diagonal arrangements providing more uniform heating across the surface.

The study confirmed that the number of heater lines, their width, and layout critically influence thermal performance and uniformity. Heaters with higher line counts (≥10) reached physiologically relevant temperatures above 33 °C while maintaining low voltage operation (12 V, 500 mA), demonstrating potential for wearable and therapeutic applications such as wristbands. The model demonstrated good agreement with experimental results for both heater resistance and temperature distribution, especially for larger line counts. These results highlight the critical role of lead wire resistance and minimizing contact variations. These results provide practical design guidelines for scalable, low-voltage textile heaters, enabling integration into wearable devices for health, comfort, and rehabilitation purposes.

This shows how knitted textile structures can be engineered into functional sensors and actuators through the combination of knit architecture, material selection and conductive layout while preserving comfort and flexibility.

RQ2: What are the fundamental relationships between knit structure, yarn properties, and electromechanical performance?

This research aimed to establish the fundamental principles linking fabric patterns and yarn types to sensor performance, providing guidelines to facilitate the design of future smart fabrics.

When developing knitted strain sensors, several key considerations should be kept in mind. First, the selection of elastic and conductive yarns is critical; elastic yarns with high recovery, such as Lycra or Nylon blends, reduce hysteresis and help the sensor return to its original shape after deformation. For conductive yarns, silver-coated nylon is preferred, as metallic yarns like stainless steel can cause unstable performance. The knit structure also strongly influences sensor performance; 1×1 rib structures provide high stretchability, linear response, and repeatable measurements, making sensing behaviour ideal. Co-knitting the conductive and elastic yarns allows control over whether the conductive yarn is positioned on the inside or outside of the structure; placing the conductive yarn inside reduces hysteresis and improves linearity. Knitting density determines fabric elasticity and working range; higher NP numbers produce looser fabrics, enabling a wider working range and higher gauge factor, while very tight structures may restrict loop sliding and reduce sensitivity. Finally, the number of conductive courses affects sensitivity, with multiple courses generally enhancing the

gauge factor while keeping hysteresis low when combined with proper yarn placement.

When developing knitted pressure sensors, several important factors should be considered to achieve reliable, sensitive and wearable performance. Material selection plays a key role; elastic substrates such as spandex or PES blends provide high recovery and comfort, while conductive yarns like silver-plated nylon ensure stable electrical responses under repeated loading. The structural design of the sensor -whether flat or dome-like- significantly affects sensitivity, detection range and response time, with Rib 3x3 knit structures demonstrating high elasticity and favorable performance for both low- and medium-pressure applications. Stitch density directly influences fabric tightness and compressibility, where looser or higher NP fabrics allow greater deformation and higher sensitivity, whereas tighter structures limit movement and reduce responsiveness. The integration of conductive elements, either plated with non-conductive yarns or embedded within the sensor, impacts hysteresis, linearity and overall sensor stability. Dome-like designs enhance the detection range and tactile perception, making them suitable for applications requiring physical feedback, while flat-knitted sensors excel in low-pressure, high-sensitivity scenarios and can be seamlessly applied to skin or textiles for human-computer interaction. Finally, the filler content, knit geometry and yarn arrangement can be optimized to balance sensitivity, durability, and response speed, enabling the production of versatile sensors for rehabilitation, motion tracking and tactile sensing applications.

When developing knitted textile heaters for wearable applications, several important considerations should be kept in mind to ensure efficiency, safety and uniform heating. First, the overall heater resistance must be maintained within defined limits to ensure controllable heating performance while operating within safe voltage and current ranges (V<12V, I<500 mA). The selection of yarns is vital: conductive yarns such as silver-coated nylon provide good conductivity while maintaining flexibility, and elastic yarns help maintain the fabric's shape and conformability. The knit structure directly influences the electrical pathways, and the resistance of both lead wire and heater lines can be tailored by adjusting the stitch type, density, or arrangement of the yarns. This helps to fine-tune the local heating and reduce hotspots. Uniform stitch lengths and careful placement of conductive yarns help prevent uneven heating. By considering these factors, it is possible to produce wearable heaters that provide consistent warmth, respond rapidly to power changes, and remain comfortable and safe for long-term skin contact.

Modelling the relationships between material properties, knit structure, heater configuration and device performance provides deeper insight and supports rational design. For the knitted heaters, a semi-empirical model was developed to link knit structure and yarn properties to the electrical resistance of individual knitted line segments, as well as a physical model that predicts the overall resistance and local power dissipation across different heater configurations. Based on these models, temperature distributions and heating non-uniformities can be predicted and used to optimize heater design.

RQ3: What applications are possible with knitted sensors?

The intention of this question is to demonstrate the practical value of the developed knitted structures by showing how these lab-tested fabrics can be turned into products for healthcare, sports and daily life. Knitted sensors enable a wide range of wearable applications due to their intrinsic flexibility, stretchability and comfort.

Strain-sensitive knitted structures can be used for motion tracking, joint angle monitoring, posture analysis and rehabilitation assessment by detecting body movements in real time. Pressure-sensitive knitted sensors are suitable for tactile sensing, load distribution analysis, and human–computer interaction, as well as for healthcare monitoring applications such as detecting body contact forces for preventing decubitus.

When integrated into garments or accessories, these sensors can support sports performance analysis, injury prevention and remote patient monitoring. Because they are soft, conformable, and breathable, knitted sensors can be seamlessly embedded into everyday clothing, enabling continuous and unobtrusive physiological and biomechanical monitoring.

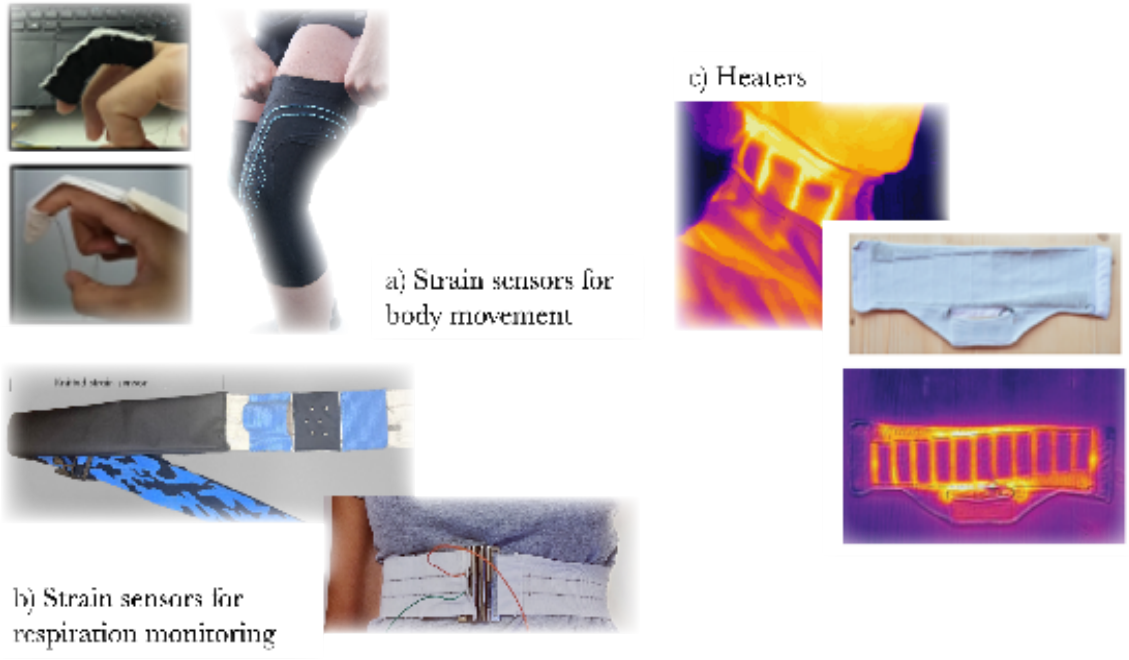


Figure 6.1 Applications of knitted textile sensors and actuators. (Refs: Figure 6.1a [1], Figure 6.1b [2], Figure 6.1c [3]).

The application studies shown in Figure 6.1 (a–c) were carried out at the Smart Textiles Lab at TU Delft and are closely related to the sensing and actuation concepts investigated in this thesis. These studies demonstrate different wearable and textile-integrated systems developed for monitoring human movement, physiological signals and user comfort. Textile-based strain sensors were explored for biomechanical monitoring by integrating flexible sensing elements into soft wearable structures.

As illustrated in Figure 6.1, strain sensors were applied to monitor finger bending, were conducted at the Smart Textiles Lab at TU Delft and are closely related to the sensing and actuation concepts investigated in this thesis. These studies demonstrate various wearable and textile-integrated systems developed for monitoring human movement, physiological signals, and user comfort.

As illustrated in Figure 6.1.a textile-based strain sensors were applied to monitor finger bending and knee flexion. These examples demonstrate the capability of soft textile sensors to capture small, repeated deformations associated with joint motion, enabling continuous biomechanical monitoring for applications such as rehabilitation, sports performance analysis, and ergonomic studies.

Furthermore, the same strain sensing principle was investigated for respiration monitoring using an elastic belt worn around the torso, as shown in Figure 6.1.b. Changes in chest circumference during inhalation and exhalation induce measurable strain in the textile sensor, facilitating continuous monitoring of breathing patterns. Validation experiments conducted during cycling activities demonstrated that the sensor could reliably capture respiration signals even under dynamic conditions, highlighting its potential for wearable physiological monitoring.

In addition to motion and respiration sensing, textile-integrated heating elements were investigated through the development of a heated collar, as shown in Figure 6.1.c. These elements were embedded into the collar to provide localized warmth around the neck area, demonstrating the potential of smart textiles to function as active comfort systems. Together, these application studies illustrate the broader context of wearable sensing and actuation research conducted at TU Delft.

These examples demonstrate the wide range of potential applications for smart textile technologies. However, the sys-

tems presented here remain at the prototype stage and have not yet been developed into commercially available products.

6.2 Contribution to the field of smart textiles

This work represents one of the first systematic studies that investigates knitted textiles as multifunctional platforms capable of acting both as sensors and actuators. While many previous studies have focused separately on strain sensors, pressure sensors or textile heaters, this research presents an integrated approach to knitted structures, demonstrating how knit architecture, yarn selection, and structural parameters can be engineered to achieve controlled electromechanical and thermal performance within the same textile framework.

A major contribution of this study is the development of strain sensors exhibiting negligible hysteresis with reproducible and reliable behavior. Achieving near-zero hysteresis in knitted strain sensors provides a stable sensing mechanism that can enable accurate monitoring of physiological movements such as respiration and joint motion. This represents a significant advancement, as hysteresis has traditionally limited the reliability of textile-based strain sensors.

The broader impact of this research lies in its potential for real-world healthcare and sports applications. The ability to embed sensing elements directly into fabrics in a non-obtrusive and comfortable manner opens new opportunities for continuous and long-term monitoring. Importantly, the proposed designs can be manufactured using existing knitting technologies, supporting scalability and industrial adjustment. However, large-scale upscaling and process standardization remain challenges that must be addressed for a better commercialization.

In addition to sensing, this study contributes to the development of fully textile-based knitted heaters. Unlike conventional textile heaters that rely on metallic wires integrated into non-stretchable substrates, the heaters developed here use conductive yarns within stretchable knit structures, enabling integration into body-conforming garments such as underwear. Furthermore, a physics-based modeling approach establishes practical design guidelines for predicting resistance, temperature distribution and heating efficiency in knitted heaters.

6.3 Limitations

Functional knitted sensors for strain and pressure have been developed in this study, but further optimization could improve their sensitivity, linearity, and working range. A good understanding of the structure–performance relationship has been established for these sensors, yet additional systematic studies could enable predictive performance models like those developed for the knitted heaters. This work also reviews smart textiles, conductive yarns, and integration techniques, but relies mainly on existing literature rather than experimental validation. Challenges such as durability, washability, and environmental effects like humidity, temperature, and long-term wear were discussed but not experimentally tested, limiting assessment of real-world performance.

Knitted strain sensors were studied using a limited set of yarns and a single knit structure under controlled, uniaxial testing. Results show improved linearity and reduced hysteresis, but may not generalize to other materials, knit patterns, or real-life multidirectional movements. Finger-worn prototypes were tested in the lab with a small range of movements, without long-term trials or diverse user conditions.

Knitted pressure sensors and heaters were evaluated in controlled conditions with specific materials and structures. Large-scale integration, long-term durability, washing effects, and real-use factors like body movement and airflow were not assessed, limiting practical applicability. This study did not provide a clear set of design rules but rather focused on optimizing designs for the best performance. To truly support designers, concise guidelines should be developed, and the findings from this work can help inform those guidelines.

One primary area of concern is the long-term durability and maintenance of these garments; specifically, the effects of

washability have not yet been investigated. For a sensing textile to be practical for daily use, it must withstand repeated washing cycles and varying environmental conditions, such as humidity and temperature, without significant changes in electromechanical performance. Newly developed conductive yarns, such as AB65 yarns [4], are evolving toward improved water resistance and durability. However, the long-term effects of washing and aging on performance have not yet been systematically evaluated. Future mechanical testing should also move beyond uniaxial strain to include multi-axial deformations that better represent real-life use. Without rigorous testing on how these factors affect the knit, the commercial longevity and overall reliability of integrated sensors remain uncertain.

For more advanced applications like knitted heated textiles, future efforts must focus on improving temperature uniformity and contact stability within flexible garment configurations. Testing larger-area prototypes will be essential to assess how temperature distribution and power consumption affect wearer comfort and performance in real-life conditions.

Sustainability represents a significant challenge in the current design. Because the sensing elements are fully embedded within the fabric matrix to preserve comfort and flexibility, silver-coated yarns are difficult to separate and recover at the end of the product's life cycle, limiting recyclability and increasing material waste. This problem becomes even more critical in large-scale production, where circular design principles and material efficiency are essential. In addition, the long-term durability of conductive coatings under repeated deformation and washing may further affect environmental performance. Scaling these innovations requires systematic optimization of knitting parameters such as yarn tension, stitch density, loop length, and machine settings to ensure consistent electromechanical behavior in industrial manufacturing. Furthermore, the present smart garments still rely on external hardware components, including batteries and microprocessors, which increase system complexity and electronic waste. While alternative conductive yarns and improved material combinations may enhance sustainability and electrical stability, exploring self-powered solutions such as triboelectric nanogenerators (TENGs) could reduce dependence on rigid power supplies and support the development of more autonomous and environmentally responsible smart textile systems.

6.4 Future work on smart textiles

To further improve this study, future work should focus on expanding material and structural diversity, testing under realistic and long-term use conditions, and enhancing sustainability and scalability. For knitted strain and pressure sensors, exploring a broader range of elastic and conductive yarns, multiple knit patterns, and multi-axial deformations would provide more generalizable insights and predictive performance models. Long-term durability, washability, and environmental factors such as humidity, temperature, and repeated wear should be systematically evaluated to ensure real-world reliability. For knitted heaters, larger-area prototypes and varied garment configurations should be tested to assess temperature uniformity, power efficiency, and wearer comfort. Additionally, standardizing knitting parameters such as yarn tension, loop length, and stitch density is critical for consistent industrial-scale production. From a sustainability perspective, future studies should investigate recyclable or biodegradable conductive yarns, circular design strategies, and the integration of self-powered elements, such as triboelectric nanogenerators, to reduce dependency on rigid power sources and minimize electronic waste. Finally, the development of concise design guidelines that integrate these findings would support designers in creating wearable smart textiles that are functional, durable, and environmentally responsible.

Another critical direction involves strengthening the interconnections between soft, stretchable textile components and rigid electronic elements. The interface between conductive yarns and hard components such as microprocessors, connectors and power units remains a mechanical and electrical weak point. Future studies should explore flexible interconnection strategies, including stretchable conductive inks, embroidered connectors, soft encapsulation techniques and mechanically solder alternatives. Developing hybrid integration approaches that reduce stress concentration at hard–soft transition zones will be essential for improving reliability under repeated deformation and daily wear.

Material sustainability must also be addressed through the development of recyclable conductive yarns, detachable sensor architectures and modular electronic units that can be separated before disposal or recycling. Research into alternative conductive materials with improved environmental compatibility, as well as coating technologies with enhanced abrasion and washing resistance, will support circular design strategies.

Finally, advancing self-powered systems through energy harvesting technologies such as TENGs should continue, particularly in combination with low-power electronics and optimized circuit design. Integrating energy harvesting with improved interconnection reliability and wash-resistant materials will move smart textiles closer to fully autonomous, durable and scalable wearable systems. By addressing these challenges, future developments can move smart knitted textiles from laboratory-scale demonstrations toward robust, commercially viable wearable systems. Strengthening washability, improving hard–soft integration, enhancing sustainability and ensuring scalable manufacturing will be decisive steps in establishing reliable and environmentally responsible e-textiles. Through interdisciplinary collaboration between textile engineering, materials science and electronics design, future knitted systems can evolve into durable and user-centered platforms that seamlessly integrate sensing and heating functionalities into everyday garments.

References

1. Bozali, B., Ghodrat, S., and K. M. Jansen, “Design of wearable finger sensors for rehabilitation applications,” Micromachines, vol. 14, no. 4, p. 710, 2023.

2. K.M.B. Jansen, R.B.G., D. van der Gracht, P. van Luijk, Validation tests on a knitted respiration sensor, in E-textiles conference 2024.

3. Loopstra Mark, Feel the heat - EXPLORATIVELY DESIGNING A WEARABLE WEFT-KNITTED HEATER, TU Delft, 2024

4. AB65ft. AB65FT yarn]. Available from: https://ab65ft.com/home/textile/.

List of publications

1. Bozali, B., van Dam, J. J., Plaude, L., & Jansen, K. M. (2021, October), Development of hysteresis-free and linear knitted strain sensors for smart textile applications. In 2021 IEEE Sensors (pp. 1-4). IEEE.
2. Bozali, B., van Dam, J., Ghodrat, S., & Jansen, K. "Design of Knitted Pressure Sensors for Tactile Perception Applications", SensorsCom, 2022
3. Bozali, B., Ghodrat, S., Plaude, L., van Dam, J. J., & Jansen, K. M. (2022). Development of low-hysteresis, linear weft-knitted strain sensors for smart textile applications. Sensors, 22(19), 7688.
4. Bozali, B., Ghodrat, S., and Jansen, Kaspar M. B., Design of wearable finger sensors for rehabilitation applications, Micromachines, vol. 14, no. 4, p. 710, 2023.
5. Bozali, B., Ghodrat, S., & Jansen, K. M. (2023). Development of a knitted strain sensor for health monitoring applications. Engineering Proceedings, 30(1), 10.
6. Bozali, B., Ghodrat, S., & Jansen, K. M. (2025). Structural Design and Optimization of Knitted Heaters for Optimized Heat Distribution. Thermo, 5 (4), 54.